

# Towards quantifiable temperatures from mollusk shells

Dissertation  
zur Erlangung des akademischen Grades  
“Doktor der Naturwissenschaften”  
im Promotionsfach Geologie/Paläontologie

Am Fachbereich 09 für Chemie, Pharmazie und Geowissenschaften  
der Johannes Gutenberg-Universität Mainz

von  
Christoph Simon Füllenbach  
geb. in Neuwied am Rhein

(D77)  
Mainz 2016



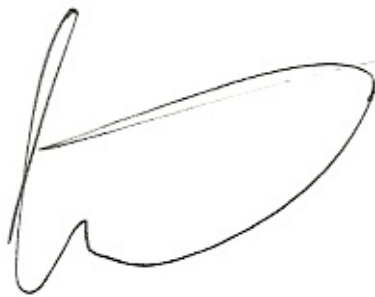
Dekan: Not displayed for reasons of data protection.

1. Berichterstatter: Not displayed for reasons of data protection.

2. Berichterstatter: Not displayed for reasons of data protection.

Datum der mündlichen Prüfung: 16 Juni 2016

Hiermit erkläre ich, dass ich die vorliegende Arbeit selbstständig verfasst  
und keine anderen als die angegebenen Quellen und Hilfsmittel benutzt habe.

A handwritten signature in black ink, consisting of a large, stylized 'C' followed by a horizontal line and a wavy tail.

---

(Christoph Simon Füllenbach)

Mainz, 25. April 2016

„Alles Wissen und alle Vermehrung unseres Wissens endet nicht mit einem Schlusspunkt, sondern mit Fragezeichen. Ein Plus an Wissen bedeutet ein Plus an Fragstellungen und jede von ihnen wird immer wieder von neuen Fragestellungen abgelöst.“

*Hermann Hesse, Auszug aus Brief von 1937*

## Abstract

Mollusk shells meet nearly all requirements of an ideal climate archive. For example, mollusks have an exceptionally wide geographical distribution, occurring from boreal to tropical regions as well as from the deep sea to the near shore. Shell parameters, such as the geochemical composition, vary relative to the physico-chemical state of the ambient water and thus record the prevailing environmental conditions during growth. Each shell portion and the corresponding proxy information can be precisely temporally aligned via annual, daily or circatidal growth patterns. Since growth of contemporaneous specimens of the same region is highly synchronized, annual growth increment chronologies can be combined into so-called master chronologies that allow high-resolution paleoclimate reconstruction over centuries and millennia. Hence, mollusk shells can provide means to study climate variability with a geographical and temporal resolution that is superior to other paleoclimatic archives.

However, quantified estimates of water temperature from mollusk shells are still limited. In fact, the only accepted paleothermometer,  $\delta^{18}\text{O}_{\text{shell}}$ , is a dual proxy that simultaneously records temperature and oxygen isotopic composition of the ambient water and thus only provides accurate environmental reconstructions if either of them is known. Other, less frequently applied temperature proxies such as growth rates, trace element ratios or clumped isotopes are likewise influenced by multiple parameters and need further refinements before they can be routinely applied. Consequently, it is currently impossible to benefit from the full potential offered by mollusk shells. This study tackles this deficit by developing new and optimizing existing proxies. Special emphasis is put on shell microstructures, element-to-element as well as  $\text{Sr}/\text{Ca}_{\text{shell}}$  ratios. Results are presented in three manuscripts, published (submitted in the case of manuscript III) in international, peer-reviewed scientific journals.

The first manuscript explores if shell microstructures of cultured specimens of the freshwater gastropod *Viviparus viviparus* are temperature-sensitive and may thus serve as an alternative temperature proxy. When water temperature was cold and variable, crossed-lamellar microstructures, i.e., the predominating microstructure in shells of *V. viviparus*, were highly unordered and heterogeneous. During warm and stable conditions, however, crossed-lamellar structures displayed a much more ordered and homogenous appearance. If new shell material was formed onto pre-existing, well-ordered crossed-lamellar structures, shell microstructures were always homogenous and ordered, irrespective of the prevailing temperature. It is hypothesized that the growth front forms an organic template that guides the appearance of crossed-lamellar structures. If this template is missing, for example when new material is formed *de novo* along the ventral margin, it is primarily the environment

that controls the appearance of the microstructure. Hence, microstructures of specific shell portions can likely be used to estimate water temperature during growth.

Manuscript II tests if  $\text{Sr}/\text{Li}_{\text{shell}}$  ratios in shells of the common cockle *Cerastoderma edule* can potentially serve as proxy for water temperature. Using LA-ICP-MS, strontium and lithium concentrations in shells of live-collected specimens from the intertidal zone of the North Sea (Schillig, Germany), were determined for the growing season of 2013 and compared to temperature records and other instrumental data. As expected,  $\text{Sr}/\text{Ca}_{\text{shell}}$  and  $\text{Li}/\text{Ca}_{\text{shell}}$  were vitally affected. However,  $\text{Sr}/\text{Li}_{\text{shell}}$  ratios were strongly negatively and linearly correlated with water temperature, with up to 81% of explained variability. It was possible to reconstruct temperature based on  $\text{Sr}/\text{Li}$  to the nearest  $\pm 1.5$  °C. It is hypothesized that normalizing  $\text{Sr}/\text{Ca}_{\text{shell}}$  to  $\text{Li}/\text{Ca}_{\text{shell}}$  mathematically reduces vital effects that hamper the application of traditional element/ $\text{Ca}_{\text{shell}}$  ratios as reliable proxies for water temperature in mollusk shells.

Manuscript III aims to advance  $\text{Sr}/\text{Ca}_{\text{shell}}$  ratios as proxy for water temperature in bivalve shells. In order to understand why strontium concentrations of bivalves are challenging to interpret, ultra-high-resolution geochemical and microstructural analyses were performed in a shell of *Cerastoderma edule* collected alive from the intertidal zone of the North Sea (Schillig, Germany). Results of this study demonstrate that strontium and sulfur (S = proxy for organics) are heterogeneously distributed and co-vary with microstructural changes. For example, circatidal growth lines of the outer portion of the outer shell layer (= irregular simple prisms;  $2.9 \pm 0.4$  mmol/mol) contained much higher Sr levels than portions between consecutive growth lines (= growth increments; nondenticular prismatic structure;  $2.5 \pm 0.2$  mmol/mol). In contrast,  $\text{S}/\text{Ca}_{\text{shell}}$  ratios displayed an inverted pattern with higher values at circatidal increments ( $2.4 \pm 0.3$  mmol/mol) and lower values at circatidal growth lines ( $2.1 \pm 0.5$  mmol/mol). It is hypothesized that microstructures or processes controlling their formation control the incorporation of  $\text{Sr}^{2+}$  ions into the shell. A lower sampling resolution that does not resolve these fine-scaled variations is therefore likely to result in  $\text{Sr}/\text{Ca}_{\text{shell}}$  ratios inadequate for temperature reconstructions, because strontium values of shell portions with different microstructures are averaged. It is suggested that  $\text{Sr}/\text{Ca}_{\text{shell}}$ -based temperature estimates can likely be improved by limiting chemical analyses to shell portions with the same microstructure.

This study proposes two alternatives to estimate water temperature from mollusk shells that aim to make better use of this highly versatile climate archive. The new proxies need to be rigorously tested in subsequent studies. Moreover, results of this study emphasize that a detailed knowledge on biomineralization of mollusk shells is required to improve the accuracy of temperature estimates.

## Zusammenfassung

Molluskenschalen erfüllen nahezu alle Anforderungen eines idealen Klimaarchivs. So haben Mollusken beispielsweise eine außerordentlich weite geographische Verbreitung mit Vorkommen in borealen bis in tropischen Regionen sowie in der Tiefsee bis in die Gezeitenzone. Während des Wachstums variieren verschiedene Schalenparameter, wie etwa die geochemische Zusammensetzung, relativ zur physikochemischen Beschaffenheit des umgebenden Wassers und zeichnen so die vorherrschenden Umweltbedingungen zur Zeit der Schalenbildung auf. Mittels Schalenwachstumsmustern, welche im Rhythmus von Jahreszeiten, Tag/Nacht-Zyklen oder Gezeiten gebildet werden, ist es möglich, Schalenbereiche und darin enthaltene Umweltinformationen zeitlich exakt einzugliedern. Da das Wachstum koexistierender Individuen derselben Region synchron verläuft, lassen sich jährliche Wachstumsmuster verschiedener Individuen verknüpfen, sodass die klimatische Entwicklung über tausende von Jahren hinweg verfolgt werden kann.

Die Rekonstruktion absoluter Wassertemperaturen durch die Analyse von Molluskenschalen ist jedoch nach wie vor eine Herausforderung. So ist beispielsweise der einzig weithin anerkannte Indikator für Wassertemperatur,  $\delta^{18}\text{O}_{\text{Schale}}$ , gleichzeitig von der Sauerstoffisotopenzusammensetzung und der Temperatur des Wassers beeinflusst. Verlässliche Umweltrekonstruktionen sind dementsprechend nur möglich, wenn eine der beiden Variablen bekannt ist. Andere, weniger häufig genutzte Methoden, wie beispielsweise Schalenwachstumsraten oder das Verhältnis von Spurenelementen bzw. Isotopologen, sind ebenfalls meist von mehreren Parametern beeinflusst und bedürfen vor einer routinemäßigen Anwendung noch weiterer Verbesserungen. Folglich ist es derzeit nicht möglich das Potential des Klimaarchivs „Molluskenschale“ voll auszuschöpfen. Das Ziel dieser Studie ist es, dieses Defizit durch die Entwicklung neuer sowie die Verbesserung vorhandener Methoden zur Rekonstruktion der Wassertemperatur zu beheben. Schwerpunkte liegen insbesondere auf Schalenmikrostrukturen, Element/Element<sub>Schale</sub>- sowie Sr/Ca<sub>Schale</sub>-Verhältnissen. Die Ergebnisse dazu werden in drei Manuskripten präsentiert, welche in internationalen Fachzeitschriften publiziert sind (Manuskript III ist eingereicht).

Manuskript I dokumentiert Untersuchungen zu einer möglichen Temperatursensitivität der Schalenmikrostruktur gehälterter Individuen des Süßwassergastropoden *Viviparus viviparus*. Es wurde beobachtet, dass kühle, stark schwankende Wassertemperaturen zur Bildung ungeordneter und heterogener kreuzlamellarer Strukturen führten, wohingegen geordnete und homogene Strukturen mit gleichbleibend warmen Wassertemperaturen im Zusammenhang standen.



Wurde neues Schalenmaterial auf bereits vorhandenen, geordneten Mikrostrukturen abgelagert, so waren diese neuen Schalenbereiche unabhängig von der vorherrschenden Wassertemperatur immer von geordneten homogenen Mikrostrukturen geprägt. Aus diesen Beobachtungen folgt die Annahme, dass die Wachstumsfront ein organisches Templat formt, welches einen starken Einfluss auf die Mikrostruktur des neuen Schalenbereiches hat. Wenn neues Material, wie beispielsweise am ventralen Schalenrand, *de novo* geformt wird, ist dieses Templat nicht vorhanden und die Mikrostrukturen werden maßgeblich durch die vorherrschenden Umweltbedingungen beeinflusst. Mikrostrukturen bestimmter Schalenbereiche könnten also möglicherweise zur Abschätzung der Wassertemperatur während der Schalenbildung genutzt werden.

In Manuskript II wird diskutiert, ob das Verhältnis von Strontium zu Lithium ( $\text{Sr/Li}_{\text{Schale}}$ ) in Schalen der gemeinen Herzmuschel *Cerastoderma edule* möglicherweise zur Rekonstruktion von Wassertemperaturen geeignet ist. Dafür wurden Sr- und Li-Konzentrationen der Wachstumsaison 2013 in Schalen lebend aus der Gezeitenzone der Nordsee (Schillig, Deutschland) gesammelter Individuen mittels LA-ICP-MS bestimmt, zeitlich alieniert und mit einem umfangreichen Umweltdatensatz verglichen. Wie erwartet erwiesen sich  $\text{Sr/Ca}_{\text{Schale}}$ - und  $\text{Li/Ca}_{\text{Schale}}$ -Verhältnisse als stark biologisch beeinflusst. Nichtsdestotrotz korrelierten  $\text{Sr/Li}_{\text{Schale}}$ -Werte stark negativ und linear mit der Wassertemperatur, welche bis zu 81% deren Variabilität erklärte. Es war möglich, die vorherrschende Wassertemperatur zur Zeit der Schalenbildung mit einer durchschnittlichen Genauigkeit von  $\pm 1,5$  °C zu rekonstruieren. Die Ergebnisse lassen vermuten, dass die Normierung von  $\text{Sr/Ca}_{\text{Schale}}$ - zu  $\text{Li/Ca}_{\text{Schale}}$ -Werten mathematisch zu einer Verringerung der biologischen Effekte führt, die für gewöhnlich die Anwendung von  $\text{Element/Ca}_{\text{Schale}}$ -Werten als Temperaturindikator verhindern.

Die in Manuskript III vorgestellten Untersuchungen tragen zu einem besseren Verständnis der Verteilung von Strontium in Molluskenschalen und so zu einer optimierten Anwendbarkeit von  $\text{Sr/Ca}_{\text{Schale}}$ -Verhältnissen als Indikator der Wassertemperatur bei. Dazu wurden an der Schale von *Cerastoderma edule* räumlich extrem hoch aufgelöste geochemische und mikrostrukturelle Analysen durchgeführt. Strontium- und Schwefel-Konzentrationen ( $\text{S}$  = Anzeiger für Organikgehalt) waren heterogen verteilt und variierten mit mikrostrukturellen Veränderungen. So wurden besonders hohe Strontiumwerte an ungefähr im Tidenrhythmus gebildeten Wachstumslinien gemessen (äußere äußere Schalenlage; irreguläre simple Prismen;  $2,9 \pm 0,4$  mmol/mol), während dazwischenliegende Bereiche deutlich geringere Werte aufwiesen (= Wachstumsinkrement; nicht-dentikulare prismatische Struktur;  $2,5 \pm 0,2$  mmol/mol).  $\text{S/Ca}_{\text{Schale}}$ -Verhältnisse zeigten ein gegensätzliches Muster, mit erhöhten Werten in den Wachstumsinkrementen ( $2,4 \pm 0,3$  mmol/mol) im Vergleich zu niedrigeren Werten an den ungefähr im Tidenrhythmus geformten Wachstumslinien

( $2,1 \pm 0,5$  mmol/mol). Der enge Zusammenhang zwischen Schalenmikrostruktur,  $\text{Sr}/\text{Ca}_{\text{Schale}}$ - sowie  $\text{S}/\text{Ca}_{\text{Schale}}$ -Verhältnissen lässt vermuten, dass Mikrostrukturen, beziehungsweise Prozesse, die deren Bildung steuern, ebenfalls den Einbau von Strontium-Ionen in die Schale der *C. edule* beeinflussen. Analytische Verfahren mit geringer räumlicher Auflösung können diese kleinräumigen Strontiumvariationen vermutlich nicht auflösen. Entsprechend sind die so ermittelten  $\text{Sr}/\text{Ca}_{\text{Schale}}$ -Werte höchstwahrscheinlich nicht zur Temperaturrekonstruktion geeignet, da sie lediglich Mittelwerte von Schalenbereichen unterschiedlicher Mikrostrukturen darstellen. Es ist daher anzunehmen, dass eine optimierte Beprobungsstrategie, bei der nur geochemische Daten der gleichen Mikrostruktur erfasst werden, die Applikation von  $\text{Sr}/\text{Ca}_{\text{Schale}}$ -Verhältnissen als Temperaturindikator verbessern könnte.

Die vorliegende Studie präsentiert zwei alternative Methoden der Temperaturrekonstruktion aus Molluskenschalen, die die Anwendungsmöglichkeiten dieses vielseitigen Klimaarchivs deutlich erweitern könnten. Um das Potential der beiden Möglichkeiten zu evaluieren, bedarf es weiterer, ausgiebiger Tests. Zusätzlich verdeutlicht diese Studie, dass ein detailliertes Wissen der Biomineralisation von Molluskenschalen maßgeblich zu einer erhöhten Genauigkeit rekonstruierter Temperaturen beitragen kann.



## **Danksagung**

Not displayed for reasons of data protection.



# Table of contents

Approval page	I
Declaration	II
Citation	III
Abstract	IV
Zusammenfassung	VI
Danksagung	X
Table of contents	XII
List of figures	XVIII
List of tables	XX

## **Chapter 1 – Introduction** **1**

1.1 On the importance of climate reconstructions	2
1.2 Mollusk shells – an extraordinary paleoclimate archive	3
1.3 A brief introduction to the formation of mollusk shells	4
1.4 Opportunities and limitations of temperature reconstructions based on mollusk shells	6
<i>a. Stable oxygen isotopes (<math>\delta^{18}O_{shell}</math>)</i>	7
<i>b. Shell growth rate</i>	7
<i>c. Clumped-isotope thermometer (<math>\Delta_{47}</math>)</i>	8
<i>d. Element-to-calcium ratios</i>	8
1.5 Aim of this study	9
<i>a. Manuscript I: Shell microstructures</i>	10
<i>b. Manuscript II: Trace element ratios</i>	10
<i>c. Manuscript III: Contextualization of Sr/Ca<sub>shell</sub> ratios and     microstructure on the ultra-scale</i>	11
1.6 Principal strategy	12
<i>a. Aquaculture</i>	12

<i>b. Natural laboratory</i>	13
1.7 Overview of research	14
<i>a. Manuscript I</i>	14
<i>b. Manuscript II</i>	14
<i>c. Manuscript III</i>	15
1.8 References	16

## **Chapter 2 – Manuscripts** **29**

### **Manuscript I:**

‘ <b>Microstructures in shells of the freshwater gastropod <i>Viviparus viviparus</i>: A potential sensor for temperature change?</b> ’	<b>30</b>
Abstract	31
1 Introduction	32
2 Material and methods	33
2.1 <i>Fluorescence microscopy</i>	34
2.2 <i>Scanning electron microscopy</i>	36
2.3 <i>Image processing</i>	36
3 Results	36
3.1 <i>Growth rates under experimental conditions</i>	36
3.2 <i>Shell microstructure</i>	37
3.3 <i>Growth lines and XLM 3<sup>rd</sup>-order lamellae</i>	39
3.4 <i>Variations within the simple crossed-lamellar structure:             1<sup>st</sup>-order lamellae</i>	41
4 Discussion	43
4.1 <i>Growth rates under experimental conditions</i>	43
4.2 <i>Growth lines and higher order microstructure changes:             Physiology and environment</i>	43
4.3 <i>Environmentally induced changes of the shell architecture</i>	45
5 Conclusions and outlook	47
6 Acknowledgments	48

7 References	49
Concluding remark	55

## **Manuscript II:**

<b>‘Strontium/lithium ratio in aragonitic shells of <i>Cerastoderma edule</i> (Bivalvia) – A new potential temperature proxy for brackish environments’</b>	<b>56</b>
Abstract	57
1 Introduction	58
2 <i>Cerastoderma edule</i>	59
3 Material and methods	61
3.1 <i>Shell preparation and growth pattern analysis</i>	62
3.2 <i>Chemical analysis of the shells via LA-ICP-MS</i>	63
3.3 <i>Chemical analysis of the water via ICP-OES</i>	64
3.4 <i>Oxygen isotope values of water and carbonate powder via CF-IRMS</i>	65
4 Results	66
4.1 <i>Water parameters</i>	66
4.2 <i>Timing and rate of shell growth of <i>Cerastoderma edule</i></i>	69
4.3 <i>Oxygen isotope values of shell carbonate and reconstructed temperatures</i>	72
4.4 <i>Element chemistry of shell carbonate and environmental variables</i>	72
5 Discussion	76
5.1 <i>Vital effects</i>	76
5.2 <i>Growth rate and crystal kinetic effects</i>	78
5.3 <i>Rayleigh fractionation</i>	79
5.4 <i>Salinity and elemental chemistry of the water</i>	81
5.5 <i>Ocean productivity</i>	83
5.6 <i>Occurrence of trace and minor elements in bivalve shells</i>	83



5.7 $Sr/Ca_{shell}$ , $Li/Ca_{shell}$ and $Sr/Li_{shell}$ of <i>C. edule</i> as temperature proxies	84
6 Summary and conclusions	85
7 Acknowledgments	85
8 References	86

### Manuscript III:

<b>‘Minute co-variations of Sr/Ca ratios and microstructures in the aragonitic shell of <i>Cerastoderma edule</i> (Bivalvia) – Are geochemical variations on the ultra-scale masking potential environmental signals?’</b>	<b>97</b>
Abstract	98
1 Introduction	99
2 Material and Methods	100
2.1 <i>Cerastoderma edule</i>	101
2.2 <i>Biomineralization</i>	101
2.3 <i>Sample locality and shell preparation</i>	102
2.4 <i>Shell microstructures and growth patterns</i>	103
2.5 <i>Semi-quantitative mapping using NanoSIMS</i>	103
2.6 <i>Quantitative spot measurements using electron probe microanalyzer</i>	105
3 Results	106
3.1 <i>Shell microstructure</i>	106
3.2 <i>Intra-annual <math>Sr/Ca_{shell}</math> and <math>S/Ca_{shell}</math> variations</i>	107
3.3 <i><math>Sr/Ca_{shell}</math> and <math>S/Ca_{shell}</math> ratios at annual growth lines</i>	112
4 Discussion	116
4.1. <i>Controls on the distribution of <math>Sr/Ca_{shell}</math> at growth lines and increments</i>	116
4.1.1 <i>Water temperature and <math>Sr/Ca_{water}</math></i>	116
4.1.2. <i>Crystal kinetics and shell growth rate</i>	117
4.1.3. <i>Biomineralization processes and shell microstructures</i>	117

4.2 $Sr/Ca_{shell}$ enrichment at circatidal and annual growth lines	119
4.3 Implications for future analysis of $Sr/Ca_{shell}$	119
5 Summary and Conclusions	120
6 Acknowledgments	121
8 References	122
<b>Chapter 3 – Summary &amp; future perspectives</b>	<b>129</b>
3.1 Summary & Conclusions	130
<i>a. Manuscript I</i>	130
<i>b. Manuscript II</i>	131
<i>c. Manuscript III</i>	132
3.2 Open questions and future outlook	134
3.3 References	136
<b>Appendix</b>	<b>138</b>
Curriculum vitae	139
Conference contributions	141



# List of figures

All figures listed are part of chapter 2.

## Manuscript I

Figure 1.	(A) Shell of <i>Viviparus viviparus</i> . (B) Temperature during the experimental period.	34
Figure 2.	Shell growth near the aperture of <i>V. viviparus</i> under experimental conditions.	35
Figure 3.	SEM images of the microstructures in shells of <i>V. viviparus</i> .	38
Figure 4.	Shell architecture (XLM structure) of <i>V. viviparus</i> close to the aperture.	39
Figure 5.	Different types of growth lines in shells of <i>V. viviparus</i> .	40
Figure 6.	Quantification of 3 <sup>rd</sup> -order lamellae cross section (perpendicular to l-axes) variations in shells of <i>V. viviparus</i> .	42
Figure 7.	Variations in XLM microstructure in shells of <i>V. viviparus</i> .	46

## Manuscript II

Figure 1.	Sclerochronology of <i>Cerastoderma edule</i> .	60
Figure 2.	Map of the North Sea coast of Germany showing the sampling locality.	62
Figure 3.	Physico-chemical parameters of the study locality between March 2013 and April 2014.	67
Figure 4.	Lunar daily growth increment (LDGI) width chronologies of the studied <i>C. edule</i> specimens.	69
Figure 5.	Tidal cycle at the study locality between June and September 2013 and corresponding shell portion of specimen A28.	70
Figure 6.	Time-series of measured and reconstructed water temperature. Reconstructed values are based on oxygen isotope values of four shells.	72
Figure 7.	Sr/Ca <sub>shell</sub> and Li/Ca <sub>shell</sub> time-series of the outer shell portion of the studied shells.	73
Figure 8.	Sclerochronological data of the shell and physico-chemical properties of the ambient water.	80
Figure 9.	Relationship between Sr/Li <sub>shell</sub> ratios and water temperature.	82

Figure 10. Sr/Li <sub>shell</sub> paleothermometry.	84
---	----

### **Manuscript III**

Figure 1. Synopsis of studied shell portions and applied sample techniques.	104
Figure 2. SEM images of microstructures of <i>C. edule</i> within circatidal and annual growth patterns.	107
Figure 3. Semi-quantitative Sr/Ca <sub>shell</sub> ratios and microstructures along circatidal growth patterns in the oOSL and TZ of ontogenetic year three.	108
Figure 4. Quantitative Sr/Ca <sub>shell</sub> and S/Ca <sub>shell</sub> ratios of 71 consecutively measured circatidal growth lines and growth increments.	110
Figure 5. Semi-quantitative and quantitative Sr/Ca <sub>shell</sub> and S/Ca <sub>shell</sub> ratios across the annual growth line of winter 2012/2013.	113
Figure 6. Quantitative Sr/Ca <sub>shell</sub> and S/Ca <sub>shell</sub> variations across annual growth lines.	115

## List of tables

All tables listed are part of chapter 2.

### Manuscript I

Table 1.	Shell growth of <i>Viviparus viviparus</i> during each of the three experimental periods.	37
Table 2.	Summary of variations of the microstructure in shells of <i>V. viviparus</i> initiated by different environmental conditions.	44

### Manuscript II

Table 1.	Timing and rate of shell growth of the studied <i>Cerastoderma edule</i> specimens.	61
Table 2.	Quality control of LA-ICP-MS measurements.	64
Table 3.	Physico-chemical properties of the water at the study locality monitored between March 2013 and March 2014.	68
Table 4.	Oxygen isotope values and temperatures reconstructed thereof of the studied specimens.	71
Table 5.	Correlations between geochemical properties of the studied shells of <i>C. edule</i> and environmental parameters during the growing season of 2013.	74

### Manuscript III

Table 1.	Quantitative Sr/Ca <sub>shell</sub> and S/Ca <sub>shell</sub> ratios of circatidal growth structures formed during the growing season of 2010.	111
Table 2.	Quantitative Sr/Ca <sub>shell</sub> and S/Ca <sub>shell</sub> across annual growth lines.	114







# **Chapter 1**

---

# **Introduction**

## 1.1 On the importance of climate reconstructions

*Homo sapiens* has unambiguously changed the global climate, amongst others, through the escalating emission of greenhouse gases. According to the IPCC (2014), this has contributed to the rise in globally averaged annual temperature of 0.85 °C over the last century (1880 – 2012). Even though the absolute temperature increase appears marginal, the impact on nature and humankind is clearly visible. This is alarming as the majority of numerical climate models predict an even stronger temperature increase during the 21<sup>st</sup> century. Besides this gradual warming trend, the number of climatic extremes has increased since the 1950s (IPCC, 2014).

To understand modern global warming, we need to progress our knowledge of climate forcings and distinguish natural from man-made climate changes. Therefore, we have to put current climate extremes into context with climate anomalies of the (geological) past, specifically the most relevant climate factor, i.e., temperature. Whereas modern temperatures can be readily studied from instrumental records, comparisons to deep-time climates depend on the accuracy of temperature reconstructions based on proxy data recorded in paleoclimate archives (Mann et al., 2008). Many climate archives were periodically formed by biogenic or abiogenic processes. Thus, the proxy data contained in these archives can be precisely temporally aligned. Prominent examples for abiogenic climate archives are ice cores (Johnsen et al., 1992; Dansgaard et al., 1993; Petit et al., 1999), speleothems (Hellstrom et al., 1998; Vollweiler et al., 2006; Scholz et al., 2012) as well as layered marine and freshwater sediments (Kissel et al., 1999; Lamy et al., 1999; Sirocko et al., 2013; Anhäuser et al., 2014). Biogenic climate archives include tree-rings (Briffa et al., 1990; D'Arrigo et al., 2001; Roig et al., 2001; Esper et al., 2002; Büntgen et al., 2009), corals (Beck et al., 1992; Mitsugushi et al., 1996; Goodkin et al., 2008), microfossils (Kennett and Ingram, 1995; Zachos et al., 2001), fish otoliths (Patterson, 1999; Ivany et al., 2000; Vanhove et al., 2011) and mollusks (Davenport, 1938; Jones, 1983; Witbaard et al., 1997; Schöne et al., 2005a). Depending on the respective paleoclimate archive, temperature estimates are often inferred from stable isotopes (e.g.,  $\delta^{18}\text{O}$ ,  $\delta\text{D}$ ,  $\Delta_{47}$ ) and/or element ratios (e.g., Sr/Ca, Mg/Ca). Furthermore, layer thickness can inform about the environmental conditions prevailing during formation (e.g., shell growth increment width, tree-ring widths, sediment layer thickness).

Proxy-based temperature reconstructions have been successfully applied to climate archives that cover long (geological) time-scales and provide a decadal to millennial resolution (Petit et al., 1999; Zachos et al., 2001; Mann et al., 2008). Whereas the understanding of long-term climate oscillations greatly benefitted from these particularly long time-series, temperature extremes as well as climate fluctuations

on shorter timescales are still poorly understood. This is especially true for the marine extratropical regime, where the majority of climate archives are either absent or do not provide a sufficiently temporal resolution. Reconstructing the climate variability of these regions with high temporal resolution can help to understand climate processes operating between the tropics and the polar regions and how these processes might influence the global climate system. Furthermore, as short-term climate events turned out to be particularly hazardous, it is of high importance to understand how these phenomena emerge and evolve.

In order to improve the understanding of short-term climate variability, quantifiable proxies are urgently needed. If such tools existed, temporally highly resolved climate reconstructions from the distant past could serve as a laboratory for short-term climate variations. This would allow studying how short-term climate extremes changed over time and how they impacted the overall climate of the Earth. Furthermore, sub-seasonally resolved temperature time-series could help to calibrate and validate the sensitivity of numerical climate models and thus optimize estimates of future climate change.

## **1.2 Mollusk shells – an extraordinary paleoclimate archive**

Mollusk shells are versatile archives, which record climate information with particularly high temporal resolution. Furthermore, not only do mollusks inhabit freshwater and marine environments, they also occur in various water depths ranging from deep-sea to shallow coastal habitats and live in high and low latitudes. Thus, sclerochronological analysis<sup>1</sup> of mollusk shells can provide means to explore the climate of the Earth with a geographical and temporal resolution that is superior to other paleoclimate archives.

Mollusk shells are accretionary hardparts composed of a mixture of carbonatic and organic substances (see chapter 1.3 for details). The addition of new shell material along the inner shell surface and the ventral margin occurs periodically. When viewed under reflected light, fast growth usually results in broad whitish increments, whereas dark and narrow growth lines are associated with slow growth. The periodicity of growth patterns is defined by endogenous timekeeping mechanisms (biological clocks), which approximately mirror environmental cycles (e.g., light/dark cycle; food availability; temperature), through which they are constantly reset (Schöne, 2008). For example, in many species annual growth lines

---

<sup>1</sup> Study of accretionary formed biogenic hardparts (Hudson et al., 1976).

form when water temperature drops below or rises above species-specific thresholds. However, in some species the periodic annual growth line is not linked to known environmental signals (Schöne et al., 2005a; Walliser et al., 2015). Additionally and more important for this study, numerous mollusk species also form sub-seasonal growth patterns. For instance, specimens inhabiting the tidal zone can exhibit circalunidian (~24.8 h) and/or circatidal (~12.4 h) growth patterns, because shell growth is limited to the time when bivalves are immersed in water, i.e., during high tide (Richardson et al., 1979; Ohno, 1985). Circadian (~24 h) growth patterns, however, were observed in various mollusk species living in subtidal regimes (e.g., Clark II, 1968; Chauvaud et al., 2005; Schöne et al., 2005b). In some species, ultradian growth periods have been reported (Rodland et al., 2006; Guzman et al., 2007).

Annual growth patterns allow to assign calendar years to each shell portion and thus to temporally align the proxy information. Sub-annual growth patterns permit a higher temporal control that sets mollusk shells apart from most other paleoclimate archives. Moreover, as growth rates are synchronized among coeval specimens individual chronologies can be combined into master chronologies that span over hundreds of years (Witbaard et al., 1997; Butler et al., 2013; Holland et al., 2014; Marali et al., 2015).

### **1.3 A brief introduction to the formation of mollusk shells**

Mollusk shells consist of a complex network of organic macromolecules and  $\text{CaCO}_3$  crystals with stunning mechanical properties. For example, the strength of nacre is 3,000 times larger than that of pure  $\text{CaCO}_3$  (Jackson et al., 1988).

Shell formation occurs in the inner and outer extrapallial spaces, reaction compartments separated from each other at the pallial line and from the ambient water by the inner shell surface, the outer mantle epithelium and the periostracum. It has been suggested that the extrapallial spaces are filled with a fluid (i.e., the extrapallial fluid = EPF) that contains all building materials for shell formation. Although some authors reported the composition of these fluids (Wada and Fujinuki, 1976; Moura et al., 2000; Planchon et al., 2013), the existence has been questioned (Addadi et al., 2006; Cuif et al., 2012; Marin et al., 2012). If extrapallial fluids exist, the volume of these is probably rather small, because an almost direct contact between mantle and the calcification front has been suggested (Rousseau et al., 2009).

Regardless of the existence of a fluid, major components necessary for the formation of new shell material (i.e., primarily  $\text{Ca}^{2+}$  and  $\text{HCO}_3^-$ ) need to be transported from the ambient water to the site of biomineralization. Cations (predominantly  $\text{Ca}^{2+}$ ) likely cross the epithelial membranes via both active intracellular and passive intercellular pathways. Thereby, energy-consuming  $\text{Ca}^{2+}$ -ATPase enzymes are suggested to promote active cation transport (Wilbur and Saleuddin, 1983; Gillikin et al., 2005a). Cations can also be passively transported across the mantle epithelium through ion-specific channels (Carré et al., 2006) or via diffusion along septate junctions (Bleher and Machado, 2004). It is assumed that cationic impurities (e.g.,  $\text{Mg}^{2+}$ ,  $\text{Sr}^{2+}$ ) co-precipitated with the shell can likewise be transported via these calcium-specific pathways, if they have similar ionic characteristics (i.e., charge, size). Carbonate anions ( $\text{CO}_3^{2-}$ ) predominantly reach the site of biomineralization by passive diffusion as hydrogen carbonate ( $\text{HCO}_3^-$ ) molecules and in minor proportions as  $\text{CO}_2$  (transformed to  $\text{HCO}_3^-$  by carbonic anhydrase) from metabolic (Wilbur and Saleuddin, 1983; Marin et al., 2012) and respiratory processes (McConnaughey and Gillikin, 2008). Furthermore, the role of membrane-coated vesicles containing amorphous calcium carbonate (= ACC), trace amounts of other metal ions and organic substances is discussed (Addadi et al., 2003). These nano-scaled globules are assumed to function as precursor phase that can temporarily store but also transport components necessary for shell formation to the biomineralization front at which they are transformed into calcite or aragonite (Jacob et al., 2011; Cartwright et al., 2012). High concentrations of  $\text{Mg}^{2+}$  and specific organic components likely prevent the amorphous carbonate from crystallization before reaching the EPS. If ACC functions as precursor phase in all mollusk species and to which proportion it constitutes to the process of shell formation however has to be clarified.

The process of shell formation is a prime example of a fully biologically controlled crystallization. Although knowledge of the underlying mechanisms is still in its infancy, it is commonly accepted that the type of  $\text{CaCO}_3$  polymorph as well as morphology, orientation, size and habit of each newly formed crystal is orchestrated via an inter- and intracrystalline organic matrix at the site of biomineralization (Addadi et al., 2006; Cuif et al., 2012; Marin et al., 2012). The minute control on morphological as well as mineralogical characteristics gives rise to seven different main categories of microstructures, which can be divided into numerous classes (see Carter and Clark, 1985; De Paula and Silveira, 2009; Marin et al., 2012 for review). For reasons of geometrical simplicity and size of the individual sub-units, nacre (= mother-of-pearl) has become the most studied microstructure, serving as a reference microstructure to understand the principles of shell formation.

Shell formation is assumed to begin with mantle epithelial cells secreting organic substances (proteins, [sulfated] polysaccharides, lipids, free amino acids and peptides) into the extrapallial spaces. Specific parts of the secreted components self-assemble to form the intercrystalline matrix, a layered organic template suggested to orchestrate the crystal formation (Bevelander and Nakahara, 1969; Addadi et al., 2006; Marin et al., 2012). In a next step, the template is covered with a gel-like phase, potentially ACC, containing major shell building elements. This layer is subsequently transformed into crystalline calcium carbonate (Addadi et al., 2006). The formation of individual crystals from the amorphous phase covering the organic matrix is initiated by nucleation at negatively charged sulfated polysaccharides as well as carboxylates (Nudelman et al., 2006). Other parts of the organic phase that are incorporated into the forming crystal (i.e., intracrystalline organic matrix) demonstrably alter its crystallographic properties (Pokroy et al., 2006). It is important to keep in mind that even though the microstructural units behave as a single crystal with respect to their optical extinction as well as to X-ray diffraction patterns, they are amalgamates of nanometer-scaled sub-units (Cölfen and Antonietti, 2005; Dauphin, 2008; Zhang and Xu, 2013). Interestingly, it has been suggested that these sub-units are similar in appearance, but differ in their organic and mineralogical characteristics (Cuif et al., 2011).

The hypothesis of shell formation described above is strongly simplified and primarily based on findings of the nacreous microstructure. Thus, it does not account for all the details of the various assumptions describing the process of crystallization under biological control. However, basic principles such as the full biological control through organic macromolecules including the formation of templates and the guided nucleation are likely also true for other microstructures, e.g., crossed-lamellar structures.

## **1.4 Opportunities and limitations of temperature reconstructions based on mollusk shells**

During growth, geochemical composition and growth rate of shells are affected by the physico-chemical conditions of the environment. Since these influences can be expressed by mathematical functions, it is possible to use specific shell parameters as proxies for environmental conditions that prevailed during shell formation. By means of re-occurring growth patterns (see chapter 1.2), proxy data can be placed into temporal context. In the following, assets and drawbacks of the most commonly applied proxy systems used to reconstruct water temperature from mollusk shells are discussed.

### a. Stable oxygen isotopes ( $\delta^{18}\text{O}_{\text{shell}}$ )

The most commonly used proxy to reconstruct water temperature from mollusk shells is the ratio of the two most abundant stable oxygen isotopes ( $^{18}\text{O}/^{16}\text{O}$ ; commonly expressed in delta-notation:  $\delta^{18}\text{O}$ ; McKinney et al., 1950). During crystallization, the distribution of both isotopes between the solution and the crystal is predominantly controlled by a temperature-dependent equilibrium fractionation. The heavier  $^{18}\text{O}$  isotope is preferentially incorporated into the crystal lattice during lower temperatures and vice versa. This inverse temperature- $\delta^{18}\text{O}_{\text{shell}}$  relationship can be used to compute temperature from  $\delta^{18}\text{O}_{\text{shell}}$  values (Epstein et al., 1953; Grossman and Ku, 1986; Dettman et al., 1999). Actually, most mollusks secrete their shells near equilibrium with the ambient water. Since  $\delta^{18}\text{O}_{\text{shell}}$  also changes as a function of  $\delta^{18}\text{O}_{\text{water}}$ ,  $\delta^{18}\text{O}_{\text{shell}}$  is a dual proxy, that simultaneously records temperature and isotopic composition of the water. Hence, the accuracy of reconstructed temperatures largely depends on knowledge of  $\delta^{18}\text{O}_{\text{water}}$  changes during shell formation. Small unnoticed variations of  $\delta^{18}\text{O}_{\text{water}}$ , for instance by means of freshwater input or evaporation ( $\delta^{18}\text{O}_{\text{water}}$  and salinity are linearly correlated: Epstein et al., 1951; Chauvaud et al., 2005; Schöne et al., 2007; Hallmann et al., 2009), can severely distort reconstructed temperatures. Since there is currently no additional proxy available to reliably track changes of  $\delta^{18}\text{O}_{\text{water}}$ , reconstructing accurate temperatures from mollusks inhabiting environments where  $\delta^{18}\text{O}_{\text{water}}$  is known to undergo large-scale variations is challenging (Gillikin et al., 2005b). Furthermore, the application to fossil specimens has a large margin for error, because  $\delta^{18}\text{O}_{\text{water}}$  needs to be estimated or inferred from other paleoclimate archives (Walliser et al., 2015).

### b. Shell growth rate

Shell growth rate and hence increment width varies as a function of temperature (Davenport, 1938; Jones et al., 1989; Schöne et al., 2003; Hallmann et al., 2011; Marali et al., 2015). Many species grow faster at higher temperatures and slower in colder waters (Rhoads and Lutz, 1980). However, mollusk growth rates are also sensitive to others factors including food availability (Jones et al., 1989), fitness (Soniati et al., 2009), pollution/anthropogenic influence (Kennish and Olsson, 1975) and ontogenetic age (Jones, 1983). The latter follows a predictable trend and can be mathematically eliminated (Cook and Kairiukstis, 1990), whereas an evaluation of the other factors is much more complex. Furthermore, it is challenging to quantify the effect of individual factors in increment width. For instance, particularly narrow growth increments may not necessarily have formed in response to low temperatures, but might equally be caused by low food quality etc. Hence, in most cases variable growth rates comprise information on a number of different factors and must therefore be interpreted with particular care.

### c. Clumped-isotope thermometer ( $\Delta_{47}$ )

The composition of the CO<sub>3</sub>-isotopologues<sup>2</sup> in a carbonate crystal changes as a function of a thermodynamically controlled equilibrium reaction. In contrast to the  $\delta^{18}\text{O}$ -paleothermometer, this process is not affected by the isotopic composition of the ambient water, because the reaction is homogeneous and thus only occurs within a single phase (i.e., the crystal; Ghosh et al., 2006). With decreasing temperature the abundance of bonded ('clumped') heavy isotopes (<sup>13</sup>C<sup>18</sup>O) within the CO<sub>3</sub>-isotopologue increases and can thus be utilized as a gauge for the prevailing temperature during crystallization (Ghosh et al., 2006). The abundance of clumped isotopes is typically derived from  $\Delta_{47}$  (simplified: abundance of CO<sub>2</sub>-isotopologue with mass 47: <sup>13</sup>C<sup>18</sup>O<sup>16</sup>O) measured in CO<sub>2</sub> resulting from acid digestion of carbonate (Ghosh et al., 2006). However, because of a large amount of sample material required for each analysis (1.2 – 4 mg) and the low sample throughput (~6 samples in ~24 h; compared to ~60 samples in ~24 h,  $\delta^{18}\text{O}_{\text{shell}}$  ratios analyzed by CF-IRMS + GasBench II), it is currently not possible to reconstruct sub-seasonally resolved temperature records with this novel technique. Furthermore, the straightforward application to biogenic carbonates needs to be rigorously tested, because vital effects may compromise  $\Delta_{47}$ -based temperature reconstructions (Eiler, 2011; Eagle et al., 2013).

### d. Element-to-calcium ratios

The concentration of trace elements such as strontium or magnesium in calcium carbonates produced in abiogenic precipitation experiments varies as a function of temperature (Kinsman and Holland, 1969; Oomori et al., 1987; Dietzel et al., 2004; Gaetani and Cohen, 2006). Similar correlations between element-to-calcium ratios (e.g., Sr/Ca, Mg/Ca) and water temperature exist in various carbonate-secreting organisms (e.g., Beck et al., 1992; Mitsugushi et al., 1996; Nürnberg et al., 1996; Rosenthal et al., 1997; Martin et al., 2002). In mollusk shells, however, the concentration of most trace element ions is actively controlled by the animal, in other words vitally affected and thus not directly applicable as a gauge for the temperature during shell formation. This is indicated by metal/Ca<sub>shell</sub> ratios strongly underestimating those of the ambient water (e.g., strontium: ~1.5 – 3.8 mmol/mol, Foster et al., 2009; 0.54 – 5.17 mmol/mol, Schöne et al., 2011; versus Sr/Ca<sub>water</sub> = ~8.5 mmol/mol, de Villiers et al., 1994) and by significantly different distribution coefficients ( $K^D$ ) reported for biogenic and abiogenic carbonates (e.g., strontium: molluscan aragonite ~0.2 – 0.3 (0 – 30 °C), Gillikin et al., 2005a; Zhao et al., 2016; versus abiogenic aragonite: ~1.2

<sup>2</sup> Molecules that differ in their isotopic composition. For carbonate 20 different isotopologues exist (Ghosh et al., 2006).



(25 °C), Dietzel et al., 2004). Considering the strong vital effects, it is still a matter of debate whether metal/ $\text{Ca}_{\text{shell}}$  ratios of mollusk shells are thermodynamically controlled and may thus serve as gauge for temperature. Strontium, for instance, co-varies with temperature (Dodd, 1965; Hallam and Price, 1968; Richardson et al., 2004; Schöne et al., 2011; Yan et al., 2013), but is also associated with the composition of the water (Chen et al., 2016; Zhao et al., 2016) as well as metabolism (Klein et al., 1996; Carré et al., 2006), growth rate (Takesue and van Geen, 2004; Gillikin et al., 2005a), kinetic effects (Vander Putten et al., 2000; Lorrain et al., 2005) and ontogenic age (Swan, 1956). Complex control on uptake and incorporation into shells were also reported for other elements (e.g., magnesium: Freitas et al., 2006; Wanamaker et al., 2008; lithium: Thébault et al., 2009; Thébault and Chauvaud, 2013). The interpretation of metal/ $\text{Ca}_{\text{shell}}$  ratios is further complicated by species-specific, habitat-specific aspects. For instance,  $\text{Sr}/\text{Ca}_{\text{shell}}$  ratios show both a positive and negative correlation with water temperature in different mollusk species (c.f. Dodd, 1965; Toland et al., 2000; Schöne et al., 2011). However, it has to be mentioned that not all analyzed shells were of the same calcium carbonate polymorph.

As seen from the brief review, there is currently no proxy available to reliably estimate temperatures from mollusk shells. If such a proxy would exist, shells of mollusks would represent an extraordinary climate archive, because annual, daily or tidally growth patterns allow to place the proxy information in precise chronological order.

## 1.5 Aim of this study

This study aims to develop new and optimize existing proxies to ultimately improve the capabilities to reconstruct sub-seasonally resolved temperatures from mollusk shells. This will advance the possibilities to reconstruct past climate variations and temperature, a necessity for testing and improving numerical climate models. The goal to unlock sub-seasonally resolved temperature data is addressed in three projects, interrelated by the underlying endeavor to gain a deeper understanding of the climate archive mollusk shell. In the following, the motivation of each project is briefly presented along with a working hypothesis.

**a. Manuscript I: Shell microstructures**

Microstructures of mollusk shells have been extensively studied to understand the evolution of phylogenetic lineages (MacClintock, 1967; Carter and Clark, 1985; Shimamoto, 1986) as well as, based on their superior mechanical properties, as blueprints for biomimetic materials (Barthelat, 2007; Finnemore et al., 2012; Mirkhalaf et al., 2014; Weber and Pokroy, 2015). However, the number of studies on their potential to serve as environmental recorders is still small. This is unexpected as the formation of the complex structures is a delicate process and thus likely to be influenced by environmental stress, for instance, by abrupt temperature changes. In fact, the proportion of the two microstructures comprising the outer shell layer of some mollusks changes as a function of temperature (Dodd, 1964; Tan Tiu, 1988; Nishida et al., 2012). Moreover, the morphology of sub-units of the nacreous microstructure is temperature-sensitive (Lutz, 1984; Olson et al., 2012). Nacre, however, predominantly forms the inner shell layer, which, due to dissolution processes during shell closure, only represents a fragmentary archive. Crossed-lamellar structures on the other hand are the most common structure of the outer shell layer and would thus offer a great archive if temperature also influenced the formation of the sub-units of this microstructure.

→ **Hypothesis: The morphology of crossed-lamellar structures is sensitive to water temperature and serves as a (paleo) thermometer.**

**b. Manuscript II: Trace element ratios**

The incorporation of some trace elements into abiogenic calcium carbonate, such as strontium in aragonite (Kinsman and Holland, 1969) or magnesium in calcite (Oomori et al., 1987), changes as a function of temperature. However, in bivalve shells the incorporation of the same trace elements is influenced by strong vital effects (Gillikin et al., 2005a; Zhao et al., 2016). If there would be means to adjust for these vital effects, trace elements could serve as valuable proxy archives. Recently, a promising approach to correct for vital effects on trace element in tests of foraminifera (Bryan and Marchitto, 2008) and coral skeletons (Case et al., 2010; Hathorne et al., 2013; Raddatz et al., 2013; Montagna et al., 2014) has been documented. By dividing one element/Ca ratio with another one (Mg/Ca and Li/Ca to Mg/Li and Li/Mg, respectively), these authors were able to extract much more accurate temperature signals than by using either one of the original element-to-calcium ratios.

Magnesium is preferably bond to the organic phase of aragonitic shells (Schöne et al., 2010). Hence,  $\text{Mg}/\text{Ca}_{\text{shell}}$  ratios of aragonitic shells are likely to vary in relation to

the organic concentration instead of temperature. Strontium, however, can substitute for  $\text{Ca}^{2+}$  in the crystal lattice of bivalve aragonite (Foster et al., 2009). If this process is thermodynamically controlled, the concentration of  $\text{Sr}^{2+}$  may change as a function of temperature. Because *Cerastoderma edule*, the studied species, forms an aragontic shell, Sr/Li ratios instead of Mg/Li ratios were evaluated as a potential temperature proxy.

→ **Hypothesis: The combination of two element-to-calcium ratios is a possibility to adjust for vital effects and thus to improve the capabilities to reconstruct water temperature based on trace element concentrations of mollusk shells.**

### c. Manuscript III: Contextualization of $\text{Sr}/\text{Ca}_{\text{shell}}$ ratios and microstructure on the ultra-scale

Strontium is one of the most extensively studied trace elements that co-precipitates with  $\text{Ca}^{2+}$  during shell formation. Unlike in other marine organisms, in which the strontium concentration clearly changes as a function of temperature, Sr/Ca ratios of mollusk shells are still challenging to interpret. The knowledge of factors controlling the incorporation into shells is still in its infancy. Deviations from published temperature relationships or crystal kinetic effects observed in abiogenic precipitation experiments (e.g., negative temperature dependency in abiogenic aragonite; Gaetani and Cohen, 2006) are typically summarized as ‘vital effects’<sup>3</sup>. Recently, microstructures and associated organic macromolecules were suggested to influence the amounts strontium incorporated into mollusk shells on the annual scale (Shirai et al., 2014). In fact, strontium concentrations change with the microstructure, for instance, those found at annual growth lines and between adjacent growth lines (Schöne et al., 2013; Shirai et al., 2014) as well as within contemporaneously formed shell portions (Hallam and Price, 1968). In *Cerastoderma edule*, microstructural variations were also observed across circatidal growth patterns (Deith, 1985). If these microstructural variations were likewise associated with changing  $\text{Sr}/\text{Ca}_{\text{shell}}$  ratios, this small-scale element-microstructure link might hamper the applicability of  $\text{Sr}/\text{Ca}_{\text{shell}}$  ratios as a paleothermometer in mollusk shells.

→ **Hypothesis: Microstructure and  $\text{Sr}/\text{Ca}_{\text{shell}}$  ratios change synchronously.**

<sup>3</sup> First mentioned by Urey (1951) in the context of biologically influenced oxygen isotope ratios.

## 1.6 Principal strategy

In order to empirically test, but also to further understand potential driving factors of geochemical and microstructural variations in mollusk shells, it is essential to establish comprehensive datasets of environmental parameters. This can be either accomplished in ‘natural laboratories’ where a natural habitat is closely monitored, or in controlled artificial environments (= tanks).

Natural laboratories come with the advantage to study animals living in their natural environment. Thus, as long as no intrusive mark-and-recovery techniques are applied, animals are not caged or transplanted into a new environment, studied specimens are most likely not at all or only marginally influenced by the experiment. A drawback of this strategy, however, is often the incompleteness of instrumental data on environmental parameters. The geochemical composition, microstructure or growth patterns of studied shells can be influenced by additional, unmonitored factors. Furthermore, the compilation of high-resolution time-series of the ambient environmental conditions requires frequent visits of the study site.

Aquacultures on the other hand allow to precisely monitor and control most environmental parameters. For instance, water temperature can be changed gradually or abruptly while food supply and chemical composition of the water are kept at a constant level. However, as the environment is artificial, animals are likely to be stressed and hence potentially show an atypical behavior. Thus, correlations established under controlled conditions might differ from results obtained in the natural environment and consequently need to be interpreted carefully and verified by natural experiments. To ensure best and most reliable results, studies realized in the course of this thesis make use of both approaches.

### a. Aquaculture

Shell microstructures are very delicate constructs, which are most likely sensitive to various parameters such as water composition and temperature, food availability and predatory pressure. Since the influence of water temperature was of particular interest, other factors were required to remain constant. This was accomplished by means of an aquacultural experiment in which parameters, except of water temperature, were kept at approximate constant levels. Detailed information on the experimental setup is given in manuscript I. The freshwater gastropod *Viviparus viviparus* was chosen as study species because it is (i) fast growing, (ii) less selective regarding food supply compared to bivalves, (iii) forming a shell predominantly characterized by the microstructure of interest, i.e. crossed-lamellar structure.

## **b. Natural laboratory**

Sub-annually resolved trace element ratios were studied in specimens of the common cockle, *Cerastoderma edule*, collected from the high intertidal zone of the North Sea, close to Schillig, Germany (manuscript II and III). *Cerastoderma edule* was chosen as study species because (i) it has a wide geographical distribution and (ii) it is fast growing. From March 2013 to April 2014, water temperature (hourly) and chemistry (approximately biweekly) were monitored at the study locality and several field trips were conducted for sample collection. To increase the number of environmental data, additional water samples were collected by local colleagues. Time-series of recorded environmental parameters are presented in manuscript II.

Independent of the experimental setup, sample preparation and processing followed a similar procedure. The basic routine is given below, for details the reader is referred to the ‘Material and Methods’ section of each manuscript.

Shells were separated from soft tissues, cleaned thoroughly, mounted on plexiglass cubes and covered with a layer of epoxy resin (JB KWIK) to ensure stabilization during subsequent preparation steps. Shell thick-sections were cut parallel to maximum axis of growth from each shell using a low-speed saw (Buehler Isomet 1000). Depending on the intended analysis, shell slabs were either mounted on glass slides (low resolution: light microscopy, milling of carbonate powder for  $\delta^{18}\text{O}$  analyses) or fully embedded into epoxy resin (high resolution: LA-ICP-MS, SEM, NanoSIMS). Subsequently to both methods, various grinding and polishing steps were applied.

Prior to any further analysis, samples were extensively studied using light and/or electron microscopy. This included establishing time reference points within each shell, either by identification of shell portions previously labeled with a fluorescent marker (manuscript I) or via comparison of periodic growth patterns (fortnight-cycles) with the tidal cycle as well as by counting circatidal and annual growth lines (manuscript II, III). If needed, different etching methods were applied to improve the visibility of the studied growth patterns. A detailed description of the different analytical techniques is given in each manuscript.

Data were placed into precise temporal context by using sclerochronological methods and compared with time-series of environmental parameters, growth rates and microstructures using qualitative (manuscript I, III) and quantitative methods (manuscript II).

## 1.7 Overview of research

The results of this thesis are published (submitted in case of manuscript III) in high-ranked, internationally renowned, peer-reviewed scientific journals. A summary of the results as well as of future perspectives is presented in chapter 3. In the following, the scope of each of the three manuscripts contributing to this thesis is briefly discussed.

### a. Manuscript I

*‘Microstructures in shells of the freshwater gastropod Viviparus viviparus: A potential sensor for temperature change?’*

This study tests if microstructural characteristics of mollusk shells change as a function of water temperature and can thus be utilized as a (paleo) thermometer. To exclude the majority of potential confounding factors, the studied specimens of the freshwater gastropod, *Viviparus viviparus* were exposed to different temperature regimes in a controlled tank experiment. Fluorescent marking with calcein allowed for a precise temporal alignment of shell portions and thus to test for a potential influence of water temperature on shell growth and microstructure. Furthermore, the influence of particularly stressful situations (i.e., removal from habitat, staining) as well as small-scale variations of microstructural sub-units in the context of reoccurring growth patterns were studied.

### b. Manuscript II

*‘Strontium/lithium ratio in aragonitic shells of Cerastoderma edule (Bivalvia) – A new potential temperature proxy for brackish environments’*

This study explores  $\text{Sr}/\text{Li}_{\text{shell}}$  as a new potential temperature proxy in shells of *Cerastoderma edule*. Specimens were collected from the intertidal zone of the North Sea (Schillig, Germany). In order to test for potential influences of different factors on this new trace element ratio, temporal aligned  $\text{Sr}/\text{Li}_{\text{shell}}$  ratios of the growing season 2013 were compared to extensive datasets of environmental parameters compiled during a one-year monitoring experiment at the sample locality whereby intrinsic factors such as growth rate were also considered. To evaluate the applicability of  $\text{Sr}/\text{Li}_{\text{shell}}$  ratios as a gauge for temperature in *C. edule*, a linear water temperature- $\text{Sr}/\text{Li}_{\text{shell}}$  regression model was constructed and applied to values of an additional specimen. Reconstructed temperatures were compared to logged temperatures as well as reconstructed temperatures based on  $\delta^{18}\text{O}_{\text{shell}}$ .

**c. Manuscript III**

*‘Minute co-variations of Sr/Ca ratios and microstructures in the aragonitic shell of Cerastoderma edule (Bivalvia) – Are geochemical variations on the ultra-scale masking potential environmental signals?’*

The manuscript aims to understand the variability and trends of Sr/Ca<sub>shell</sub> ratios that currently hamper the use of strontium concentrations as a reliable paleothermometer in most bivalve species. Strontium and sulfur concentrations along with shell microstructure of shells of *C. edule* were determined on the sub-micrometer scale. NanoSIMS mapping and ion microprobe spot analyses combined with modern SEM-techniques allowed for the comparison of geochemical and microstructural variations with ultra-high spatial resolution. Special attention was given to potential geochemical and microstructural variations along annual and circatidal growth patterns.

## 1.8 References

- Addadi, L., Raz, S., Weiner, S., 2003. Taking advantage of disorder: Amorphous calcium carbonate and its roles in biomineralization. *Adv. Mater.* 15, 959–970.
- Addadi, L., Joester, D., Nudelman, F., Weiner, S., 2006. Mollusk shell formation: a source of new concepts for understanding biomineralization processes. *Chemistry* 12, 980–987.
- Anhäuser, T., Sirocko, F., Greule, M., Esper, J., Keppler, F., 2014. D/H ratios of methoxyl groups of the sedimentary organic matter of Lake Holzmaar (Eifel, Germany): A potential palaeoclimate/-hydrology proxy. *Geochim. Cosmochim. Acta* 142, 39–52.
- Barthelat, F., 2007. Biomimetics for next generation materials. *Philos. Trans. R. Soc. A.* 365, 2907–2919.
- Beck, J.W., Edwards, R.L., Ito, E., Taylor, F.W., Recy, J., Rougerie, F., Joannot, P., Henin, C., 1992. Sea-surface temperature from coral skeletal strontium/calcium ratios. *Science* 257, 644–647.
- Bevelander G., Nakahara, H., 1969. An electron microscope study of the formation of the nacreous layer in the shell of certain bivalve molluscs. *Calc. Tiss. Res.* 3, 84–92.
- Bleher, R., Machado, J.P., 2004. Paracellular pathway in the shell epithelium of *Anodonta cygnea*. *J. Exp. Zool. A* 301, 419–27.
- Briffa, K.R., Bartholin, T.S., Eckstein, D., Jones, P.D., Karlén, W., Schweingruber, F.H., Zetterberg, P., 1990. A 1,400-year tree-ring record of summer temperatures in Fennoscandia. *Nature* 346, 434–439.
- Bryan, S.P., Marchitto, T.M., 2008. Mg/Ca-temperature proxy in benthic foraminifera: New calibrations from the Florida Straits and a hypothesis regarding Mg/Li. *Paleoceanography* 23, PA2220.
- Büntgen, U., Tegel, W., Nicolussi, K., McCormick, M., Frank, D., Trouet, V., Kaplan, J.O., Herzig, F., Heussner, K.-U., Wanner, H., Luterbacher, J., Esper, J., 2011. 2500 years of European climate variability and human susceptibility. *Science* 331, 578–582.
- Butler, P.G., Wanamaker Jr., A.D., Scourse, J.D., Richardson, C.A., Reynolds, D.J., 2013. Variability of marine climate on the North Icelandic Shelf in a 1357-year proxy archive based on growth increments in the bivalve *Arctica islandica*. *Palaeogeogr. Palaeoclimatol. Palaeoecol.* 373, 141–151.
- Carré, M., Bentaleb, I., Bruguier, O., Ordinola, E., Barrett, N.T., Fontugne, M., 2006. Calcification rate influence on trace element concentrations in aragonitic bivalve shells: Evidences and mechanisms. *Geochim. Cosmochim. Acta* 70, 4906–4920.



- Carter, J.G., Clark II, G.R., 1985. Classification and phylogenetic significance of molluscan shell microstructure. In: Bottjer, D.J., Hickman, C.S., Ward, P.D. (Eds.), *Mollusks Notes for a Short Course*. University of Tennessee, pp. 50–71.
- Cartwright, J.H.E., Checa, A.G., Gale, J.D., Gebauer, D., Sainz-Díaz, C.I., 2012. Calcium carbonate polymorphism and its role in biomineralization: How many amorphous calcium carbonates are there? *Angew. Chem. Int. Edit.* 51, 11960–11970.
- Case, D.H., Robinson, L.F., Auro, M.E., Gagnon, A.C., 2010. Environmental and biological controls on Mg and Li in deep-sea scleractinian corals. *Earth Planet. Sci. Lett.* 300, 215–225.
- Chauvaud, L., Lorrain, A., Dunbar, R.B., Paulet, Y.-M., Thouzeau, G., Jean, F., Guarini, J.M., Mucciarone, D., 2005. Shell of the Great Scallop *Pecten maximus* as a high-frequency archive of paleoenvironmental changes. *Geochem. Geophys. Geosyst.* 6, Q08001.
- Chen, F., Feng, J.-L., Hu, H.-P., 2015. Relationship between the shell geochemistry of the modern aquatic gastropod *Radix* and water chemistry of lakes of the Tibetan Plateau. *Hydrobiologia*. doi:10.1007/s10750-015-2634-1
- Clark II, G.R., 1968. Mollusk shell: daily growth lines. *Science* 161, 800–802.
- Cölfen, H., Antonietti, M., 2005. Mesocrystals: inorganic superstructures made by highly parallel crystallization and controlled alignment. *Angew. Chem. Int. Edit.* 44, 5576–5591.
- Cuif, J.-P., Dauphin, Y., Sorauf, J.E., 2011. *Biominerals and fossils through time*. Cambridge University Press, Cambridge (490 pp.).
- Cook, E.R., Kairiukstis, L.A. (Eds.), 1990. *Methods of dendrochronology. Applications in the environmental sciences*. Kluwer Academic Publishers, Dordrecht (394 pp.).
- Cuif, J.-P., Dauphin, Y., Nehrke, G., Nouet, J., Perez-Huerta, A., 2012. Layered growth and crystallization in calcareous biominerals: Impact of structural and chemical evidence on two major concepts in invertebrate biomineralization studies. *Minerals* 2, 11–39.
- D'Arrigo, R., Villalba, R., Wiles, G., 2001. Tree-ring estimates of Pacific decadal climate variability. *Clim. Dyn.* 18, 219–224.
- Dansgaard, W., Johnsen, S.J., Clausen, H.B., Dahl-Jensen, D., Gundestrup, N.S., Hammer, C.U., Hvidberg, C.S., Steffensen, J.P., Sveinbjörnsdóttir, A.E., Jouzel, J., Bond, G., 1993. Evidence for general instability of past climate from a 250-kyr ice-core record. *Nature* 364, 218–220.
- Dauphin, Y., 2008. The nanostructural unity of mollusc shells. *Mineral. Mag.* 72, 243–246.
- Davenport, C.B., 1938. Growth lines in fossil pectens as indicators of past climates. *J. Paleontol.* 12, 514–515.

- de Paula, S.M., Silveira, M., 2009. Studies on molluscan shells: Contributions from microscopic and analytical methods. *Micron* 40, 669–90.
- de Villiers, S., Shen, G.T., Nelson, B.K., 1994. The Sr/Ca-temperature relationship in coralline aragonite: Influence of variability in (Sr/Ca) seawater and skeletal growth parameters. *Geochim. Cosmochim. Acta* 58, 197–208.
- Deith, M.R., 1985. The composition of tidally deposited growth lines in the shell of the edible cockle, *Cerastoderma edule*. *J. Mar. Biol. Assoc. U. K.* 65, 573–581.
- Dettman, D.L., Reische, A.K., Lohmann, K.C., 1999. Controls on the stable isotope composition of seasonal growth bands in aragonitic fresh-water bivalves (unionidae). *Geochim. Cosmochim. Acta* 63, 1049–1057.
- Dietzel, M., Gussone, N., Eisenhauer, A., 2004. Co-precipitation of Sr<sup>2+</sup> and Ba<sup>2+</sup> with aragonite by membrane diffusion of CO<sub>2</sub> between 10 and 50 °C. *Chem. Geol.* 203, 139–151.
- Dodd, J.R., 1964. Environmentally controlled variation in the shell structure of a pelecypod species. *J. Paleontol.* 38, 1065–1071.
- Dodd, J.R., 1965. Environmental control of strontium and magnesium in *Mytilus*. *Geochim. Cosmochim. Acta* 29, 385–398.
- Eagle, R.A., Eiler, J.M., Tripathi, A.K., Ries, J.B., Freitas, P.S., Hiebenthal, C., Wanamaker Jr., A.D., Taviani, M., Elliott, M., Marensi, S., Nakamura, K., Ramirez, P., Roy, K., 2013. The influence of temperature and seawater carbonate saturation state on <sup>13</sup>C–<sup>18</sup>O bond ordering in bivalve mollusks. *Biogeosci.* 10, 4591–4606.
- Eiler, J.M., 2011. Paleoclimate reconstruction using carbonate clumped isotope thermometry. *Quat. Sci. Rev.* 30, 3575–3588.
- Epstein, S., Buchsbaum, R., Lowenstam, H.A., Urey, H.C., 1951. Carbonate-water isotopic temperature scale. *Geol. Soc. Am. Bull.* 62, 417–426.
- Epstein, S., Buchsbaum, R., Lowenstam, H.A., Urey, H.C., 1953. Revised carbonate-water isotopic temperature scale. *Geol. Soc. Am. Bull.* 64, 1315–1326.
- Esper, J., Cook, E.R., Schweingruber, F.H., 2002. Low-frequency signals in long tree-ring chronologies for reconstructing past temperature variability. *Science* 295, 2250–2253.
- Finnemore, A., Cunha, P., Shean, T., Vignolini, S., Guldin, S., Oyen, M., Steiner, U., 2012. Biomimetic layer-by-layer assembly of artificial nacre. *Nat. Commun.* 3, 966.
- Foster, L.C., Allison, N., Finch, A.A., Andersson, C., 2009. Strontium distribution in the shell of the aragonite bivalve *Arctica islandica*. *Geochem. Geophys. Geosyst.* 10, Q03003.
- Freitas, P.S., Clarke, L.J., Kennedy, H.A., Richardson, C.A., Abrantes, F., 2006. Environmental and biological controls on elemental (Mg/Ca, Sr/Ca and Mn/Ca) ratios in shells of the king scallop *Pecten maximus*. *Geochim. Cosmochim. Acta* 70, 5119–5133.

- Gaetani, G.A., Cohen, A.L., 2006. Element partitioning during precipitation of aragonite from seawater: A framework for understanding paleoproxies. *Geochim. Cosmochim. Acta* 70, 4617–4634.
- Ghosh, P., Adkins, J.F., Affek, H.P., Balta, B., Guo, W., Schauble, E., Schrag, D.P., Eiler, J.M., 2006.  $^{13}\text{C}$ – $^{18}\text{O}$  bonds in carbonate minerals: A new kind of paleothermometer. *Geochim. Cosmochim. Acta* 70, 1439–1456.
- Gillikin, D.P., Lorrain, A., Navez, J., Taylor, J.W., André, L., Keppens, E., Baeyens, W., Dehairs, F., 2005a. Strong biological controls on Sr/Ca ratios in aragonitic marine bivalve shells. *Geochem. Geophys. Geosyst.* 6, Q05009.
- Gillikin, D.P., De Ridder, F., Ulens, H., Elskens, M., Keppens, E., Baeyens, W., Dehairs, F., 2005b. Assessing the reproducibility and reliability of estuarine bivalve shells (*Saxidomus giganteus*) for sea surface temperature reconstruction: Implications for paleoclimate studies. *Palaeogeogr. Palaeoclimatol. Palaeoecol.* 228, 70–85.
- Goodkin, N.F., Hughen, K.A., Doney, S.C., Curry, W.B., 2008. Increased multidecadal variability of the North Atlantic Oscillation since 1781. *Nat. Geosci.* 1, 844–848.
- Grossman, E.L., Ku, T.-L., 1986. Oxygen and carbon isotope fractionation in biogenic aragonite: Temperature effects. *Chem. Geol. Isot. Geosci. Sect.* 59, 59–74.
- Guzman, N., Ball, A.D., Cuif, J.-P., Dauphin, Y., Denis, A., Ortlieb, L., 2007. Subdaily growth patterns and organo-mineral nanostructure of the growth layers in the calcitic prisms of the shell of *Concholepas concholepas* Bruguière, 1789 (Gastropoda, Muricidae). *Microsc. Microanal.* 13, 397–403.
- Hallam, A., Price, N.B., 1968. Environmental and biochemical control of strontium in shells of *Cardium edule*. *Geochim. Cosmochim. Acta* 32, 319–328.
- Hallmann, N., Burchell, M., Schöne, B.R., Irvine, G. V, Maxwell, D., 2009. High-resolution sclerochronological analysis of the bivalve mollusk *Saxidomus gigantea* from Alaska and British Columbia: techniques for revealing environmental archives and archaeological seasonality. *J. Archaeol. Sci.* 36, 2353–2364.
- Hallmann, N., Schöne, B.R., Irvine, G. V, Burchell, M., Cokelet, E.D., Hilton, M.R., 2011. An improved understanding of the Alaska Coastal Current: the application of a bivalve growth-temperature model to reconstruct freshwater-influenced paleoenvironments. *Palaios* 26, 346–363.
- Hathorne, E.C., Felis, T., Suzuki, A., Kawahata, H., Cabioch, G., 2013. Lithium in the aragonite skeletons of massive *Porites* corals: A new tool to reconstruct tropical sea surface temperatures. *Paleoceanography* 28, 143–152.

- Hellstrom, J., McCulloch, M., Stone, J., 1998. A detailed 31,000-year record of climate and vegetation change, from the isotope geochemistry of two New Zealand speleothems. *Quat. Res.* 178, 167–178.
- Holland, H.A., Schöne, B.R., Lipowski, C., Esper, J., 2014. Decadal climate variability of the North Sea during the last millennium reconstructed from bivalve shells (*Arctica islandica*). *The Holocene* 24, 771–786.
- Hudson, J.H., Shinn, E.A., Halley, R.B., Lidz, B., 1976. Sclerochronology: A tool for interpreting past environments. *Geology* 4, 361–364.
- IPCC, 2014. Summary for Policymakers. In: Field, C.B., Barros, V.R., Dokken, D.J., Mach, K.J., Mastrandrea, M.D., Bilir, T.E., Chatterjee, M., Ebi, K.L., Estrada, Y.O., Genova, R.C., Girma, B., Kissel, E.S., Levy, A.N., MacCracken, S., Mastrandrea, P.R., White, L.L., (Eds.), *Climate Change 2014: Impacts, Adaptation, and Vulnerability. Part A: Global and Sectoral Aspects. Contribution of Working Group II to the Fifth Assessment Report of the Intergovernmental Panel on Climate Change*. Cambridge University Press, Cambridge and New York (32 pp.).
- Ivany, L.C., Patterson, W.P., Lohmann, K.C., 2000. Cooler winters as a possible cause of mass extinctions at the Eocene/Oligocene boundary. *Nature* 407, 887–890.
- Jackson, A.P., Vincent, J.F.V., Turner, R. M., 1988. The mechanical design of nacre. *Proc. R. Soc. Lond. B, Biol. Sci.* 234, 415–440.
- Jacob, D.E., Wirth, R., Soldati, A.L., Wehrmeister, U., Schreiber, A., 2011. Amorphous calcium carbonate in the shells of adult *Unionoida*. *J. Struct. Biol.* 173, 241–249.
- Johnsen, S.J., Clausen, H.B., Dansgaard, W., Fuhrer, K., Gundestrup, N.S., Hammer, C.U., Iversen, P., Jouzel, J., Stauffer, B., Steffensen, J.P., 1992. Irregular glacial interstadials recorded in a new Greenland ice core. *Nature* 359, 311–313.
- Jones, D.S., 1983. Sclerochronology: reading the record of the molluscan shell. *Am. Sci.* 71, 384–391.
- Jones, D.S., Arthur, M.A., Allard, D.J., 1989. Sclerochronological records of temperature and growth from shells of *Mercenaria mercenaria* from Narragansett Bay, Rhode Island. *Mar. Biol.* 102, 225–234.
- Kennett, J.P., Ingram, B.L., 1995. A 20,000 year record of ocean circulation and climate-change from the Santa-Barbara basin. *Nature* 377, 510–514.
- Kennish, M.J., Olsson, R.K., 1975. Effects of thermal discharges on the microstructural growth of *Mercenaria mercenaria*. *Environ. Geol.* 1, 41–64.
- Kinsman, D.J.J., Holland, H.D., 1969. The co-precipitation of cations with  $\text{CaCO}_3$  – IV. The co-precipitation of  $\text{Sr}^{2+}$  with aragonite between 16° and 96 °C. *Geochim. Cosmochim. Acta* 33, 1–17.

- Kissel, C., Laj, C., Labeyrie, L., Dokken, T., Voelker, A., Blamart, D., 1999. Rapid climate variations during marine isotope stage 3: Magnetic analysis of sediments from Nordic Seas and Atlantic. *Earth Planet. Sci. Lett.* 171, 489–502.
- Klein, R.T., Lohmann, K.C., Thayer, C.W., 1996. Sr/Ca and  $^{13}\text{C}/^{12}\text{C}$  ratios in skeletal calcite of *Mytilus trossulus*: Covariation with metabolic rate, salinity, and carbon isotopic composition of seawater. *Geochim. Cosmochim. Acta* 60, 4207–4221.
- Lamy, F., Hebbeln, D., Wefer, G., 1999. High-resolution marine record of climatic change in mid-latitude Chile during the last 28,000 years based on terrigenous sediment parameters. *Quat. Res.* 51, 83–93.
- Lorrain, A., Gillikin, D.P., Paulet, Y.-M., Chauvaud, L., Le Mercier, A., Navez, J., André, L., 2005. Strong kinetic effects on Sr/Ca ratios in the calcitic bivalve *Pecten maximus*. *Geology* 33, 965–968.
- Lutz, R.A., 1984. Paleoecological implications of environmentally-controlled variation in molluscan shell microstructure. *Geobios Mémoires* 8, 93–97.
- MacClintock, C., 1967. Shell structure of patelloid and bellerophonoid gastropods (Mollusca). *Peabody Museum Nat. Hist. Yale Univ. Bull.* 22, 1–140.
- Mann, M.E., Zhang, Z., Hughes, M.K., Bradley, R.S., Miller, S.K., Rutherford, S., Ni, F., 2008. Proxy-based reconstructions of hemispheric and global surface temperature variations over the past two millennia. *Proc. Natl. Acad. Sci. U. S. A.* 105, 13252–13257.
- Marali, S., Schöne, B.R., 2015. Oceanographic control on shell growth of *Arctica islandica* (Bivalvia) in surface waters of Northeast Iceland – implications for paleoclimate reconstructions. *Palaeogeogr. Palaeoclimatol. Palaeoecol.* 420, 138–149.
- Marin, F., Le Roy, N., Marie, B., 2012. The formation and mineralization of mollusk shell. *Front. Biosci.* S4, 1099–1125.
- Martin, P.A., Lea, D.W., Rosenthal, Y., Shackleton, N.J., Sarnthein, M., Papenfuss, T., 2002. Quaternary deep sea temperature histories derived from benthic foraminiferal Mg/Ca. *Earth Planet. Sci. Lett.* 198, 193–209.
- McConnaughey, T.A., Gillikin, D.P., 2008. Carbon isotopes in mollusk shell carbonates. *Geo-Mar. Lett.* 28, 287–299.
- McKinney, C.R., McCrea, J.M., Epstein, S., Allen, H.A., Urey, H.C., 1950. Improvements in mass spectrometers for the measurement of small differences in isotope abundance ratios. *Rev. Sci. Instrum.* 21, 724–730.
- Mirkhalaf, M., Dastjerdi, A.K., Barthelat, F., 2014. Overcoming the brittleness of glass through bio-inspiration and micro-architecture. *Nat. Commun.* 5, 3166.

- Mitsuguchi, T., Matsumoto, E., Abe, O., Uchida, T., Isdale, P.J., 1996. Mg/Ca thermometry in coral skeletons. *Science* 274, 961–963.
- Montagna, P., McCulloch, M.T., Douville, E., López Correa, M., Trotter, J., Rodolfo-Metalpa, R., Dissard, D., Ferrier-Pagès, C., Frank, N., Freiwald, A., Goldstein, S., Mazzoli, C., Reynaud, S., Rüggeberg, A., Russo, S., Taviani, M., 2014. Li/Mg systematics in scleractinian corals: Calibration of the thermometer. *Geochim. Cosmochim. Acta* 132, 288–310.
- Moura, G., Vilarinho, L., Santos, A.C., Machado, J.P., 2000. Organic compounds in the extrapalial fluid and haemolymph of *Anodonta cygnea* (L.) with emphasis on the seasonal biomineralization process. *Comp. Biochem. Physiol. B* 125, 293–306.
- Nishida, K., Ishimura, T., Suzuki, A., Sasaki, T., 2012. Seasonal changes in the shell microstructure of the bloody clam, *Scapharca broughtonii* (Mollusca: Bivalvia: Arcidae). *Palaeogeogr. Palaeoclimatol. Palaeoecol.* 363–364, 99–108.
- Nudelman, F., Gotliv, B.A., Addadi, L., Weiner, S., 2006. Mollusk shell formation: mapping the distribution of organic matrix components underlying a single aragonitic tablet in nacre. *J. Struct. Biol.* 153, 176–187.
- Nürnberg, D., Bijma, J., Hemleben, C., 1996. Assessing the reliability of magnesium in foraminiferal calcite as a proxy for water mass temperatures. *Geochim. Cosmochim. Acta* 60, 803–814.
- Ohno, T., 1985. Experimentelle Analysen zur Rhythmik des Schalenwachstums einiger Bivalven und ihre palaeobiologische Bedeutung. *Palaeontogr. A* 189, 63–123.
- Olson, I.C., Kozdon, R., Valley, J.W., Gilbert, P.U.P.A., 2012. Mollusk shell nacre ultrastructure correlates with environmental temperature and pressure. *J. Am. Chem. Soc.* 134, 7351–7358.
- Oomori, T., Kaneshima, H., Maezato, Y., Kitano, Y., 1987. Distribution coefficient of Mg<sup>2+</sup> ions between calcite and solution at 10–50 °C. *Mar. Chem.* 20, 327–336.
- Patterson, W.P., 1999. Oldest isotopically characterized fish otoliths provide insight to Jurassic continental climate of Europe. *Geology* 27, 199–202.
- Petit, R.J., Raynaud, D., Basile, I., Chappellaz, J., Ritz, C., Delmotte, M., Legrand, M., Lorius, C., Pe, L., 1999. Climate and atmospheric history of the past 420,000 years from the Vostok ice core, Antarctica. *Nature* 399, 429–413.
- Planchon, F., Poulain, C., Langlet, D., Paulet, Y.-M., André, L., 2013. Mg-isotopic fractionation in the manila clam (*Ruditapes philippinarum*): New insights into Mg incorporation pathway and calcification process of bivalves. *Geochim. Cosmochim. Acta* 121, 374–397.
- Pokroy, B., Fitch, A.N., Marin, F., Kapon, M., Adir, N., Zolotoyabko, E., 2006. Anisotropic lattice distortions in biogenic calcite induced by intra-crystalline organic molecules. *J. Struct. Biol.* 155, 96–103.

- Raddatz, J., Liebetrau, V., Rüggeberg, A., Hathorne, E.C., Krabbenhöft, A., Eisenhauer, A., Böhm, F., Vollstaedt, H., Fietzke, J., López Correa, M., Freiwald, A., Dullo, W.C., 2013. Stable Sr-isotope, Sr/Ca, Mg/Ca, Li/Ca and Mg/Li ratios in the scleractinian cold-water coral *Lophelia pertusa*. *Chem. Geol.* 352, 143–152.
- Rhoads, D.C., Lutz, R.A. (Eds.), 1980. Skeletal growth of aquatic organisms. Biological records of environmental change. Plenum Press, New York and London (750 pp.).
- Richardson, C.A., Crisp, D.J., Runham, N.W., 1979. Tidally deposited growth bands in the shell of the common cockle, *Cerastoderma edule* (L.). *Malacologia* 18, 277–290.
- Richardson, C.A., Peharda, M., Kennedy, H.A., Kennedy, P., Onofri, V., 2004. Age, growth rate and season of recruitment of *Pinna nobilis* (L) in the Croatian Adriatic determined from Mg:Ca and Sr:Ca shell profiles. *J. Exp. Mar. Bio. Ecol.* 299, 1–16.
- Rodland, D.L., Schöne, B.R., Helama, S.O., Nielsen, J.K., Baier, S., 2006. A clockwork mollusc: Ultradian rhythms in bivalve activity revealed by digital photography. *J. Exp. Mar. Bio. Ecol.* 334, 316–323.
- Roig, F.A., Le-Quesne, C., Boninsegna, J.A., Briffa, K.R., Lara, A., Grudd, H., Jones, P.D., Villagrán, C., 2001. Climate variability 50,000 years ago in mid-latitude Chile as reconstructed from tree rings. *Nature* 410, 567–570.
- Rosenthal, Y., Boyle, E.A., Slowey, N., 1997. Temperature control on the incorporation of magnesium, strontium, fluorine, and cadmium into benthic foraminiferal shells from Little Bahama Bank: Prospects for thermocline paleoceanography. *Geochim. Cosmochim. Acta* 61, 3633–3643.
- Rousseau, M., Meibom, A., Gèze, M., Bourrat, X., Angellier, M., Lopez, E., 2009. Dynamics of sheet nacre formation in bivalves. *J. Struct. Biol.* 165, 190–195.
- Scholz, D., Frisia, S., Borsato, A., Spötl, C., Fohlmeister, J., Mudelsee, M., Miorandi, R., Mangini, A., 2012. Holocene climate variability in north-eastern Italy: Potential influence of the NAO and solar activity recorded by speleothem data. *Clim. Past* 8, 1367–1383.
- Schöne, B.R., 2003. A “clam-ring” master-chronology constructed from a short-lived bivalve mollusc from the northern Gulf of California, USA. *The Holocene* 1, 39–49.
- Schöne, B.R., Fiebig, J., Pfeiffer, M., Gleß, R., 2005a. Climate records from a bivalved *Methuselah* (*Arctica islandica*, Mollusca; Iceland). *Palaeogeogr. Palaeoclimatol. Palaeoecol.* 228, 130–148.
- Schöne, B.R., Houk, S.D., Freyre Castro, A.D., Fiebig, J., Oschmann, W., Kroncke, I., Dreyer, W., Gosselck, F., 2005b. Daily growth rates in shells of *Arctica islandica*: Assessing sub-seasonal environmental controls on a long-lived bivalve mollusk. *Palaios* 20, 78–92.

- Schöne, B.R., Rodland, D.L., Wehrmann, A., Heidel, B., Oschmann, W., Zhang, Z., Fiebig, J., Beck, L., 2007. Combined sclerochronologic and oxygen isotope analysis of gastropod shells (*Gibbula cineraria*, North Sea): life-history traits and utility as a high-resolution environmental archive for kelp forests. *Mar. Biol.* 150, 1237–1252.
- Schöne, B.R., 2008. The curse of physiology - challenges and opportunities in the interpretation of geochemical data from mollusk shells. *Geo-Mar. Lett.* 28, 269–285.
- Schöne, B.R., Zhang, Z., Jacob, D., Gillikin, D.P., Tütken, T., Garbe-Schönberg, D., McConnaughey, T., Soldati, A., 2010. Effect of organic matrices on the determination of the trace element chemistry (Mg, Sr, Mg/Ca, Sr/Ca) of aragonitic bivalve shells (*Arctica islandica*) – comparison of ICP-OES and LA-ICP-MS data. *Geochem. J.* 44, 23–37.
- Schöne, B.R., Zhang, Z., Radermacher, P., Thébault, J., Jacob, D.E., Nunn, E.V., Maurer, A.-F., 2011. Sr/Ca and Mg/Ca ratios of ontogenetically old, long-lived bivalve shells (*Arctica islandica*) and their function as paleotemperature proxies. *Palaeogeogr. Palaeoclimatol. Palaeoecol.* 302, 52–64.
- Schöne, B.R., Radermacher, P., Zhang, Z., Jacob, D.E., 2013. Crystal fabrics and element impurities (Sr/Ca, Mg/Ca, and Ba/Ca) in shells of *Arctica islandica* - Implications for paleoclimate reconstructions. *Palaeogeogr. Palaeoclimatol. Palaeoecol.* 373, 50–59.
- Shimamoto, M., 1986. Shell microstructure of Veneridae (Bivalvia) and its phylogenetic implications. *Tohoku Univ., Sci. Rep., 2<sup>nd</sup> ser.* 56, 1–39.
- Shirai, K., Schöne, B.R., Miyaji, T., Radermacher, P., Krause, R., Tanabe, K., 2014. Assessment of the mechanism of elemental incorporation into bivalve shells (*Arctica islandica*) based on elemental distribution at the microstructural scale. *Geochim. Cosmochim. Acta* 126, 307–320.
- Sirocko, F., Dietrich, S., Veres, D., Grootes, P.M., Schaber-Mohr, K., Seelos, K., Nadeau, M.J., Kromer, B., Rothacker, L., Röhner, M., Krbetschek, M., Appleby, P., Hambach, U., Rolf, C., Sudo, M., Grim, S., 2013. Multi-proxy dating of Holocene maar lakes and Pleistocene dry maar sediments in the Eifel, Germany. *Quat. Sci. Rev.* 62, 56–76.
- Soniat, T.M., Hofmann, E.E., Klinck, J.M., Powell, E.N., 2009. Differential modulation of eastern oyster (*Crassostrea virginica*) disease parasites by the El-Niño-Southern Oscillation and the North Atlantic Oscillation. *Int. J. Earth Sci.* 98, 99–114.
- Swan, E.F., 1956. The meaning of strontium-calcium ratios. *Deep-Sea Res.* 4, 71.
- Takesue, R.K., van Geen, A., 2004. Mg/Ca, Sr/Ca, and stable isotopes in modern and Holocene *Protothaca staminea* shells from a northern California coastal upwelling region. *Geochim. Cosmochim. Acta* 68, 3845–3861.



- Tan Tiu, A., 1988. Temporal and spatial variation of shell microstructure of *Polymesoda carolinia* (Bivalvia: Heterodonta). *Am. Malacol. Bull.* 6, 199–206.
- Thébault, J., Schöne, B.R., Hallmann, N., Barth, M., Nunn, E.V., 2009. Investigation of Li/Ca variations in aragonitic shells of the ocean quahog *Arctica islandica*, northeast Iceland. *Geochem. Geophys. Geosyst.* 10, Q12008.
- Thébault, J., Chauvaud, L., 2013. Li/Ca enrichments in great scallop shells (*Pecten maximus*) and their relationship with phytoplankton blooms. *Palaeogeogr. Palaeoclimatol. Palaeoecol.* 373, 108–122.
- Toland, H., Perkins, B., Pearce, N.J.G., Keenan, F., Leng, M.J., 2000. A study of sclerochronology by laser ablation ICP-MS. *J. Anal. At. Spectrom.* 15, 1143–1148.
- Urey, H.C., 1951. Measurement of paleotemperatures and temperatures of the Upper Cretaceous of England, Denmark, and the southeastern United States. *Geol. Soc. Am. Bull.* 62, 399–416.
- Vander Putten, E., Dehairs, F., Keppens, E., Baeyens, W., 2000. High resolution distribution of trace elements in the calcite shell layer of modern *Mytilus edulis*: Environmental and biological controls. *Geochim. Cosmochim. Acta* 64, 997–1011.
- Vanhove, D., Stassen, P., Speijer, R.P., Steurbaut, E., 2011. Assessing paleotemperature and seasonality during the early Eocene climatic optimum (EECO) in the Belgian Basin by means of fish otolith stable O and C isotopes. *Geol. Belgica* 14, 143–158.
- Vollweiler, N., Scholz, D., Mühlinghaus, C., Mangini, A., Spötl, C., 2006. A precisely dated climate record for the last 9 kyr from three high alpine stalagmites, Spannagel Cave, Austria. *Geophys. Res. Lett.* 33, 1–5.
- Wada, K., Fujinuki, T., 1976. Biomineralization in bivalve molluscs with emphasis on the chemical composition of the extrapallial fluid. In: Bryan, N.M., Wilbur, K.M. (Eds.), *Mechanisms of Mineralization in the Invertebrates and Plants*. University of South Carolina Press, Georgetown, pp. 175–190.
- Walliser, E.O., Schöne, B.R., Tütken, T., Zirkel, J., Grimm, K.I., Pross, J., 2015. The bivalve *Glycymeris planicostalis* as a high-resolution paleoclimate archive for the Rupelian (Early Oligocene) of central Europe. *Clim. Past* 11, 653–668.
- Wanamaker Jr., A.D., Kreutz, K.J., Wilson, T., Borns, H.W., Introne, D.S., Feindel, S., 2008. Experimentally determined Mg/Ca and Sr/Ca ratios in juvenile bivalve calcite for *Mytilus edulis*: implications for paleotemperature reconstructions. *Geo-Mar. Lett.* 28, 359–368.
- Weber, E., Pokroy, B., 2015. Intracrystalline inclusions within single crystalline hosts: from biomineralization to bio-inspired crystal growth. *CrystEngComm* 17, 5873–5883.
- Wilbur, K.M., Saleuddin, A.S.M., 1983. Shell formation. In: Saleuddin, A.S.M., Wilbur, K.M. (Eds.), *The Mollusca*. Vol. 4. Physiology, Part 1. Academic Press, Toronto, pp. 235–287.

- Witbaard, R., Duineveld, G.C.A., De Wilde, P.A.W.J., 1997. A long-term growth record derived from *Arctica Islandica* (Mollusca, Bivalvia) from the Fladen Ground (northern North Sea). *J. Mar. Biol. Assoc. U. K.* 77, 801–816.
- Yan, H., Shao, D., Wang, Y., Sun, L., 2013. Sr/Ca profile of long-lived *Tridacna gigas* bivalves from South China Sea: A new high-resolution SST proxy. *Geochim. Cosmochim. Acta* 112, 52–65.
- Zachos, J.C., Pagani, M., Sloan, L., Thomas, E., Billups, K., 2001. Trends, rhythms, and aberrations in global climate 65 Ma to Present. *Science* 292, 686–693.
- Zhang, G., Xu, J., 2013. From colloidal nanoparticles to a single crystal: New insights into the formation of nacre's aragonite tablets. *J. Struct. Biol.* 182, 36–43.
- Zhao, L., Schöne, B.R., Mertz-Kraus, R., 2016. Controls on strontium and barium incorporation into freshwater bivalve shells (*Corbicula fluminea*). *Palaeogeogr. Palaeoclimatol. Palaeoecol.* (article in press).





# **Chapter 2**

---

# **Manuscripts**

# Manuscript I

## Microstructures in shells of the freshwater gastropod *Viviparus viviparus*: A potential sensor for temperature change?

Published in Acta Biomaterialia

Christoph S. Füllenbach<sup>1</sup>, Bernd R. Schöne<sup>1</sup>, Robert Branscheid<sup>2</sup>

<sup>1</sup>Institute of Geosciences, University of Mainz,  
Johann-Joachim-Becher-Weg 21, 55128 Mainz, Germany

<sup>2</sup>Institut of Micro- and Nanostructure Research, University of Erlangen,  
Cauerstraße 6, 91058 Erlangen, Germany

### Authors contribution

Concept: CSF, BRS

Execution: CSF

Analyses: Growth patterns: CSF; SEM: RB, CSF, BRS

Data analysis: CSF

Writing: CSF, BRS, RB

Füllenbach, C.S., Schöne, B.R., Branscheid, R., 2014. Microstructures in shells of the freshwater gastropod *Viviparus viviparus*: A potential sensor for temperature change? Acta Biomater. 10, 3911–3921.

## Abstract

Mollusk shells contain a plethora of information on past climate variability. However, only a limited toolkit is currently available to reconstruct such data from the shells. The environmental data of some proxies (e.g., Sr/Ca ratios) is obscured by physiological effects, whereas other proxies such as  $\delta^{18}\text{O}$  simultaneously provide information on two or more different environmental variables. The present study investigates if microstructures of the freshwater gastropod, *Viviparus viviparus* provide an alternative means to reconstruct past water temperature. Cold and highly variable temperature regimes resulted in the precipitation of highly unordered 1<sup>st</sup>-order lamellae of simple crossed-lamellar structures if new shell formed from scratch. However, during stable and warm conditions, well-ordered 1<sup>st</sup>-order lamellae were laid down irrespective of pre-existing shell material. Homogeneous 1<sup>st</sup>-order lamellae also formed during times of cold and highly variable temperatures if the new shell was deposited onto existing shell material with well-ordered 1<sup>st</sup>-order lamellae. The growth front seems to contain instructions for building specific microstructure variants irrespective of environmental conditions. However, if this template is missing, the animal forms a deviating microstructure. Under extremely stressful situations (e.g., removal from habitat, calcein staining, extreme temperature shifts), the gastropod precipitates evolutionarily older microstructure (irregular simple prisms) rather than simple crossed-lamellar structures. These shell portions were macroscopically described as disturbance lines. In addition, repetitive, presumably periodic growth patterns were observed which consisted of gradually changing 3<sup>rd</sup>-order lamellae between consecutive faint, organic-rich growth lines. These growth patterns were likely controlled by intrinsic biological clocks and exhibited a two-daily periodicity. Results of our study may provide the basis for using changes of the microstructure of shell sections as a new sensor (environmental proxy) for past water temperature.

Keywords: Gastropod shell; Microstructure; Crossed-lamellar; Environmental influence; Sclerochronology

## 1 Introduction

Mollusk shells are becoming increasingly recognized as powerful tools for paleoclimate reconstructions (Jones, 1983; Wanamaker et al., 2008; Schöne and Gillikin, 2013). During growth, ambient environmental conditions are recorded in the shells in the form of variable geochemical properties (Dettman et al., 1999; Schöne et al., 2005a) and variable growth rates (Witbaard et al., 1997; Butler et al., 2013). Since mollusk shell formation occurs periodically (tidal cycles, diurnally, annually etc.), environmental proxy data can be precisely temporally aligned. Such data are essential to validate and optimize numerical climate models and identify forcing mechanisms operating within the Earth system (e.g., Delworth and Mann, 2000).

However, it still remains extremely challenging to obtain quantifiable environmental data, specifically paleotemperature from mollusk shells. The only well accepted proxy for temperature in mollusks,  $\delta^{18}\text{O}_{\text{shell}}$ , is a dual proxy that simultaneously records temperature and the oxygen isotope signature of the ambient water ( $\delta^{18}\text{O}_{\text{water}}$ ). To reconstruct past water temperature from  $\delta^{18}\text{O}_{\text{shell}}$  values,  $\delta^{18}\text{O}_{\text{water}}$  (or salinity) must be known which is rarely available for ancient environments. Attempts have been made to infer water temperature from other physicochemical properties such as Mg/Ca and Sr/Ca ratios (Klein et al., 1996; Wanamaker et al., 2008),  $\Delta_{47}$  values (Gosh et al., 2006),  $\delta^{44/40}\text{Ca}$  values (Immenhauser et al., 2005) and growth patterns (Kennish and Olsson, 1975; Schöne et al., 2002; Hallmann et al., 2011). However, vital effects typically result in a strong biologically filtering of the temperature signal in these proxies (Schöne, 2008). For example, Sr/Ca and Mg/Ca values of mollusk shells remain far below that of the ambient water, and their relative changes are not always linked to temperature shifts (Lazareth et al., 2007; Freitas et al., 2008; Foster et al., 2009; Schöne et al., 2011). The sensitivity of the  $\Delta_{47}$  clumped isotope thermometer is much lower (Eagle et al., 2013) than previously assumed (Gosh et al., 2006) and requires large amounts of sample material which precludes high-resolution analyses (between 4 and 14 mg of carbonate powder (Came et al., 2007; Eiler, 2007; Affek et al., 2008; Wacker et al., 2013). Temperature uncertainties for an assumed  $\Delta_{47}$  precision error of 0.05 ‰ would be on the order of  $\pm 1.4$  °C (Eagle et al., 2013). Furthermore, variations in shell growth rate are controlled by multiple different environmental and physiological parameters, which make it rather difficult to extract information specifically on temperature (Schöne, 2008). In conclusion, no proxy is currently available to reconstruct water temperature quantitatively and reliably from mollusk shells.

Interestingly, microstructures of mollusk shells (Bøggild, 1930; Taylor and Kennedy, 1969; Kobayashi, 1969) have attracted little attention as potential recorders



of environmental change (e.g., Dodd, 1964; Lutz, 1984; Stemmer et al., 2013). Instead, they have largely been used for phylogenetic reconstructions (e.g., Carter and Clark, 1985; MacClintock, 1967) and inspired the design of novel biomimetic materials (e.g., Finnemore et al., 2012). The term ‘microstructure’ combines information on crystallographic textures and morphological appearances of shells on the  $\mu\text{m}$ -scale (Chateigner et al., 2000). We here focus strictly on the morphological arrangement of crystals / assemblage of crystals, which is characterized by the combined visual appearance of their size, shape and orientation (as seen under the SEM). Since the formation of biominerals is controlled by physiological processes in epithelial cells of the outer mantle, it is not unlikely that environmental conditions influence the biomineralization process and, in turn, can be reconstructed from the product of this formation, the microstructure. In fact, temperature seems to modify microstructures in bivalves (Dodd, 1964; Lutz, 1984; Tan Tiu, 1988; Nishida et al., 2012).

The present authors studied the effect of temperature changes on the microstructure of shells from cultured freshwater gastropods, *Viviparus viviparus* (Linnaeus, 1758). Specifically, we analyzed if and how cold and strongly varying temperatures as well as more stable, warm regimes influence the shell architecture at the  $\mu\text{m}$ -scale. Results of this study can pave the way to develop new techniques for more precise paleotemperature estimates from mollusk shells.

## 2 Material and methods

The freshwater gastropod, *Viviparus viviparus* forms a fully aragonitic shell (tested by Raman spectroscopy). Specimens (Fig. 1A) were grown in a tank (180 L) with a 5 cm-thick loess substrate. All three specimens were cultured from the larval stage on and had a maximum age of 6 month at the beginning of the experiment that was conducted in November and December 2010. Specimens were exposed to simulated 12:12 light/dark cycles and fed every third day with fine ground fish food (‘Tetra Pond Sterlet Sticks’). To study the potential effect of changing water temperature on shell microstructure, the observational period was partitioned into three two-weekly intervals with different temperature regimes (Fig. 2B). During the first interval, water temperature was kept constantly warm ( $21.2\text{ }^{\circ}\text{C} \pm 0.4\text{ }^{\circ}\text{C}$ ). During the subsequent interval, water temperature was more variable and, on average, ca.  $4\text{ }^{\circ}\text{C}$  colder (interval II:  $17.1\text{ }^{\circ}\text{C} \pm 2.6\text{ }^{\circ}\text{C}$ ). Interval III was characterized by a ca.  $10\text{ }^{\circ}\text{C}$  temperature shift ( $11\text{ }^{\circ}\text{C}$  to  $21\text{ }^{\circ}\text{C}$ ; on average  $16\text{ }^{\circ}\text{C} \pm 7\text{ }^{\circ}\text{C}$ ).

For a later temporal alignment of shell growth and comparison with ambient environmental conditions, shells were labeled with a fluorescent marker at the beginning of each interval. For this purpose, specimens were immersed in a solution of calcein (100 mg/L) for three hours followed by cleaning under tap water. Calcein becomes incorporated into the shell during biomineralization (Kaehler and McQuaid, 1999; Moran, 2000) and fluoresces under blue light.

At the end of the experiment, all specimens were sacrificed by physical removal of the operculum and the soft tissues. Shells were ultrasonically cleaned and embedded in JB KWIK Weld epoxy resin. Using a low-speed saw (Buehler Isomet 1000; 225 rpm), shell thick-sections were cut from the youngest whorl along the axis of maximum growth. Two millimeter-thick shell slabs were mounted on glass slides, ground on glass plates (800, 1200 grit SiC powder) and polished on a Buehler G-cloth using 1  $\mu\text{m}$   $\text{Al}_2\text{O}_3$  powder.

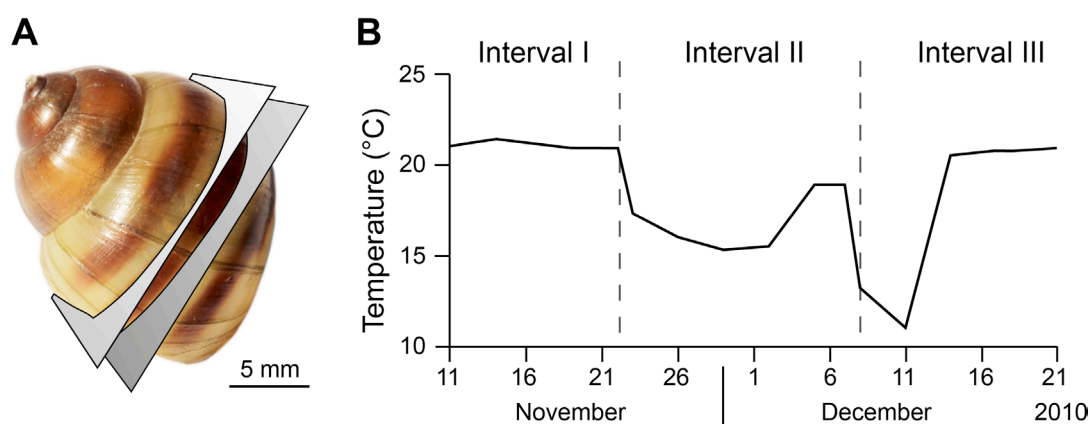


**Fig. 1.** (A) The shell of *Viviparus viviparus*. Sketch showing the position where a 2-mm-thick shell section was cut from the youngest whorl. (B) Temperature during the experimental period. During the first 2-weekly interval, the temperature remained warm and stable. During intervals II and III, the temperature was lower and more variable.

## 2.1 Fluorescence microscopy

Samples were studied using a Zeiss Axiolmager.A1m microscope connected to a Zeiss HBO100 mercury lamp. When a Zeiss Filter Set 38 (Excitation wavelength: ~450-500 nm; Emission wavelength: ~500 – 550 nm) was added to the optical path, fluorochrome marks appeared as distinct, green lines (Fig. 2A). Distances measured between consecutive calcein lines were used to quantify the increase in shell thickness during each two-weekly interval (Fig. 2A). Increase in shell length was assessed by measuring the distance between the previous and the new shell margin (Fig. 2A).

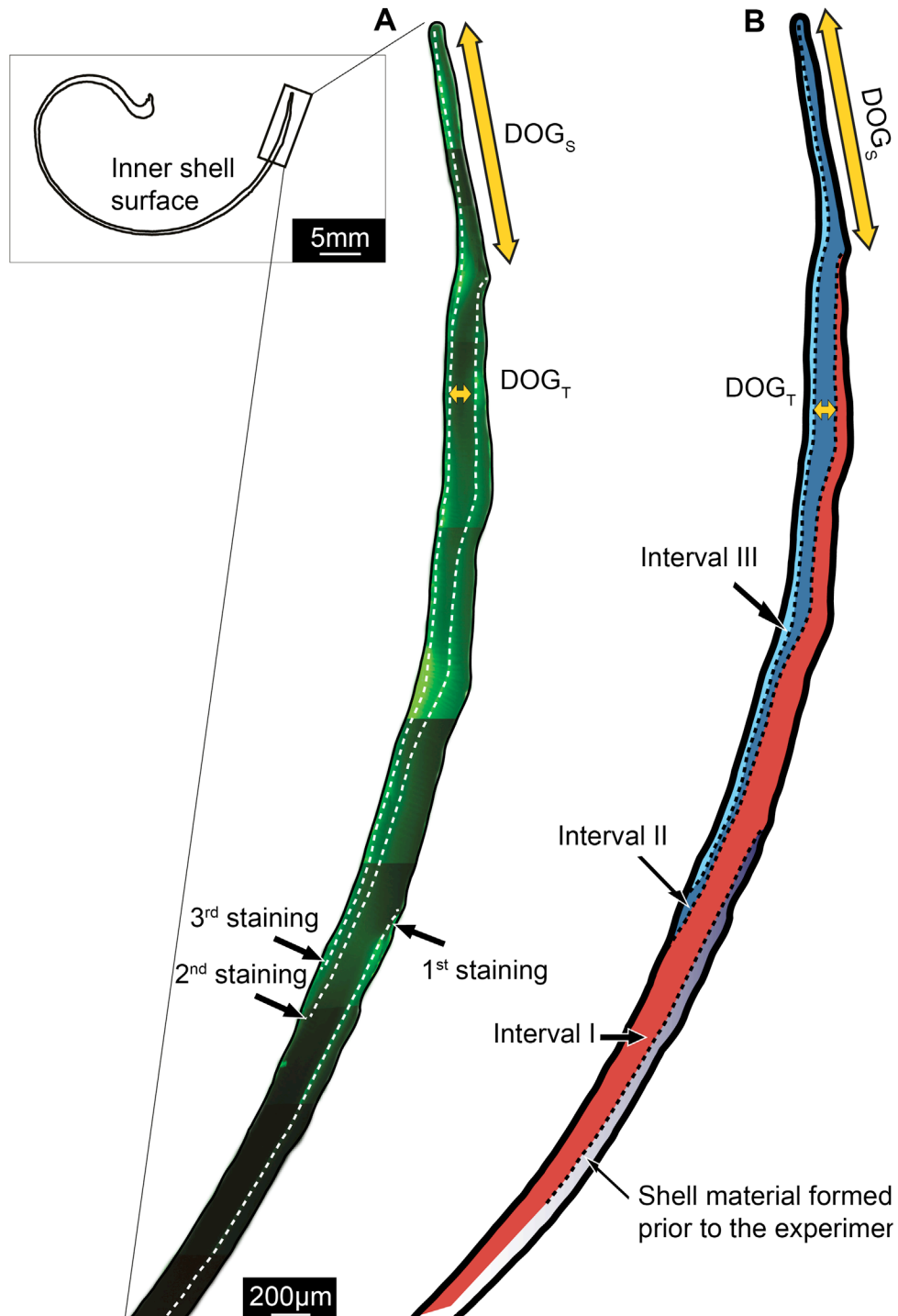


**Fig. 2.** Shell growth near the aperture of *Viviparus viviparus* under experimental conditions. (A) Fluorescence microscopy image showing the most recently formed shell portion. White, dashed lines indicate positions of calcein marks. Shells were labeled with this fluorochrome every 14 days, i.e. before each of the three 2-weekly experimental time intervals. Short and long yellow arrows indicate shell material added in thickness and length (size), respectively, during interval II. (B) Schematic illustration of the shell portions laid down during each of the three experimental time intervals. DOG = direction of growth;  $DOG_S$  = growth in size;  $DOG_T$  = growth in shell thickness.

## 2.2 Scanning electron microscopy

Examination for changing microstructures was focused on polished shell sections that were analyzed without any further sample treatment using a FEI NanoSEM 630 (Department of Nanobiotechnology; University of Mainz). Electron accelerating voltage applied to the Schottky-FEG was set to 4.5 keV and the working distance was fixed to 4.5 mm. In addition, lightly etched shell sections were analyzed (specific etching techniques are given in figure captions).

## 2.3 Image processing

The free image processing software ImageJ (<http://rsbweb.nih.gov/ij/>; last checked on 29<sup>th</sup> Jan. 2016) was used to quantify small-scale variations of microstructures. For this purpose, we used SEM images of shell sections that revealed cross-sections approximately perpendicular to the longitudinal axes (l-axis) of the objects of interest on the 100 nm scale (so-called 3<sup>rd</sup>-order lamellae, see section 3.4 and 4.2). A change in the orientation of the section has a dramatic effect on the generated data. Therefore, a proper sample orientation is essential. For automatic image analysis, images were re-sharpened and converted to black / white using a threshold of 65 (gray-scale value). False pixels were manually corrected. Subsequently, surface area, elongation of shape and orientation of cross-sections were measured automatically. See on-line supplementary material (Fig. S1) for more details.

# 3 Results

## 3.1 Growth rates under experimental conditions

Calcein staining produced distinct ~3.5 mm long fluorescent lines (Fig. 2A) running subparallel to the inner shell surface of *V. viviparus*. These lines were used to quantify the increase in shell thickness and size during each of the three two-weekly intervals. As illustrated in Figure 2B, the CaCO<sub>3</sub> production declined with decreasing water temperature and increasing temperature variability (Table 1). Fastest growth occurred during constantly warm conditions (interval I; Fig. 2B). During lower and unstable temperatures (interval II), however, much less CaCO<sub>3</sub> was added to the shell (Fig. 2B). When temperature shifts were particularly large (10 °C during interval III), shell elongation ceased completely and only little shell thickening was observed (Fig. 2B).

**Table 1** Shell growth of *Viviparus viviparus* in thickness, size and area during each of the three experimental intervals

	Thickness [ $\mu\text{m}$ ]	Size [ $\mu\text{m}$ ]	Area [ $\text{mm}^2$ ]
Interval I	160	3200	0.68
Interval II	130	1300	0.33
Interval III	50	0	0.19

### 3.2 Shell microstructure

Shells of *V. viviparus* showed three different microstructures, namely simple crossed-lamellar (= XLM), irregular simple prismatic (= ISP) and a third structure consisting of elongated crystals (= ECL)<sup>1</sup>. The majority of the examined shell sections consisted of XLM structure exhibiting the typical hierarchy of 1<sup>st</sup>-, 2<sup>nd</sup>- and 3<sup>rd</sup>-order lamellae (Fig. 3).

First-order lamellae were arranged in a fence-like manner with light and dark planks, orientated with their maximum elongation approximately perpendicular to the outer and inner shell surfaces (Fig. 3A). These lamellae measured between 1 and 23  $\mu\text{m}$  in width. At higher magnification (10,000 X), 2<sup>nd</sup>-order lamellae became visible which were arranged in a card deck style (Fig. 3B). On average, the height (h-axis) of 2<sup>nd</sup>-order lamellae (i.e., ‘card height’) measured 63 nm. Within the same 1<sup>st</sup>-order lamella, all 2<sup>nd</sup>-order lamellae were dipping in approximately the same direction either toward the inner or outer shell surfaces (average inclination of ca. 45° relative to the outer or inner shell surface, respectively). The dipping direction of 2<sup>nd</sup>-order lamellae l-axes (i.e., ‘card length’; length axis) alternated regularly between adjacent 1<sup>st</sup>-order lamellae resulting in a light or dark appearance (Fig. 3A). Third-order lamellae (Fig. 3B) split the 2<sup>nd</sup>-order units parallel to their l-axis into laths with an average width (w-axis) of 255 nm (Fig. 4). Thus, 2<sup>nd</sup>-order lamellae can be described as a layer of converged 3<sup>rd</sup>-order lamellae. The assignment of length, width- and height-axes to the 2<sup>nd</sup>- / 3<sup>rd</sup>-order lamellae is illustrated in Figure 3B. In addition, a three-dimensional model of the overall arrangement of the simple crossed-lamellar microstructure in *V. viviparus* is shown in Figure 4.

Minor proportions of the shells were made of elongated crystals (ECL) and ISP. For example, the inner shell surface of the youngest whorl was covered by a layer of elongated crystals (Figs. 3C+D) orientated perpendicular to the inner shell

<sup>1</sup> ECL = Elongated crystal layer. A possible subdivision into smaller subunits of the crystals assembling this layer could not be experimentally verified with the methods applied. None of the known microstructural types could be assigned to these structures with certainty.

surface. The thickness of the layer measured ca.  $2.5\ \mu\text{m}$  throughout the studied shell section. The transition between the ECL and XLM was abrupt (Figs. 3C+D). ISP, the third microstructural type occurred in distinct growth lines disrupting the XLM structure (Figs. 3C+E). Shell material formed prior to the experiment exhibited all three microstructural types, with ECL being present in some, but not all analyzed samples (see on-line supplementary material, Fig. S2).

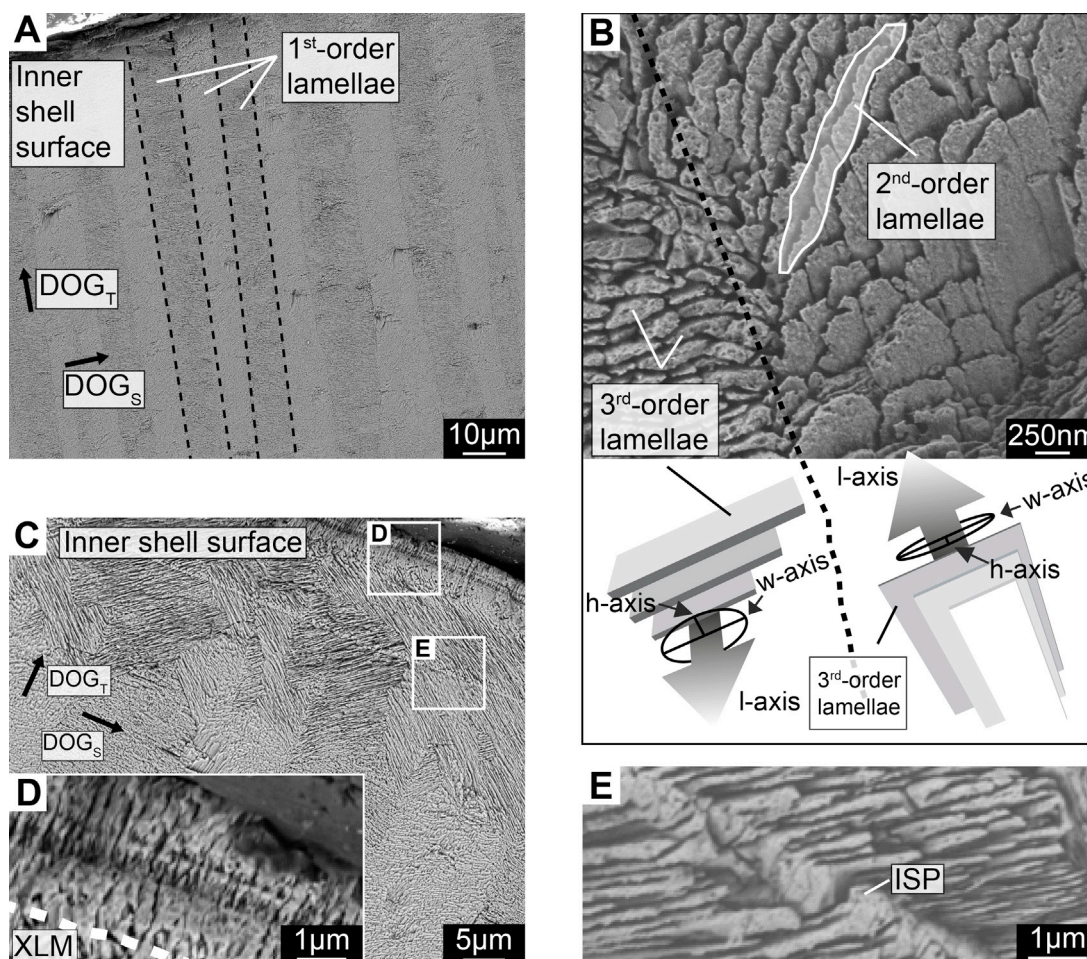


**Fig. 3.** SEM images of the microstructures in shells of *Viviparus viviparus*. (A) First-order lamellae of XLM structure; alternating light and dark planks result from different dipping angles of higher-order lamellae highlighted in (B). (B) Lamellae of second order (white highlighted area) subdividing 1<sup>st</sup>-order lamellae. Black dotted line highlights the boundary between adjacent 1<sup>st</sup>-order lamellae. Note the different dipping directions of 2<sup>nd</sup>-order lamellae in adjacent 1<sup>st</sup>-order lamellae. Third-order lamellae with a rod/lath-like appearance subdivide 2<sup>nd</sup>-order lamellae. Orientation of length, width and height axes of second-/third-order lamellae in respective image sections are illustrated below. (C) Shell portion near the inner shell surface. (D) Layer of elongated crystals (thickness  $\sim 2.5\ \mu\text{m}$ ) covering the inner shell surface. Orientation of the crystals is approximately perpendicular to the inner shell surface. (E) Layer of irregular simple prisms (thickness  $0.3\ \mu\text{m}$ ) running subparallel to the inner shell surface.  $\text{DOG}_s$  = growth in size;  $\text{DOG}_T$  = growth in shell thickness.

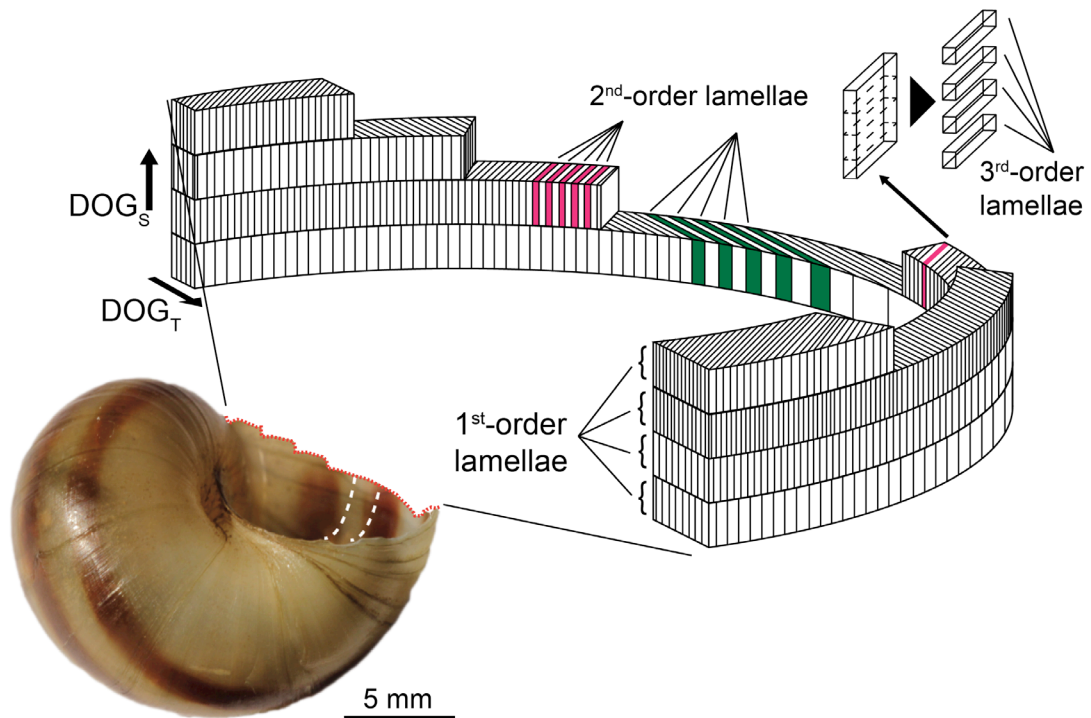


**Fig. 4.** Shell architecture (XLM structure) of *V. viviparus* close to the aperture.  $DOG_S$  = growth in size;  $DOG_T$  = growth in shell thickness.

### 3.3 Growth lines and XLM 3<sup>rd</sup>-order lamellae

The simple crossed-lamellar structures were disrupted by growth lines running subparallel to the inner shell surface and thus nearly perpendicularly to the maximal extension of the 1<sup>st</sup>-order lamellae (Fig. 5). Two types of growth lines were distinguishable:

1. Type-1 lines consisted of an approximately 5 nm dark layer and were best viewed in shell portions formed during interval II (Figs. 5A+B, 6). In such two-weekly intervals, we counted up to seven lines. Identification of type-1 lines was greatly facilitated by distinct and repetitive changes of the surface area, the shape (width-to-height ratio) and the orientation of cross-sections perpendicular to the l-axes of 3<sup>rd</sup>-order lamellae between two consecutive type-1 lines (Fig. 6). From one to the next type-1 line (see Figs. 6A-D), the surface area of the cross-sections decreased from  $\sim 45 \text{ nm}^2$  to  $\sim 27 \text{ nm}^2$  (Figs. 6E+H, I), whereas their shape became increasingly elongated and elliptically shaped (Figs. 6F+H, I). At the same time, the 3<sup>rd</sup>-order lamellae rotated counter-clockwise along their l-axes by ca.  $30^\circ$ , resulting in an almost parallel orientation of the flattened 3<sup>rd</sup>-order lamellae and the following type-1 growth line (Figs. 6G+H, I). Type-1 growth increment widths (= distance between consecutive type-1 growth lines) measured, on average,  $10 \mu\text{m}$  (broadest increment:  $\sim 60 \mu\text{m}$ ). Repetitively formed type-1 growth lines were also observed

- in shell portions formed prior to the experiment, but could not be assigned to specific time periods due to missing time markers (see supplementary Fig. S2A).
- Type-2 lines were much broader than type-1 lines and measured, on average, ca. 1.7  $\mu\text{m}$  (max. observed width: 4  $\mu\text{m}$ ). The microstructure of type-2 lines can be characterized as ISP (i.e., irregular, blocky, slightly elongated prisms with the maximum extension oriented perpendicularly to the inner shell surface) and as such differed significantly from adjacent shell portions (XLM). Transitions from XLM to ISP and vice versa were abrupt (Figs. 5C+D). Formation of type-2 lines primarily occurred when specimens were removed from tanks for calcein staining as well as during times of cold and unstable temperature regimes. Type-2 lines occurred less regularly and were less numerous than type-1 lines. In shell portions formed prior to the experiment, type-2 lines were much less numerous.

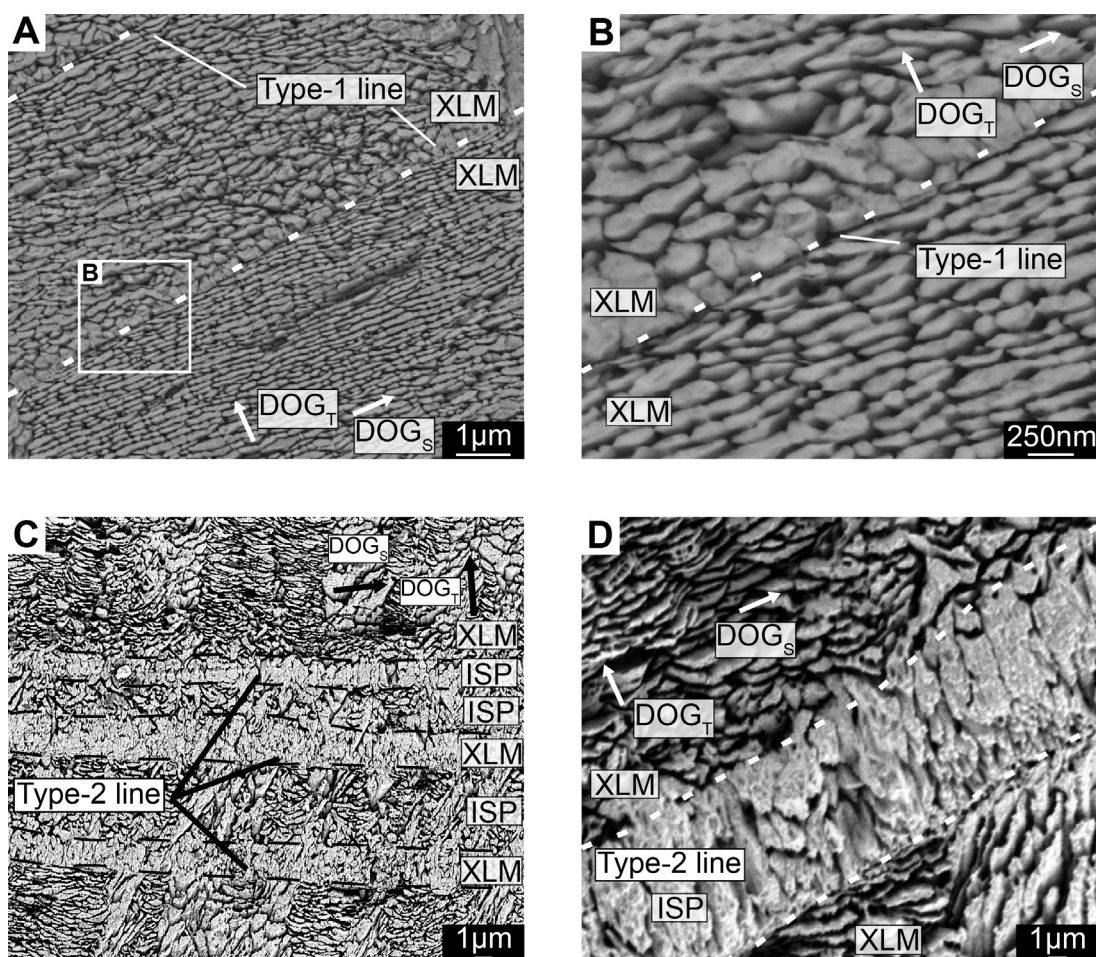


**Fig. 5.** Different types of growth lines in shells of *V. viviparus*. (A) Faint type-1 growth lines (dashed lines). Note the change in surface area, shape (width-to-height ratio) and orientation of 3<sup>rd</sup>-order lamellae cross sections (approximately perpendicular to l-axes) between the two subsequent type-1 lines. Overall microstructure remains unchanged (= XLM). (B) Magnified shell portion of (A) near a type-1 growth line. (C) Type-2 growth lines are much broader than type-1 lines, consist of irregular simple prisms and can therefore easily be distinguished from the surrounding XLM. (D) Detailed view of a type-2 line. DOG<sub>s</sub> = growth in size; DOG<sub>t</sub> = growth in shell thickness.



### **3.4 Variations within the simple crossed-lamellar structure: 1<sup>st</sup>-order lamellae**

During the experimental period, the appearance of the XLM structure, especially of 1<sup>st</sup>-order lamellae, changed significantly (Fig. 7). Shell material formed during steady warm conditions (interval I) revealed slender, uniform, well-ordered 1<sup>st</sup>-order simple crossed lamellae (Figs. 7A+B) regardless of pre-existing shell material being present or missing. From the outer toward the inner shell surface, the shape of the 1<sup>st</sup>-order lamellae remained unchanged without branching or abrupt terminations (Fig. 7B). Even during the following unstable and cold conditions (intervals II and III), the microstructural characteristics remained largely unchanged in shell portions that were deposited onto pre-existing shell material (shell thickening) with well-ordered 1<sup>st</sup>-order lamellae. In contrast, shell material formed during intervals II and III that was not deposited onto pre-existing shell material was characterized by highly unordered microstructures (Figs. 7A+C). Here, 1<sup>st</sup>-order lamellae were generally thinner (approx. 4.7  $\mu\text{m}$ ) than in well-ordered shell portions (approx. 12.5  $\mu\text{m}$ ). Additionally, 1<sup>st</sup>-order lamellae showed branching and, occasionally, abrupt terminations (Fig. 7C). (See on-line supplementary material, Fig. S3 for Figures 7B+C with higher resolution and highlighted outlines of 1<sup>st</sup>-order lamellae.)

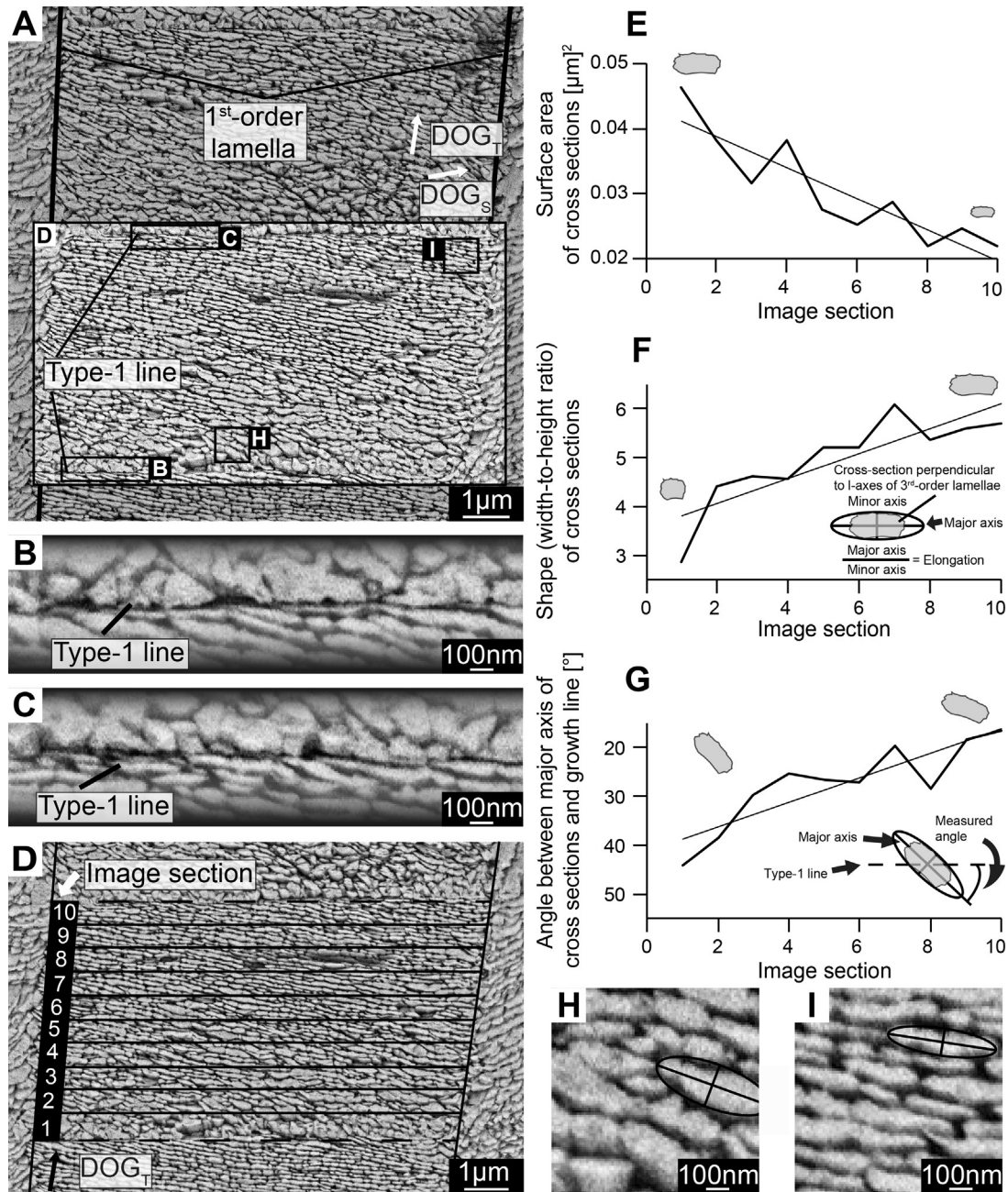


**Fig. 6.** Quantification of 3<sup>rd</sup>-order lamellae cross section (perpendicular to l-axes) variations in shells of *Viviparus viviparus*. (A) Shell portion with highlighted (bright rectangle) type-1 growth increment (delimited horizontally by two type-1 lines and vertically by adjacent 1<sup>st</sup>-order lamellae). (B, C) Higher magnification images of the lower (B) and the upper (C) delimiting type-1 line. (D) Enlarged image of the analyzed growth increment. To quantify small-scale variations in 3<sup>rd</sup>-order lamellae cross sections, the selected growth increment was subdivided into 10 image sections arranged subparallel to the delimiting type-1 growth lines. Within each image section (1 to 10), surface area, elongation of shape (major axis divided by minor axis of cross section) and orientation of cross sections were automatically analyzed step by step with ImageJ image processing software. From one to the next type-1 growth line, the surface area decreased by almost 50% (E), the shape became increasingly elongated (F) and the orientation changed gradually into a nearly subparallel orientation (G). DOG<sub>s</sub> = growth in size; DOG<sub>t</sub> = growth in shell thickness. Gray objects in (E–G) symbolize 3<sup>rd</sup>-order lamellae cross sections perpendicular to l-axes. (H, I) Higher-magnification images illustrating the differences between 3<sup>rd</sup>-order lamellae cross sections from the lower (H) and the upper (I) segment of the analyzed type-1 growth increment.

## 4 Discussion

### 4.1 Growth rates under experimental conditions

The shell growth rate of most mollusk species is positively correlated to temperature (e.g., Largen, 1967; Jones and Quitmyer, 1996; Fenger et al., 2007; Schöne et al., 2007). Findings of the present study line up with this observation. During warm temperatures, shells of *Viviparus viviparus* grew larger in size and thickness than during cold regimes. Furthermore, strong temperature shifts had adverse effects on shell growth (Table 1) and even affected the shell morphology. For example, during interval III no shell material was added at the aperture, but some shell thickening occurred. This could be interpreted as a protection mechanism. Instead of producing new thin, fragile shell, it was likely advantageous for the animals to further stabilize the existing shell. An alternative interpretation is that the shells grew in thickness rather than in size, because the soft parts grew slower during these adverse environmental conditions and, thus, did not require a more voluminous encasement. Since other environmental parameters (e.g., food supply) remained unchanged during the experiment, the observed changes of shell growth were most likely attributed to temperature.

### 4.2 Growth lines and higher order microstructure changes: Physiology and environment

In contrast to the shell growth rate, the formation of type-1 growth lines was most certainly not controlled by temperature. Although this environmental parameter was not constant during interval II, strong temperature fluctuations occurred less frequently and less periodically (3 major shifts) than type-1 lines were visible (7). Type-1 growth increments were always accompanied by repetitive changes of the surface area, elongation of shape and orientation of 3<sup>rd</sup>-order lamellae cross-sections formed during this growth increment (Fig. 6). Type-1 growth lines likely represent times during which only organic material was laid down (thin dark layer), whereas the calcium carbonate production ceased. The underlying reason for the observed repetitive changes of the 3<sup>rd</sup>-order lamellae (Fig. 6) is unclear. We hypothesize that the counterclockwise rotation of the increasingly elongated / flattened and smaller 3<sup>rd</sup>-order lamellae between consecutive type-1 growth lines fulfills biomechanical needs. The observed changes may increase the stability and robustness of the shell against shell fractures (e.g., Yang et al., 2011a, b).

It appears likely that these repetitive growth patterns formed on a periodic basis controlled by intrinsic timekeeping mechanisms, so-called biological clocks (Rensing et al., 2001). Biological clocks are genetically determined endogenous rhythms that maintain physiological cycles and are constantly reset by periodic environmental zeitgebers (pacemakers; Williams et al., 1997). The only external variable that changed periodically and could have served as zeitgeber was the simulated day/night cycle. However, the number of type-1 growth lines (7) remained well below the number of such day/night cycles (14) during the two-weekly interval. Perhaps, *V. viviparus* only formed one growth line and one growth increment every second day. Such a two-daily shell growth rhythm has previously been reported by Thébault et al. (2006) for the tropical scallop, *Comptopallium radula*. Another possible explanation is that the removal from the tanks and the calcein bath was so disturbing for the animal that it stopped growing shell for nearly a week and only then continued to grow shell on a daily (circadian) basis.

**Table 2** Summary of microstructural variations in shells of *Viviparus viviparus* triggered by differing environmental conditions: favorable conditions, calm and steady water temperature; unfavorable conditions, cold and highly variable water temperature, withdrawal from tanks, staining

	Favorable environmental conditions	Unfavorable environmental conditions
1 <sup>st</sup> -order lamellae width	Thick	Thin
Type-1 lines	Repetitive and periodic	Mostly repetitive and periodic
Type-2 lines	Not present	Frequently present

In fact, removal from the tanks and calcein immersion represented stressful situations for the gastropods as indicated by the formation of type-2 lines (Table 2). Such growth lines were also observed between calcein marks II and III and between calcein mark III and the last formed shell portion, i.e., the time intervals during which the animals experienced strong temperature shifts. Since time markers to temporally contextualize these growth lines were not available, however, it was impossible to determine whether these disturbance lines formed simultaneously with the temperature shifts. Shell portions formed prior to the experiment (calm and stable water temperature) revealed type-2 lines in a strongly reduced quantity. Disturbance lines have been reported in several previous sclerochronological studies and resulted from a variety of different environmental stressors. For example, Ramsay et al. (2000) and (2001) identified fishing and predatory attack by crabs as potential sources of scars visible in cross-sections of the dog cockle, *Glycymeris glycymeris*. Spawning, storms, and temperature extremes can induce the formation of disturbance lines in *Mercenaria mercenaria* (Kennish and Olsson, 1975; Panella and MacClintock, 1968). Furthermore, sudden pH changes leave similar growth patterns in shells of the freshwater pearl mussel, *Margaritifera margaritifera* (Dunca et al., 2005).

Structurally, disturbance lines including those observed in *V. viviparus* can hardly be distinguished from regular annual growth lines which are typically composed of irregular simple prisms (Dunca et al., 2009; Karney et al., 2012; Schöne et al., 2013; Shirai et al., 2014) or alternatively block-like objects with a strikingly similar appearance (Sumitomo et al., 2011). We speculate here that increased physiological stress favors the formation of evolutionarily older microstructures (= ISP; Taylor, 1973) that are probably easier to manufacture than more complex structures (XLM). Upon return to less hostile environmental conditions, the production of XLM commences. This agrees well with the strongly reduced number of type-2 lines visible in shell areas formed prior to the experiment (mostly very calm and stable growth conditions). The formation of type-2 lines prior to the experiment may have been triggered by others stressors (i.e., food scarcity, reproduction). It should be added that XLM is one of the most frequently occurring microstructures in modern mollusks (Dauphin, 2008; Suzuki et al., 2011; Nouet et al., 2012), likely because of its extraordinary hardness (Taylor and Layman, 1972). Furthermore, it contains much less organic material compared to other microstructural types such as nacre or prisms (Osuna-Mascaró et al., 2014), and its production thus requires much less energy.

### 4.3 Environmentally induced changes of the shell architecture

Only few existing studies have addressed the relationship between environmental change and microstructures of mollusk shells. Most of these studies observed modifications of microstructures at colder water temperatures. For example, *Mytilus californianus* grew a thicker inner prismatic layer (Dodd, 1964), whereas *Scaphara broughtonii* precipitated a thicker outer composite prismatic layer (Nishida et al., 2012). Likewise, shells of *Polymesoda caroliniana* formed predominantly pseudospiral microstructures rather than XLM during colder seasons (Tan Tiu, 1988).

Aside from the overall microstructure, however, temperature and other environmental variables can also induce more subtle modifications of the shell architecture. For example, changes of ambient pH seem to alter the preferred orientation of crystals in the outer calcitic layer of *Mytilus galloprovincialis* and *Mytilus edulis*, respectively (Hahn et al., 2012, 2014). In contrast, Stemmer et al. (2013) were unable to verify an impact of variable CO<sub>2</sub> levels on the crystal structure of *Arctica islandica* that grew under controlled laboratory conditions. Furthermore, Lutz (1984) identified smaller and more irregularly stacked nacre tablets in shells of *Geukensia demissa* that were exposed to colder regimes, and Olson et al. (2012) discovered a relationship between maximum water temperature and the angle of nacre stacks in shells of different gastropod and bivalve species.

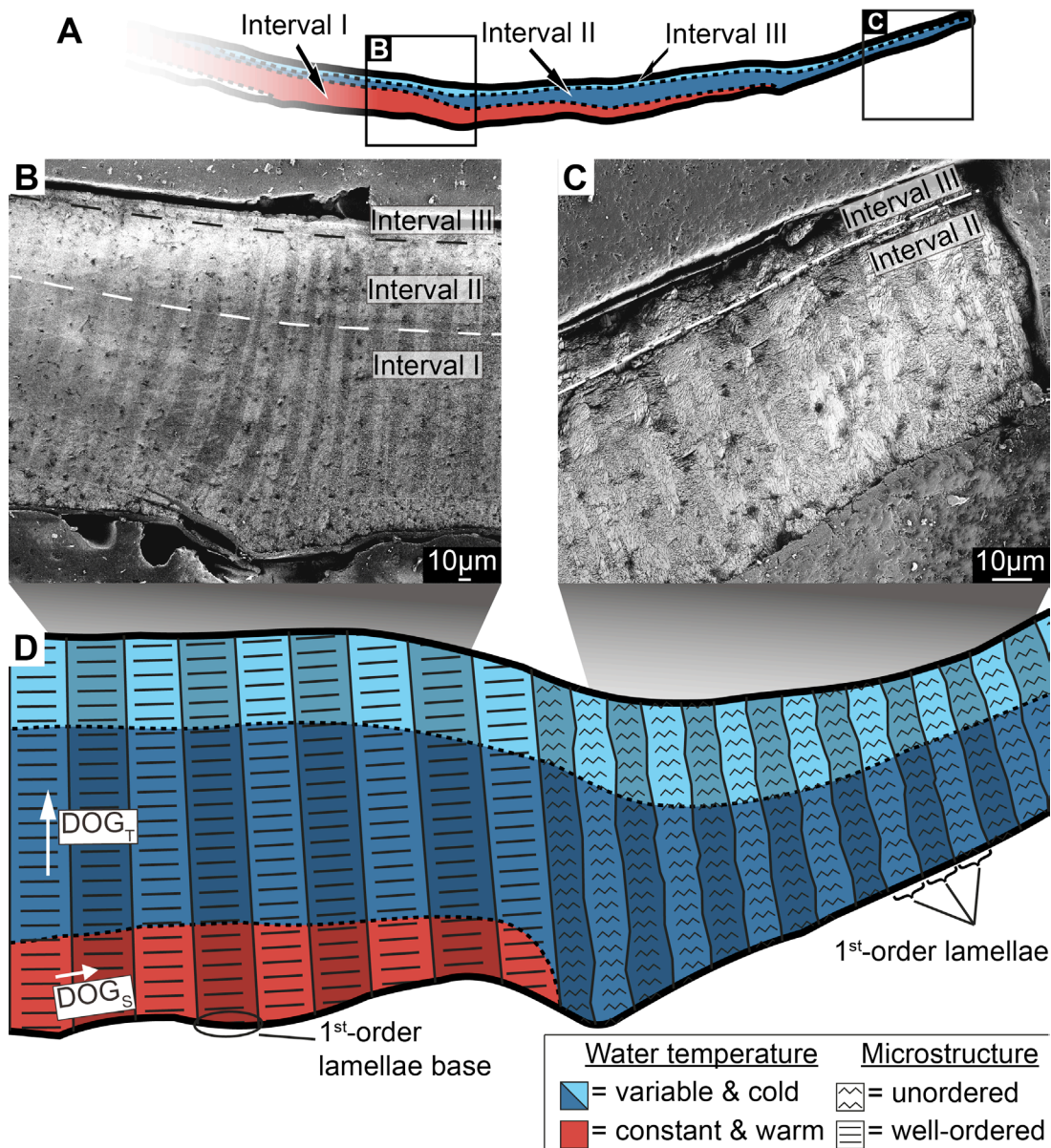


**Fig. 7.** Variations in XLM microstructure in shells of *Viviparus viviparus*. (A) Overview of the shell portion near the aperture (see Fig. 2) formed during the experiment. Dashed black lines denote calcein lines separating the shell into the three experimental intervals (interval I = stable warm; intervals II and III = variable and cold conditions). (B) Despite significant changes in ambient water temperature, the microstructure remained unchanged (= well-ordered simple crossed lamellae) in portions where new shell material was added onto pre-existing shell material. (C) Where shell material formed entirely new (= from scratch; growth in shell length) during cold and variable water temperatures, crossed-lamellar structures were highly disordered. (D) Sketch illustrating change in XLM structures described in (B) and (C).  $DOG_s$  = growth in size;  $DOG_t$  = growth in shell thickness.

In the present study, we also observed an environmentally induced precipitation of variants of a microstructure, even in contemporaneous shell portions (Table 2). Cold and more variable temperature regimes resulted in the formation of disordered and inhomogeneous 1<sup>st</sup>-order lamellae (XLM) if pre-existing shell was not available (Fig. 7), whereas well-ordered simple-crossed lamellae were precipitated onto already

existing shell (with well-ordered 1<sup>st</sup>-order lamellae). This suggests that the existing shell surface of *Viviparus viviparus* contains instructions for how to manufacture a specific XLM appearance irrespective of higher physiological stress (Fig. 7D). Such information could be present at the growth front in the form of specific matrix proteins or weak anionic peptides which are able to form specific crystal morphologies (Wheeler, 1992). Alternatively, the shape, size and orientation of existing of the lamellae at the growth front could serve as a template (blueprint) for subsequent shell precipitation (Wilbur and Saleuddin, 1983). However, if new shell was formed from scratch (= without pre-existing shell material) during adverse environmental conditions, calcification occurred without guidance and reacted directly to temperature extremes and temperature shifts. This resulted in the formation of variants of the XLM structure. Interestingly, the first few micrometers of new shell material in some specimens exhibited crystals in elongated form, which gradually changed into the typical hierarchal organization of crossed lamellae. This finding compares well with Wilmot et al. (1992), who identified a preliminary stage of unordered 3<sup>rd</sup>-order lamellae immediately at the growth front.

Subsequent studies should analyze if the observed microstructural changes occur proportionately and gradually with water temperature. For this purpose high-resolution crystallographic mapping methods such as electron backscattered diffraction (EBSD) could be used to map changes of crystallographic axes. If a relationship between temperature and crystallographic data can be verified, quantitative reconstructions of past water temperature may become possible. Further, it is mandatory to test if other environmental variables also affect the microstructure of this species, and if these different environmental controls can be distinguished based on the analysis of microstructures. It is also necessary to verify if similar microstructural changes also occur under natural conditions.

## 5 Conclusions and outlook

Temperature and physiological processes exert a distinct influence on shell growth rates and microstructures of shells of the freshwater gastropod *Viviparus viviparus*.

1. Shell production is significantly lower during cold and highly variable temperatures and occurs predominantly in the form of shell thickening.
2. First-order lamellae of simple crossed-lamellar (XLM) structures appeared highly unordered (thinning, branching, sudden stops) when formed without pre-existing shell under cold and highly variable temperature regimes. However, during stable

and warm conditions, well-ordered 1<sup>st</sup>-order lamellae were laid down. Likewise, well-ordered structures continued to form even under increased temperature stress if new shell was deposited onto already existing shell material with well-ordered 1<sup>st</sup>-order lamellae. The growth front seems to contain templates for maintaining a certain microstructural type.

3. Stress (unfavorable growth conditions, during experiment: cold and unstable water temperature) initiated the deposition of disturbance lines (type-2 lines) which were made of evolutionarily more primitive microstructure, i.e., irregular simple prisms.
4. Shell portions formed during interval II also revealed repetitive, presumably periodic growth patterns (faint organic type-1 growth line, gradual changes of 3<sup>rd</sup>-order lamellae of XLM structure). It is not unlikely that their formation was controlled by biological clocks. A couplet of one type-1 growth line and type-1 increment likely represents two days.

It is proposed here that changes of 1<sup>st</sup>-order lamellae proportions may serve as a new temperature proxy. However, subsequent experimental studies using high-resolution crystallographic mapping methods such as (EBSD) are necessary to test this hypothesis. It also needs to be verified if the observed microstructural changes are specifically related to temperature changes or if other environmental parameters can cause similar patterns. Furthermore, field experiments are advised to rule out that the observed changes only occur under artificial conditions.

## 6 Acknowledgments

The authors thank Etienne Neuhaus for his help designing Figures 1, 3 and 4. We also thank two anonymous reviewers for constructive comments, which substantially improved the quality of this paper. Financial support for this project was kindly provided by the German Research Foundation, Deutsche Forschungsgemeinschaft (DFG) to BRS (SCHO\_793/13).



## 7 References

- Affek, H.P., Bar-Matthews, M., Ayalon, A., Matthews, A., Eiler, J.M., 2008. Glacial/interglacial temperature variations in Soreq cave speleothems as recorded by ‘clumped isotope’ thermometry. *Geochim. Cosmochim. Acta* 72, 5351–5360.
- Bøggild, O.B., 1930. The shell structure of the mollusks. *D. Kgl. Danske Vidensk. Selsk. Skr., Nat. Mat. Afd.* 9, 231–326.
- Butler, P.G., Wanamaker Jr., A.D., Scourse, J.D., Richardson, C.A., Reynolds, D.J., 2013. Variability of marine climate on the North Icelandic Shelf in a 1357-year proxy archive based on growth increments in the bivalve *Arctica islandica*. *Palaeogeogr. Palaeoclimatol. Palaeoecol.* 373, 141–151.
- Came, R.E., Eiler, J.M., Veizer, J., Azmy, K., Brand, U., Weidman, C.R., 2007. Coupling of surface temperatures and atmospheric CO<sub>2</sub> concentrations during the Palaeozoic era. *Nature* 449, 198–201.
- Carter, J.G., Clark II, G.R., 1985. Classification and phylogenetic significance of molluscan shell microstructure. In: Bottjer, D.J., Hickman, C.S., Ward, P.D. (Eds.), *Mollusks Notes for a Short Course*. University of Tennessee, pp. 50–71.
- Chateigner, D., Hedegaard, C., Wenk, H., 2000. Mollusc shell microstructures and crystallographic textures. *J. Struct. Biol.* 22, 1723–1735.
- Dauphin, Y., 2008. The nanostructural unity of mollusc shells. *Mineral. Mag.* 72, 243–246.
- Delworth, T.L., Mann, M.E., 2000. Observed and simulated multidecadal variability in the Northern Hemisphere. *Clim. Dyn.* 16, 661–676.
- Dettman, D.L., Reische, A.K., Lohmann, K.C., 1999. Controls on the stable isotope composition of seasonal growth bands in aragonitic fresh-water bivalves (unionidae). *Geochim. Cosmochim. Acta* 63, 1049–1057.
- Dodd, J.R., 1964. Environmentally controlled variation in the shell structure of a pelecypod species. *J. Paleontol.* 38, 1065–1071.
- Dunca, E., Mutvei, H., Göransson, P., Mört, C.-M., Schöne, B.R., Whitehouse, M.J., Elfman, M., Baden, S.P., 2009. Using ocean quahog (*Arctica islandica*) shells to reconstruct palaeoenvironment in Öresund, Kattegat and Skagerrak, Sweden. *Int. J. Earth Sci.* 98, 3–17.
- Dunca, E., Schöne, B.R., Mutvei, H., 2005. Freshwater bivalves tell of past climates: But how clearly do shells from polluted rivers speak? *Palaeogeogr. Palaeoclimatol. Palaeoecol.* 228, 43–57.

- Eagle, R.A., Eiler, J.M., Tripathi, A.K., Ries, J.B., Freitas, P.S., Hiebenthal, C., Wanamaker Jr., A.D., Taviani, M., Elliot, M., Marensi, S., Nakamura, K., Ramirez, P., Roy, K., 2013. The influence of temperature and seawater carbonate saturation state on  $^{13}\text{C}$ - $^{18}\text{O}$  bond ordering in bivalve mollusks. *Biogeosci.* 10, 1–16.
- Eiler, J.M., 2007. “Clumped-isotope” geochemistry – The study of naturally-occurring, multiply-substituted isotopologues. *Earth Planet. Sci. Lett.* 262, 309–327.
- Fenger, T., Surge, D., Schöne, B.R., Milner, N., 2007. Sclerochronology and geochemical variation in limpet shells (*Patella vulgata*): A new archive to reconstruct coastal sea surface temperature. *Geochem. Geophys. Geosyst.* 8, Q07001.
- Finnemore, A., Cunha, P., Shean, T., Vignolini, S., Guldin, S., Oyen, M., Steiner, U., 2012. Biomimetic layer-by-layer assembly of artificial nacre. *Nat. Commun.* 3, 1–6.
- Foster, L.C., Allison, N., Finch, A.A., Andersson, C., 2009. Strontium distribution in the shell of the aragonite bivalve *Arctica islandica*. *Geochem. Geophys. Geosyst.* 10, Q03003.
- Freitas, P.S., Clarke, L.J., Kennedy, H.A., Richardson, C.A., 2008. Inter- and intra-specimen variability masks reliable temperature control on shell Mg/Ca ratios in laboratory- and field-cultured *Mytilus edulis* and *Pecten maximus* (bivalvia). *Biogeosci.* 5, 1245–1258.
- Ghosh, P., Adkins, J., Affek, H., Balta, B., Guo, W., Schauble, E.A., Schrag, D., Eiler, J.M., 2006.  $^{13}\text{C}$ - $^{18}\text{O}$  bonds in carbonate minerals: A new kind of paleothermometer. *Geochim. Cosmochim. Acta* 70, 1439–1456.
- Hahn, S., Griesshaber, E., Schmahl, W.W., Neuser, R.D., Ritter, A.-C., Hoffmann, R., Buhl, D., Niedermayr, A., Geske, A., Immenhauser, A., 2014. Exploring aberrant bivalve shell ultrastructure and geochemistry as proxies for past sea water acidification. *Sedimentology* 61, 1625–1658.
- Hahn, S., Rodolfo-Metalpa, R., Griesshaber, E., Schmahl, W.W., Buhl, D., Hall-Spencer, J.M., Baggini, C., Fehr, K.T., Immenhauser, A., 2012. Marine bivalve shell geochemistry and ultrastructure from modern low pH environments: environmental effect versus experimental bias. *Biogeosci.* 9 1897–1914.
- Hallmann, N., Schöne, B.R., Irvine, G.V., Burchell, M., Cokelet, E.D., Hilton, M.R., 2011. An improved understanding of the Alaska Coastal Current: the application of a bivalve growth-temperature model to reconstruct freshwater-influenced paleoenvironments. *Palaios* 26, 346–363.
- Immenhauser, A., Nägler, T.F., Steuber, T., Hippler, D., 2005. A critical assessment of mollusk  $^{18}\text{O}/^{16}\text{O}$ , Mg/Ca, and  $^{44}\text{Ca}/^{40}\text{Ca}$  ratios as proxies for Cretaceous seawater temperature seasonality. *Palaeogeogr. Palaeoclimatol. Palaeoecol.* 215, 221–237.
- Jones, D.S., Quitmyer, I.R., 1996. Marking time with bivalve shells: oxygen isotopes and season of annual increment formation. *Palaios* 11, 340–346.

- Jones, D.S., 1983. Reading Sclerochronology: reading the shell record of the molluscan shell. *Am. Sci.* 71, 384–391.
- Kaehler, S., McQuaid, C.D., 1999. Use of the fluorochrome calcein as an in situ growth marker in the brown mussel *Perna perna*. *Mar. Biol.* 133, 455–460.
- Karney, G.B., Butler, P.G., Speller, S., Scourse, J.D., Richardson, C.A., Schröder, M., Hughes, G.M., Czernuszka, J.T., Grovenor, C.R.M., 2012. Characterizing the microstructure of *Arctica islandica* shells using NanoSIMS and EBSD. *Geochem. Geophys. Geosyst.* 13, Q04002.
- Kennish, M.J., Olsson, R.K., 1975. Effects of thermal discharges on the microstructural growth of *Mercenaria mercenaria*. *Environ. Geol.* 1, 41–64.
- Klein, R.T., Lohmann, K.C., Thayer, C.W., 1996. Bivalve skeletons record sea-surface temperature and  $\delta^{18}\text{O}$  via Mg/Ca and  $^{18}\text{O}/^{16}\text{O}$  ratios. *Geology* 24, 415–418.
- Kobayashi, I., 1969. Internal microstructure of the shell of bivalve molluscs. *Am. Zool.* 9, 663–672.
- Largen, M.J., 1967. The influence of water temperature upon the life of the dog-whelk *Thais lapillus* (Gastropoda: Prosobranchia). *J. Anim. Ecol.* 36, 207–214.
- Lazareth, C.E., Guzman, N., Poitrasson, F., Candaudap, F., Ortlieb, L., 2007. Nyctemeral variations of magnesium intake in the calcitic layer of a Chilean mollusk shell (*Concholepas concholepas*, Gastropoda). *Geochim. Cosmochim. Acta* 71, 5369–5383.
- Linnaeus, C., 1758. *Systema Naturae per regna tria naturae, secundum classes, ordines, genera, species, cum characteribus, differentiis, synonymis, locis*. Vol. 1; 10<sup>th</sup> edition. Holmiae. (Salvius). (823 pp.).
- Lutz, R.A., 1984. Paleocological implications of environmentally-controlled variation in molluscan shell microstructure. *Geobios Mémoires* 8, 93–97.
- MacClintock, C., 1967. Shell structure of patelloid and bellerophontoid gastropods (Mollusca). *Peabody Museum of Natural History Yale University Bulletin* 22, 1–140.
- Moran, A.L., 2000. Calcein as a marker in experimental studies newly-hatched gastropods. *Mar. Biol.* 137, 893–898.
- Nishida, K., Ishimura, T., Suzuki, A., Sasaki, T., 2012. Seasonal changes in the shell microstructure of the bloody clam, *Scapharca broughtonii* (Mollusca: Bivalvia: Arcidae). *Palaeogeogr. Palaeoclimatol. Palaeoecol.* 363–364, 99–108.
- Nouet, J., Baronnet, A., Howard, L., 2012. Crystallization in organo-mineral micro-domains in the crossed-lamellar layer of *Nerita undata* (Gastropoda, Neritopsina). *Micron* 43, 456–62.

- Olson, I.C., Kozdon, R., Valley, J.W., Gilbert, P.U.P.A., 2012. Mollusk shell nacre ultrastructure correlates with environmental temperature and pressure. *J. Am. Chem. Soc.* 134, 7351–7358
- Osuna-Mascaró, A., Cruz-Bustos, T., Benhamada, S., Guichard, N., Marie, B., Plasseraud, L., Corneillat, M., Alcaraz, G., Checa, A., Marin, F., 2014. The shell organic matrix of the crossed lamellar queen conch shell (*Strombus gigas*). *Comp. Biochem. Physiol. B* 168, 76–85.
- Pannella, G., MacClintock, C., 1968. Biological and environmental rhythms reflected in molluscan shell growth. *Paleontol. Soc. Mem.* 2, 64–81.
- Ramsay, K., Kaiser, M.J., Richardson, C.A., Veale, L.O., Brand, A.R., 2000. Can shell scars on dog cockles (*Glycymeris glycymeris* L.) be used as an indicator of fishing disturbance? *J. Sea Res.* 43, 167–176.
- Ramsay, K., Richardson, C.A., Kaiser, M.J., 2001. Causes of shell scarring in dog cockles *Glycymeris glycymeris* L.. *J. Sea Res.* 45, 131–139.
- Rensing, L., Meyer-Grahe, U., Ruoff, P., 2001. Biological timing and the clock metaphor: oscillatory and hourglass mechanisms. *Chronobiol. Int.* 18, 329–369.
- Schöne, B.R., Fiebig, J., Pfeiffer, M., Gleß, R., Hickson, J., Johnson, A.L.A., Dreyer, W., Oschmann, W., 2005. Climate records from a bivalved Methuselah (*Arctica islandica*, Mollusca; Iceland). *Palaeogeogr. Palaeoclimatol. Palaeoecol.* 228, 130–148.
- Schöne, B.R., Rodland, D.L., Wehrmann, A., Heidel, B., Oschmann, W., Zhang, Z., Fiebig, J., Beck, L., 2007. Combined sclerochronologic and oxygen isotope analysis of gastropod shells (*Gibbula cineraria*, North Sea): life-history traits and utility as a high-resolution environmental archive for kelp forests. *Mar. Biol.* 150, 1237–1252.
- Schöne B.R., Gillikin, D.P., 2013. Unraveling environmental histories from skeletal diaries – Advances in sclerochronology. *Palaeogeogr. Palaeoclimatol. Palaeoecol.* 373, 1–5.
- Schöne, B.R., Goodwin, D., Flessa, K., Dettman, D., Roopnarine, P., 2002. Sclerochronology and growth of the bivalve mollusks *Chione* (*Chionista*) *fluctifraga* and *C. (Chionista) cortezi* in the northern gulf of California, Mexico. *Veliger* 45, 45–54.
- Schöne, B.R., Radermacher, P., Zhang, Z., Jacob, D.E., 2013. Crystal fabrics and element impurities (Sr/Ca, Mg/Ca, and Ba/Ca) in shells of *Arctica islandica* – Implications for paleoclimate reconstructions. *Palaeogeogr. Palaeoclimatol. Palaeoecol.* 373, 50–59.
- Schöne, B.R., Zhang, Z., Radermacher, P., Thébault, J., Jacob, D.E., Nunn, E.V., Maurer, A.F., 2011. Sr/Ca and Mg/Ca ratios of ontogenetically old, long-lived bivalve shells (*Arctica islandica*) and their function as paleotemperature proxies. *Palaeogeogr. Palaeoclimatol. Palaeoecol.* 302, 52–64.

- Schöne, B.R., 2008. The curse of physiology – challenges and opportunities in the interpretation of geochemical data from mollusk shells. *Geo-Mar. Lett.* 28, 269–285.
- Shirai, K., Schöne, B.R., Miyaji, T., Radermacher, P., Krause Jr., R.A., Tanabe, K., 2014. Assessment of the mechanism of elemental incorporation into bivalve shells (*Arctica islandica*) based on elemental distribution at the microstructural scale. *Geochim. Cosmochim. Acta* 126, 307–320.
- Stemmer, K., Nehrke, G., Brey, T., 2013. Elevated CO<sub>2</sub> levels do not affect the shell structure of the bivalve *Arctica islandica* from the Western Baltic. *PLoS ONE* 8, e70106.
- Sumitomo, T., Kakisawa, H., Kagawa, Y., 2011. Nanoscale structure and mechanical behavior of growth lines in shell of abalone *Haliotis gigantea*. *J. Struct. Biol.* 174, 31–36.
- Suzuki, M., Kogure, T., Weiner, S., Addadi, L., 2011. Formation of aragonite crystals in the crossed lamellar microstructure of limpet Shells. *Cryst. Growth Des.* 11, 4850–4859.
- Tan Tiu, A., 1988. Temporal and spatial variation of shell microstructure of *Polymesoda Carolinia* (Bivalvia: Heterodonta). *Am. Malacol. Bull.* 6, 199–206.
- Taylor, J.D., Kennedy, W.J., 1969. The influence of the periostracum on the shell structure of bivalve molluscs. *Calc. Tiss. Res.* 3, 274–283.
- Taylor, J.D., Layman, M., 1972. The mechanical properties of bivalve (Mollusca) shell structures. *Paleontol.* 15, 73–87.
- Taylor, J.D., 1973. The structural evolution of the bivalve shell. *Palaeontol.* 16, 519–534.
- Thébault, J., Chauvaud, L., Clavier, J., Fichez, R., Morize, E., 2006. Evidence of a 2-day periodicity of striae formation in the tropical scallop *Comptopallium radula* using calcein marking. *Mar. Biol.* 149, 257–267.
- Wacker, U., Fiebig, J., Schöne, B.R., 2013. Clumped isotope analysis of carbonates: comparison of two different acid digestion techniques. *Rapid Commun. Mass Spectrom.* 27, 1631–1642.
- Wanamaker Jr., A.D., Kreutz, K.J., Schöne, B.R., Pettigrew, N., Borns, H.W., Introne, D.S., Belknap, D., Maasch, K.A., Feindel, S., 2008. Coupled North Atlantic slope water forcing on Gulf of Maine temperatures over the past millennium. *Clim. Dyn.* 31, 183–194.
- Wanamaker Jr., A.D., Kreutz, K.J., Wilson, T., Borns Jr., H.W., Introne, D.S., Feindel, S., 2008. Experimentally determined Mg/Ca and Sr/Ca ratios in juvenile bivalve calcite for *Mytilus edulis*: implications for paleotemperature reconstructions. *Geo-Mar. Lett.* 28, 359–368.
- Wheeler, A.P., 1992. Mechanisms of molluscan shell formation. In: Bonucci, E. (Ed.), *Calcification in biological systems*. CRC Press, Boca Raton, pp. 77–83.

- Wilbur, K.M., Saleuddin, A., 1983. Shell formation. In: Saleuddin, A., Wilbur, K.M. (Eds.), *The Mollusca*, Vol. 4. Academic Press Inc, Toronto, pp 235–287.
- Williams, B.G., Pilditch, C.A., 1997. The entrainment of persistent tidal rhythmicity in a filter-feeding bivalve using cycles of food availability. *J. Biol. Rhythms* 12, 173–181.
- Wilmot, N.V., Barber, D.J., Taylor, J.D., Graham, A.L., 1992. Electron microscopy of molluscan crossed-lamellar microstructure. *Phil. Trans. R. Soc. B.* 337, 21–35.
- Witbaard, R., Duineveld, G.C.A., De Wilde, P.A.W.J., 1997. A long-term growth record derived from *Arctica islandica* (Mollusca, Bivalvia) from the Fladen Ground (northern North Sea). *J. Mar. Biol. Ass. U.K.* 77, 801–816.
- Yang, W., Zhang, G., Liu, H., Li, X., 2011a. Microstructural characterization and hardness behavior of a biological *Saxidomus purpuratus* shell. *J. Mater. Sci. Technol.* 27, 139–146.
- Yang, W., Zhang, G.P., Zhu, X.F., Li, X.W., Meyers, M.A., 2011b. Structure and mechanical properties of *Saxidomus purpuratus* biological shells. *J. Mech. Behav. Biomed. Mater.* 4, 1514–1530.

## Concluding remark

As suggested in manuscript I, in subsequent (unpublished) studies it was tested if the crystallographic orientation of the mesocrystals serves as proxy to estimate temperature with greater robustness. Therefore, EBSD (= electron backscatter diffraction) measurements were done on shells of *Viviparus viviparus*. Gastropods were exposed to different temperature regimes in a three-month long aquacultural experiment and labeled with calcein for a later temporal alignment of the growth record. Unfortunately, almost all specimens exhibited poor fitness and died prior to the planned ending of the experiment.

In a collaboration with Prof. Schmahl and Dr. Griesshaber (LMU München) it was tested if the crystallographic texture of crossed-lamellar structures of *Viviparus viviparus* irrespective of a potential temperature signal can be measured with EBSD. As it turned out, this is not the case. Potentially, the amalgamation of numerous sub-units forming the nanocrystal assemblage of this particularly delicate microstructure impede Kikuchi patterns to emerge and thus to map the crystallographic orientation. Possibly, the application of TEM-EBSD, an analytical technique that allows to map the orientation of the crystallographic axes of crystals on an even higher spatial resolution is more suitable.

## Manuscript II

### Strontium/lithium ratio in aragonitic shells of *Cerastoderma edule* (Bivalvia)

–

### A new potential temperature proxy for brackish environments

Published in Chemical Geology

Christoph S. Füllenbach<sup>1</sup>, Bernd R. Schöne<sup>1</sup>, Regina Mertz-Kraus<sup>1</sup>

<sup>1</sup>Institute of Geosciences, University of Mainz,  
Johann-Joachim-Becher-Weg 21, 55128 Mainz, Germany

#### Authors contribution

Concept: CSF, BRS

Execution: CSF

Analyses: Growth patterns: CSF, Stefania Milano; LA-ICP-MS: RMK, CSF;

ICP-OES: Michael Maus, CSF; CF-IRMS: Michael Maus, CSF

Data analysis: CSF

Writing: CSF, BRS, RMK

Füllenbach, C.S., Schöne, B.R., Mertz-Kraus, R., 2015. Strontium/lithium ratio in aragonitic shells of *Cerastoderma edule* (Bivalvia) – A new potential temperature proxy for brackish environments. Chem. Geol. 417, 341–355.



## Abstract

Quantitative reconstruction of water temperature from shells of bivalve mollusks is still a very challenging task. For example, in highly variable environments like intertidal zones, shell oxygen isotope values can only provide reliable temperature estimates if the  $\delta^{18}\text{O}_{\text{water}}$  signature during the exact time of growth is known. Furthermore, trace element ratios like Sr/Ca or Mg/Ca are not generally accepted as useful paleothermometer, since their incorporation in bivalve shells is known to be strongly biologically controlled. Here, we present a potential novel temperature proxy which is based on the Sr/Li<sub>shell</sub> ratio of the intertidal bivalve *Cerastoderma edule*. Up to 81% of the variability in Sr/Li<sub>shell</sub> is mathematically explained by water temperature. It is suggested that vital effects on the incorporation of Sr and Li in the aragonitic shells are largely eliminated by normalizing Sr/Ca to Li/Ca. Apparently, growth rate does not control the incorporation of Sr or Li in the shell of *C. edule*. By using this new proxy, it was possible to estimate water temperature from *C. edule* with an uncertainty of  $\pm 1.5$  °C. Future studies are required to test if Sr/Li<sub>shell</sub> also serves as a reliable temperature proxy in other bivalve species and in other environments.

Keywords: Bivalve shell, Temperature proxy, Element-to-element ratio, Strontium, Lithium

## 1 Introduction

Bivalve shells are becoming increasingly recognized as powerful tools for high-resolution paleoclimate reconstructions. This class virtually combines all requirements of an ideal paleoclimate archive. Bivalves inhabit nearly all aquatic environments, specifically extratropical shallow-marine and nearshore settings (Nicol, 1951; Lomovasky et al., 2002; Malham et al., 2012). During growth these animals store information on changes of the physico-chemical environment in their shells in the form of variable growth rates and geochemical properties (Williams et al., 1982; Chauvaud et al., 2005; Wanamaker et al., 2008; Hallman et al., 2011). Environmental proxy data can be placed in a precise temporal context by using periodic shell growth patterns, i.e., circatidal, daily, fortnightly and annual growth increments and lines (Evans, 1972; Jones, 1983; Ohno, 1985; Jones and Quitmyer, 1996). Certain boreal species are known to grow shell during both seasonal extremes and thus record the full seasonal amplitude (Schöne et al., 2005a). Some bivalves are exceptionally long-lived and attain a lifespan of more than 500 years (Schöne et al., 2005a; Wisshak et al., 2009; Butler et al., 2013). Therefore, bivalves can provide subseasonally resolved records of environmental change over coherent time intervals of many years (Schöne et al., 2005b; Wanamaker et al., 2011; Yan et al., 2015). Since shell growth of contemporaneous specimens from the same region is highly synchronized, it is also possible to combine annual growth increment time-series to form longer chronologies that cover many generations of bivalves and centuries to millennia (Witbaard et al., 1997; Marchitto et al., 2000; Butler et al., 2010, 2013; Holland et al., 2014).

Despite recent achievements in bivalve sclerochronology, quantitative reconstructions of environmental variables from shells still remains a very challenging task. This is particularly true for ocean temperature, a crucial parameter of the climate system. The most frequently used and well-accepted proxy for water temperature,  $\delta^{18}\text{O}_{\text{shell}}$ , provides reliable temperature data only if the oxygen isotope signature of the water or salinity, which is strongly coupled to  $\delta^{18}\text{O}_{\text{water}}$  during the time of growth is precisely known (Epstein et al., 1953; Mook, 1971; Grossman and Ku, 1986; Wefer and Berger, 1991). For bivalves, however, no proxy exists for  $\delta^{18}\text{O}_{\text{water}}$  or salinity. More recently, the carbonate clumped isotope method has been introduced as a novel paleothermometer (Ghosh et al., 2006; accuracy ca.  $\pm 1.4$  °C) and has already been successfully applied to bivalves (Came et al. 2007; Eagle et al., 2013; Henkes et al., 2013). However, Eiler et al. (2011) suggested that  $\Delta_{47}$  values of biogenic carbonates are biased by vital effects. Even if this effect can be mathematically eliminated, the low sample throughput (~six measurements per 24 hours; at least triplicate measurements are required for one sample) and the relatively large amounts of shell carbonate required for each analysis (ca. 1.2 to 4 mg per measurement) currently precludes the possibility

to obtain subseasonally resolved paleotemperature records using this sophisticated technique. Another potential paleothermometer that has occasionally been applied to bivalves is based on certain element-to-calcium ratios, especially Sr/Ca and Mg/Ca (Dodd, 1965; Klein et al., 1996; Yan et al., 2015). Even though crystallographic characteristics favor the incorporation of certain trace elements into specific CaCO<sub>3</sub> polymorphs (e.g., the incorporation of the larger Sr<sup>2+</sup> ion is favored in aragonite due to its looser 9-fold coordination, compared to the 6-fold coordination in calcite), trace element signatures of bivalve shells still offer great potential as paleothermometers, because the CaCO<sub>3</sub> polymorph typically does not change on a seasonal basis or throughout lifetime. However, the incorporation of trace and minor elements is also strongly influenced by physiology (Schöne et al., 2011) and vital effects (Gillikin et al., 2005; Freitas et al., 2006). In some species, the element partitioning between shell and water can further be affected by growth rate and ontogenetic age (Swan, 1956; Takesue and van Geen, 2004; Lorrain et al., 2005; Schöne et al., 2011). Moreover, the Sr/Ca and Mg/Ca ratios can also vary contradictorily among different bivalve species and even among contemporaneous specimens from one locality (Dodd, 1965; Gillikin et al., 2005; Lorrain et al., 2005; Freitas et al., 2008). Therefore, temperature typically explains only a small proportion of the element-to-calcium values of bivalve shells.

In an attempt to adjust for the influence of vital effects on the element incorporation in the tests of foraminifera, Bryan and Marchitto (2008) suggested to normalize Mg/Ca to Li/Ca. The resulting Mg/Li ratio is much more sensitive to temperature than Mg/Ca. So far, the method has been successfully applied to benthic foraminifera (Bryan and Marchitto, 2008) and corals (Case et al., 2010; Hathorne et al., 2013; Raddatz et al., 2013, 2014; Montagna et al., 2014, Rollion-Bard and Balmart, 2015). Here, we applied a similar approach by indexing Sr/Ca by Li/Ca values and tested if Sr/Li ratios can be used as an alternative temperature proxy in the intertidal bivalve mollusk species, *Cerastoderma edule*.

## ***2 Cerastoderma edule***

The common cockle, *Cerastoderma edule* (Linnaeus) is a common inhabitant of the intertidal zones of the North Sea, Baltic Sea, Mediterranean Sea and Black Sea as well as the North Atlantic Ocean (Malham et al., 2012). This small bivalve (<5 cm) lives just below the sediment surface (Burdon et al., 2014) and gathers food from suspension (Barlow and Kingston, 2001; Burdon et al., 2014). Its aragonitic shell (confirmed here by Raman spectroscopy) is subdivided into an inner shell layer (ISL)

and an outer shell layer (OSL) (Fig. 1). The latter is further subdivided into an inner portion (iOSL; simple crossed-lamellar microstructure; Deith, 1985) and an outer portion (oOSL; composite prismatic microstructure; Popov, 1986).

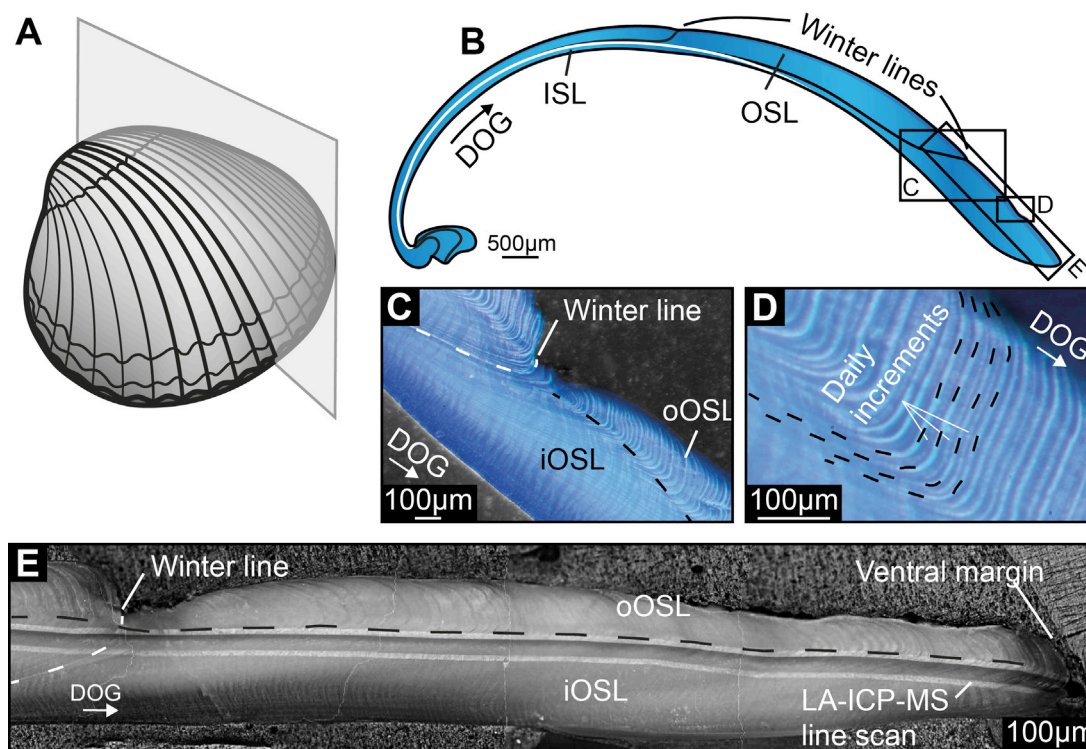


**Fig. 1.** Sclerochronology of *Cerastoderma edule*. (A) Sketch of left valve. Three thick-sections were cut from the shell along the axis of maximum growth (gray plane). (B) Schematic illustration of cross-sectioned shell with major annual growth patterns (winter lines). (C) Thick-section of specimen A24 stained with Mutvei solution (Schöne et al., 2005c) showing shell portion (outer layer) near winter line. oOSL/iOSL = outer/inner portion of outer shell layer. Transition zone between the oOSL and iOSL is indicated by dashed black line. (D) Growth patterns in the oOSL of specimen A24 showing lunar daily (circalunidian) increments delimited by growth lines (dashed). Faint line half way between lunar daily growth lines represents circatidal growth line. A couplet of two circatidal growth increments and lines forms each lunar day (~24.8 h). (E) Laser ablation line scan covering the last year of growth (2013) of specimen A24. DOG = direction of growth.

Like other bivalve species, shells of *C. edule* grow on a periodic basis resulting in distinct growth patterns that consist of narrow, organic-rich, dark lines and broad,  $\text{CaCO}_3$ -rich, whitish increments. Major growth lines visible on the outer shell surface and in cross-sections represent winter lines (Orton, 1926; Farrow, 1971; Bourget and Brock, 1990; Ponsero et al., 2009). Typically, each winter line is associated with a notch in the outer shell surface (Figs. 1B–E) (House and Farrow, 1968). Furthermore, cross-sections of the shells reveal fortnightly, circalunidian (24.8 hour cycles; lunar daily) and circatidal (12.4 hour cycles; semidiurnal) growth lines and increments (Fig. 1D; Richardson et al., 1979; Ohno, 1985; Lønne and Gray, 1988; Mahé et al., 2010).

These growth patterns can be used to determine the duration of the growing season and place each shell portion in a precise temporal context. The duration of the main growing season of this species typically lasts from early spring until late fall (Lønne and Gray, 1988; Bourget and Brock, 1990). Temperatures below 10 °C and above 30 °C result in very slow shell growth (Kingston, 1974).

### 3 Material and methods

On 1 April 2013 a temperature logger (HOBO U24) was deployed in the high intertidal zone north of Schillig, North Sea, Germany (N53° 42′ 45.68″ E8° 01′ 14.88″; Fig. 2). Since the logger was chained to a small ship wreck lying in a tideway, it was constantly immersed and recorded water temperature on an hourly basis until it was recovered a year later (11 March 2014). For comparison with the shells, a new time-series was computed that reflects the water temperature during high tide (high stand  $\pm$  1 hour; arithmetic mean), i.e. during the time when new shell material is formed. Tidal ranges and the timing of spring and neap tides at the sampling locality were computed with the software WXTide32 ver. 4.7. At the same locality, water samples for geochemical analysis were taken during low tide from a water-filled tideway nearby. Samples were taken up to four times per month between 1 April 2013 and 11 March 2014 and then stored in a refrigerator. Chlorophyll a data (approx. weekly resolution) were obtained from satellite datasets (4 km spatial resolution, MODIS NASA, available at <http://disc.sci.gsfc.nasa.gov/giovanni>; last checked January 2016). On 11 March 2014, we also collected four three-year-old living specimens of *C. edule* that lived next to the logger (Table 1). In the following, we refer to these specimens (IDs: SNS-11Mar14-A1, -A6, -A24 and -A28) as A1, A6, A24 and A28.

**Table 1** Timing and rate of shell growth of the studied *Cerastoderma edule* specimens.

Shell ID SNS-11Mar14-	# lunar daily increments	Lunar daily increment width [ $\mu$ m]			Duration of growing season 2013 ( $\pm$ 7 days)
		Average $\pm$ 1SD	Min.	Max.	
A1	135	23 $\pm$ 11	3	55	19 Apr. - 5 Sep.
A6	143	25 $\pm$ 12	6	84	19 Apr. - 13 Sep.
A24	146	23 $\pm$ 10	5	49	19 Apr. - 16 Sep.
A28	129	24 $\pm$ 14	4	78	19 Apr. - 25 Aug.

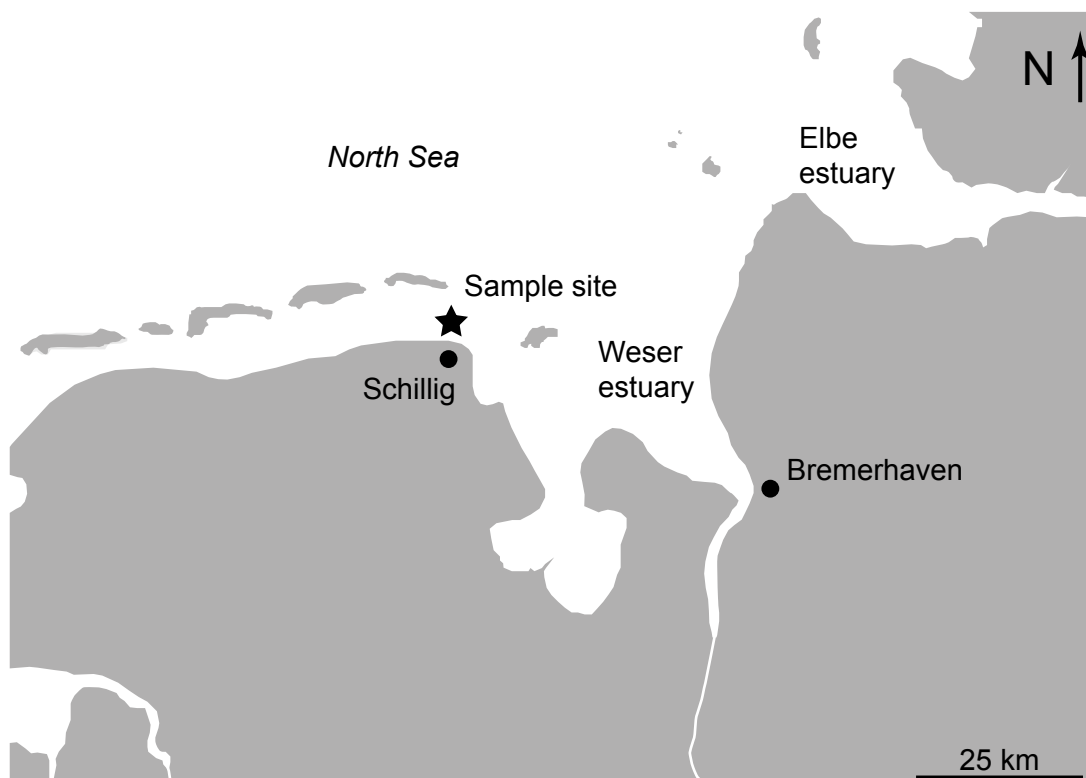


**Fig. 2.** Map of the North Sea coast of Germany. Black star marks study locality north of the village of Schillig.

### 3.1 Shell preparation and growth pattern analysis

After removing the soft tissues, shells were ultrasonically cleaned, mounted on plexiglass cubes and covered with a protective layer of a quick-drying epoxy resin (JB KWIK). Three 2-millimeter-thick sections were cut along the axis of maximum growth using a low-speed saw (Buehler Isomet 1000) (Figs. 1A+B).

For laser ablation inductively coupled plasma mass spectrometry (LA-ICP-MS) analysis, thick-sections were embedded in epoxy resin (Struers EpoFix), ground on rotating SiC-discs (320, 600, 1200, 2500 grit), polished by hand with a poly-diamond solution (3  $\mu\text{m}$ ) and then polished for 3 hours with 0.3  $\mu\text{m}$   $\text{Al}_2\text{O}_3$  powder on a Buehler Vibromet. Subsequently, samples were ultrasonically cleaned with Milli-Q water and rinsed with a few drops of ethanol.

For growth pattern analysis, additional shell slabs were mounted on glass slides, ground on glass plates (800, 1200 grit SiC powder) and polished on a Buehler G-Cloth with 1  $\mu\text{m}$   $\text{Al}_2\text{O}_3$  powder. After immersion in Mutvei's solution (Schöne et al., 2005c), thick-sections were viewed under a binocular microscope equipped with sectoral dark field illumination (Schott VisiLED MC1000) and photographed with a

Canon EOS 550D camera. The widths of lunar daily growth increments deposited in 2013 were measured to the nearest 1  $\mu\text{m}$  in the oOSL with the image processing software Panopea (Figs. 1C+D). To determine the seasonal timing of shell growth of *C. edule* at this locality and assign calendar dates to each shell portion, the study area was visited almost every month to identify when the winter line starts to form. We have deliberately not employed calcein marking (Kaehler and McQuaid, 1999; Moran, 2000) to constrain the timing of seasonal growth, because this can influence the physiology of the animal and the microstructures of the shells (Füllenbach et al., 2014).

For oxygen isotope analysis of shell carbonate, remaining shell slabs were mounted on glass slides, ground on glass plates (800, 1200 grit SiC powder) and finally polished on a Buehler G-Cloth with 1  $\mu\text{m}$   $\text{Al}_2\text{O}_3$  powder. After ultrasonically cleaning the thick-sections in de-ionized water, five to seven powder samples were obtained from the OSL of each specimen with a Rexim Minimo dental drill equipped with a conical drill bit (300  $\mu\text{m}$  diameter; Komet/Gebr. Brasseler GmbH & Co. KG, model no. H52 104 003) and mounted to a binocular microscope. Achieving a higher temporal resolution by means of milling instead of drilling remained largely impossible due to the complex architecture of the growth patterns. Drill holes measured on average 300  $\mu\text{m}$  in diameter and were equally distributed with the smallest possible overlap within shell portions formed in 2013. All powder samples weighed between 40 to 120  $\mu\text{g}$ .

### 3.2 Chemical analysis of the shells via LA-ICP-MS

Lithium (measured as  $^7\text{Li}$ ) and strontium (measured as  $^{88}\text{Sr}$ ) concentrations of the four specimens were determined by LA-ICP-MS in line scan mode at the Institute of Geosciences, University of Mainz. The majority of measurements were completed within in the iOSL with an approximately uniform distance of 10  $\mu\text{m}$  to the oOSL; only a few data points came from the oOSL (Fig. 1E). Line scans extended from the ventral margin toward the dorsal end of the shell and fully covered the third (last) growing season of each specimen, i.e. calendar year 2013.

Analyses were performed using an ArF EXCIMER laser (193 nm wavelength, NWR193 system by esi/NewWave) coupled to an Agilent 7500ce ICP-MS. The laser was operated at a repetition rate of 10 Hz with laser energy at the sample site of  $\sim 6 \text{ J/cm}^2$ . The line scans were carried out after preablation of the sample surface with a beam diameter of 55  $\mu\text{m}$ , and a scan speed of 5  $\mu\text{m/s}$ . Backgrounds

were measured for 20 s prior to each ablation. NIST SRM 612 was used for calibration, applying the preferred values reported in the GeoReM database (<http://georem.mpch-mainz.gwdg.de/>) (Jochum et al., 2005, Jochum et al., 2011) as the “true” concentrations to calculate the element concentrations in the samples. During each run synthetic NIST SRM 610 (n = 9), basaltic USGS BCR-2G (n = 9) and synthetic carbonate USGS MACS-3 (n = 9) were analyzed as unknowns to monitor accuracy and reproducibility of the analyses. For all materials  $^{43}\text{Ca}$  was used as internal standard applying for the reference materials the Ca concentrations reported in the GeoReM database and for the samples a Ca concentration of 368,000  $\mu\text{g/g}$  previously measured by ICP-OES, respectively. Data processing was performed using a Microsoft Excel spreadsheet following the methods of Longerich et al. (1996) and Jochum et al. (2007, 2011). Average detection limits ( $3\sigma_{\text{background}}$ ; Jochum et al., 2012) were  $0.490 \pm 0.047 \mu\text{g/g}$  for Li and  $0.083 \pm 0.022 \mu\text{g/g}$  for Sr, respectively. On the samples, some Li data points, primarily at the beginning of the growing season were below the limit of detection and were hence removed. Chemical data were temporally contextualized by means of growth pattern analysis (see above). The measured Li and Sr concentrations of the quality control materials agree within 7% with published values and the relative standard deviations (1 RSD) are <6% (Table 2).

**Table 2** Quality control of LA-ICP-MS measurements. Reference materials include NIST SRM610 (synthetic glass), USGS BCR-2G (basalt glass) and USGS MACS-3 (synthetic calcium carbonate). Reference values: NIST SRM610 = GeoReM preferred values (Jochum et al., 2011); USGS BCR-2G = GeoReM preferred values (Jochum et al., 2005); USGS MACS-3 = Jochum et al., 2014). Measured values represent arithmetic averages of all analyses of the respective reference material.

	Reference values		Measured values	
	Strontium [ $\mu\text{g/g}$ ]	Lithium [ $\mu\text{g/g}$ ]	Strontium [ $\mu\text{g/g}$ ]	Lithium [ $\mu\text{g/g}$ ]
NIST SRM 610	$515.5 \pm 2.89$	$468 \pm 24$	$494 \pm 8$	$460 \pm 14$
USGS BCR-2G	$342 \pm 4$	$9 \pm 1$	$319 \pm 4$	$8.9 \pm 0.6$
USGS MACS-3	$6600 \pm 430$	$58 \pm 8$	$6961 \pm 178$	$55 \pm 3$

### 3.3 Chemical analysis of the water via ICP-OES

Calcium, strontium, sodium and lithium concentrations of the water samples were determined with a Spectro CIROS Vision SOP ICP-OES system at the Institute of Geosciences, University of Mainz. Mixed standard solutions were prepared from single element standards for Ca and Sr; Na and Li were analyzed with single element standard solutions. Relative standard deviations (RSD; based on five injections of external standard) were better than 1 RSD% for all elements. Accuracy was 6% for



Ca, 8% for Sr, and 2% for Na and Li, respectively (determined by Roth SolutionX multi element standard solution Lot R459520 for Ca, Sr and Na, and by Merck multi element standard solution Lot OC492641 for Li). If more than one water sample per day was available, values were arithmetically averaged. Salinity was estimated from  $\text{Na}^+$  concentrations applying the equation of DOE (1994):

$$S_{\text{Na}} (\text{PSU}) = \text{Na}^+ (\mu\text{g} \cdot \text{g}^{-1}) \cdot 35/10783.7 \quad (1)$$

### 3.4 Oxygen isotope values of water and carbonate powder via CF-IRMS

Oxygen isotope values of water ( $\delta^{18}\text{O}_{\text{water}}$ ) and carbonate powder samples ( $\delta^{18}\text{O}_{\text{shell}}$ ) were measured with a Thermo Finnigan MAT 253 continuous flow – isotope ratio mass spectrometer equipped with a Gasbench II at the Institute of Geosciences, University of Mainz. Water samples ( $\delta^{18}\text{O}_{\text{water}}$ ) were processed using the equilibration method with  $\text{CO}_2$ . Borosilicate glass exetainers were flushed with a mixture of 0.3%  $\text{CO}_2$  in He and loaded with 0.5 ml of water sample. During 24 hours, samples equilibrated at 25 °C. GISP2, SMOW2 and SLAP2 were used for calibration. Average internal precision was better than 0.1‰.  $\delta^{18}\text{O}_{\text{water}}$  values were calculated against the Vienna Standard Mean Ocean Water (V-SMOW) scale (Gonfiantini, 1978), reported in  $\delta$ -notation and given as parts per mil (‰) (McKinney et al., 1950).

Carbonate powder samples ( $\delta^{18}\text{O}_{\text{shell}}$ ) were dissolved with concentrated phosphoric acid in He-flushed borosilicate exetainers. Data were calibrated against a NBS-19 calibrated IVA Carrara marble ( $\delta^{18}\text{O} = -1.91\text{‰}$ ). On average, internal precision ( $1\sigma$ ) and accuracy were better than 0.04‰. The  $\delta^{18}\text{O}_{\text{shell}}$  values were calculated against the Vienna Pee Dee Belemenite (V-PDB), reported in  $\delta$ -notation and given as parts per mil (‰) (McKinney et al., 1950).

Note that  $\delta^{18}\text{O}$  values of shell aragonite were not adjusted for differences in acid fractionation factors of aragonite and calcite. Using the acid fractionation factors of Kim et al. (2007) for a reaction temperature of 72 °C ( $\alpha_{\text{CO}_2(\text{acid}) - \text{calcite}} = 1.00868$ ;  $\alpha_{\text{CO}_2(\text{acid}) - \text{aragonite}} = 1.00906$ ) actual  $\delta^{18}\text{O}$  values of aragonite would be 0.38‰ more negative than reported here. However, this correction was not applied, because we used the paleotemperature equation by Grossman and Ku (1986) that assumed no differences in acid fractionation factors for the two  $\text{CaCO}_3$  polymorphs. Furthermore, this equation does not take into account temperature-induced changes of the acid fractionation factors. Grossman and Ku (1986) reacted their carbonate samples at 50 and 60 °C and, accordingly, their  $\delta^{18}\text{O}$  values of aragonite

would require a correction ( $1000 \times [\alpha_{\text{CO}_2(\text{acid}) - \text{calcite}} - \alpha_{\text{CO}_2(\text{acid}) - \text{aragonite}}]$ ) by only  $-0.34\text{‰}$  ( $=1000 \times [1.00940 - 1.00974]$ ) and  $-0.36\text{‰}$  ( $=1000 \times [1.00906 - 1.00942]$ ), respectively (acid fraction factors from Kim et al., 2007). In order to compute temperatures with the equation of Grossman and Ku (1986),  $\delta^{18}\text{O}$  values of aragonite processed at  $72\text{ °C}$  would therefore require a correction of  $-0.02$  to  $-0.04\text{‰}$ . Since this difference is smaller than the precision uncertainty of the mass spectrometer (see below), our data were not adjusted.

Since bivalves form their shell near equilibrium with the ambient water,  $\delta^{18}\text{O}_{\text{shell}}$  values can be converted to temperature. *C. edule* forms an entirely aragonitic shell. Hence, the temperature equation (2) by Grossman and Ku (1986) with a scale correction of  $-0.27\text{‰}$ , (Dettman et al., 1999) was applied.

$$T_{\delta^{18}\text{O}} (\text{°C}) = 20.40 - 4.34 \cdot (\delta^{18}\text{O}_{\text{shell}} - (\delta^{18}\text{O}_{\text{water}} - 0.27)) \quad (2)$$

Since  $\delta^{18}\text{O}_{\text{water}}$  at the study site varied by up to  $1.28\text{‰}$  within days (see section 4.1; Fig. 3A), the average seasonal  $\delta^{18}\text{O}_{\text{water}}$  of  $-0.37 \pm 0.39\text{‰}$  ( $\pm 1\sigma$ ) was used for the temperature reconstruction. Calculated temperatures were assigned to respective calendar dates by means of growth pattern analysis. Because growth increments were running nearly parallel to the shell surface in some shell areas, drill holes were partially overlapping (i.e., sampling the same increment). This required arithmetic averaging of some  $\delta^{18}\text{O}_{\text{shell}}$  values. Based on the precision uncertainty of the mass spectrometer, an average temperature uncertainty of  $\pm 0.3\text{ °C}$  was calculated following the error propagation method.

## 4 Results

### 4.1 Water parameters

Between 1 April 2013 and 11 March 2014 water temperatures around high tide varied between  $-1.5\text{ °C}$  (25 January 2014) and  $22.7\text{ °C}$  (2 August 2014) (Fig. 3A, Table 3). The average temperature of the studied time interval was  $11.4 \pm 5.8\text{ °C}$ . Sodium-derived salinity data revealed a seasonal pattern similar to temperature (Fig. 3A, Table 3). However, maxima and minima of both time-series did not occur simultaneously. Highest salinity ( $37.7\text{ PSU}$ ) was recorded in June 2013 and the lowest values ( $28.3\text{ PSU}$ ) in early November 2013 (Fig. 3A).

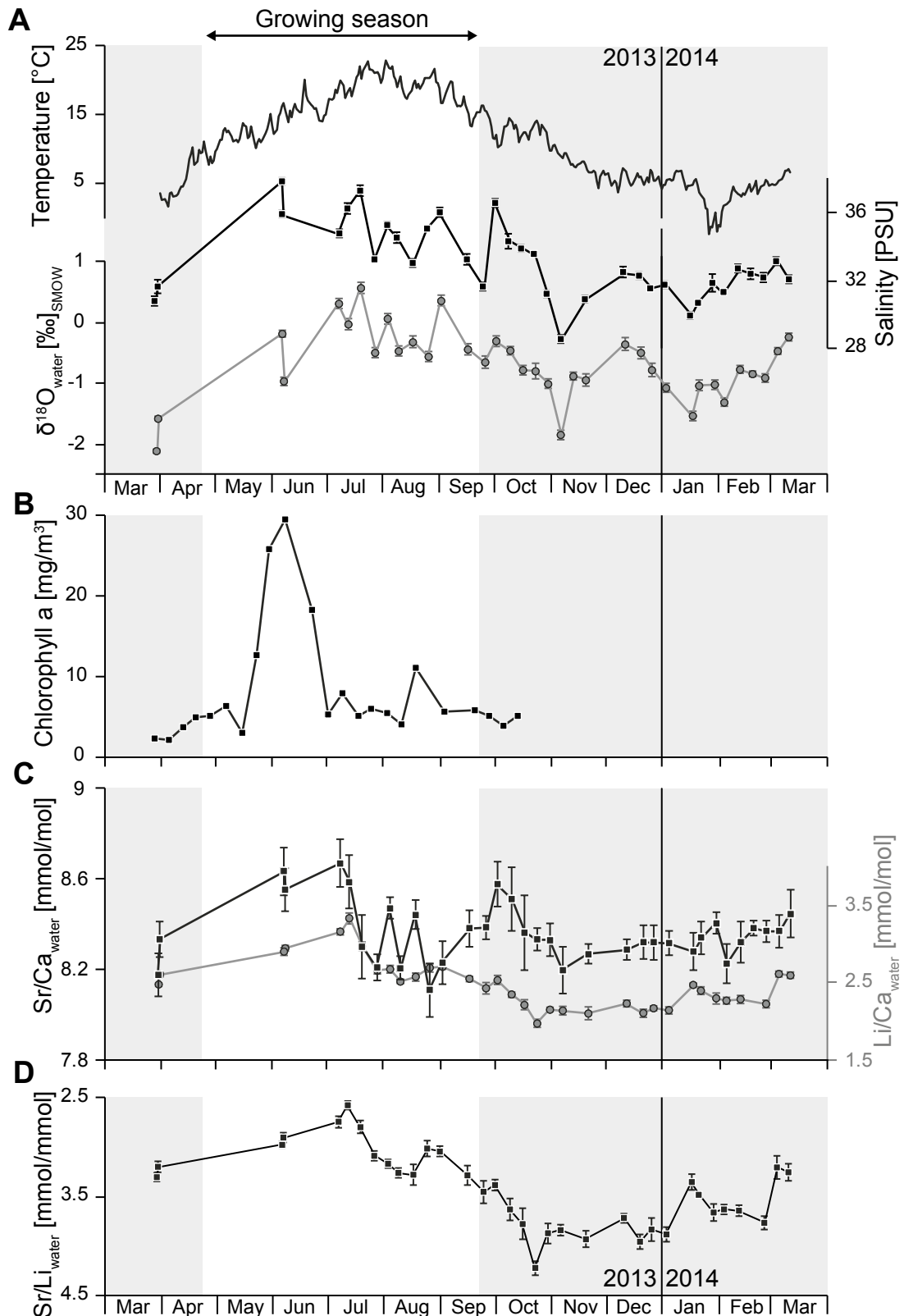


**Fig. 3.** Physico-chemical parameters of the study locality between March 2013 and March 2014. (A) Water temperature (high stand  $\pm 1$  h; arithmetic mean), salinity, and  $\delta^{18}\text{O}_{\text{water}}$ ; (B) Chlorophyll a chronology; (C)  $\text{Sr}/\text{Ca}_{\text{water}}$ ,  $\text{Li}/\text{Ca}_{\text{water}}$  and (D)  $\text{Sr}/\text{Li}_{\text{water}}$  values. Main growing season of *C. edule* during 2013 (19 April  $\pm 7$  days to 16 September  $\pm 7$  days) is indicated by white background; gray color = timing of ‘winter’ growth line formation. Error bars represent 1 $\sigma$  standard deviation.

The oxygen isotope value of the water ( $\delta^{18}\text{O}_{\text{water}}$ ) equaled on average  $-0.69 \pm 0.47\text{‰}$  ( $\pm 1\sigma$ ) and showed a seasonal amplitude of  $2.68\text{‰}$  (Fig. 3A; Table 3). Lowest values ( $-2.14\text{‰}$ ) were recorded in March, and highest values ( $0.54\text{‰}$ ) in August. Variations of up to  $1.28\text{‰}$  between two consecutive days were recorded (6 June 2013 to 7 June 2013). As expected, the  $\delta^{18}\text{O}_{\text{water}}$  values were positively and linearly correlated to salinity ( $r = 0.77$ ;  $r^2 = 0.59$ ;  $p < 0.01$ ).

Chlorophyll a concentration during the growing season of the specimens was, on average,  $10.2 \pm 8.3 \text{ mg/m}^3$  ( $\pm 1\sigma$ ), with highest concentrations ( $29.9 \text{ mg/m}^3$ ) recorded in June and lowest concentrations ( $3.1 \text{ mg/m}^3$ ) in March 2013 (Fig 3B; Table 3).

During the studied time interval,  $\text{Sr}/\text{Ca}_{\text{water}}$  ratios measured  $8.38 \pm 0.13 \text{ mmol/mol}$  (average  $\pm 1\sigma$ ; Fig. 3C; Table 3). Highest  $\text{Sr}/\text{Ca}_{\text{water}}$  ratios (up to  $8.66 \text{ mmol/mol}$ ) were recorded in June and July, lowest ( $8.10 \text{ mmol/mol}$ ) in August 2013.  $\text{Li}/\text{Ca}_{\text{water}}$  ratios were about four times lower than  $\text{Sr}/\text{Ca}_{\text{water}}$  and equaled  $2.52 \pm 0.31 \text{ mmol/mol}$  with most extreme values occurring in October ( $1.97 \text{ mmol/mol}$ ) and July ( $3.15 \text{ mmol/mol}$ ) (Fig. 3C; Table 3). Accordingly,  $\text{Sr}/\text{Li}_{\text{water}}$  ( $= \text{Sr}/\text{Ca} / \text{Li}/\text{Ca}_{\text{water}}$ ) attained lowest values in July ( $2.75 \text{ mmol/mmol}$ ) and highest in October ( $4.23 \text{ mmol/mmol}$ ), and fluctuated around  $3.37 \pm 0.38 \text{ mmol/mmol}$  (average  $\pm 1\sigma$ ) (Fig. 3D; Table 3).

**Table 3** Physico-chemical properties of the water at the study site between 29 March 2013 and 11 March 2014. Growing season = 19 April ( $\pm 1$  week) to 16 September ( $\pm 1$  week) 2013.

	Unit	Observed time interval			Growing season		
		Average $\pm$ 1SD	Min.	Max.	Average $\pm$ 1SD	Min.	Max.
Temperature	$^{\circ}\text{C}$	$11.4 \pm 5.8$	-1.5	22.7	$16.3 \pm 3.8$	8.2	22.7
Salinity	(PSU)	$33.2 \pm 2.0$	28.3	37.7	$35.0 \pm 1.1$	32.8	37.7
$\delta^{18}\text{O}_{\text{water}}$	$\text{‰}_{\text{SMOW}}$	$-0.69 \pm 0.47$	-2.14	0.54	$-0.37 \pm 0.39$	-1.18	0.54
Chlorophyll a	$[\text{mg}/\text{m}^3]$				$10.2 \pm 8.3$	3.1	29.9
$\text{Sr}/\text{Ca}_{\text{water}}$	$\text{mmol/mol}$	$8.38 \pm 0.13$	8.1	8.66	$8.44 \pm 0.15$	8.1	8.66
$\text{Li}/\text{Ca}_{\text{water}}$	$\text{mmol/mol}$	$2.52 \pm 0.31$	1.97	3.15	$2.81 \pm 0.18$	2.51	3.15
$\text{Sr}/\text{Li}_{\text{water}}$	$\text{mmol/mmol}$	$3.37 \pm 0.38$	2.75	4.23	$3.02 \pm 0.16$	2.75	3.28

## 4.2 Timing and rate of shell growth of *Cerastoderma edule*

When the logger was deployed in the field (early April 2013), a distinct annual growth line was visible in specimens of *C. edule*. Likewise, all four specimens collected in the middle of March 2014 showed an annual growth line at the ventral margin, but the growing season of 2014 had not yet started. Between the last two annual growth lines (= growing season of 2013), we counted between 129 and 146 lunar daily growth increments. This corresponds to a duration of the main growing season of ca. five months. Lunar daily growth increment width curves of the four specimens agreed well with each other and showed two peaks near increment numbers 30 ( $46 \pm 10 \mu\text{m}$ ) and 100 ( $44 \pm 16 \mu\text{m}$ ) (Fig. 4). On average, shells grew in height by  $24 \pm 12 \mu\text{m}$  per lunar day (Table 1).

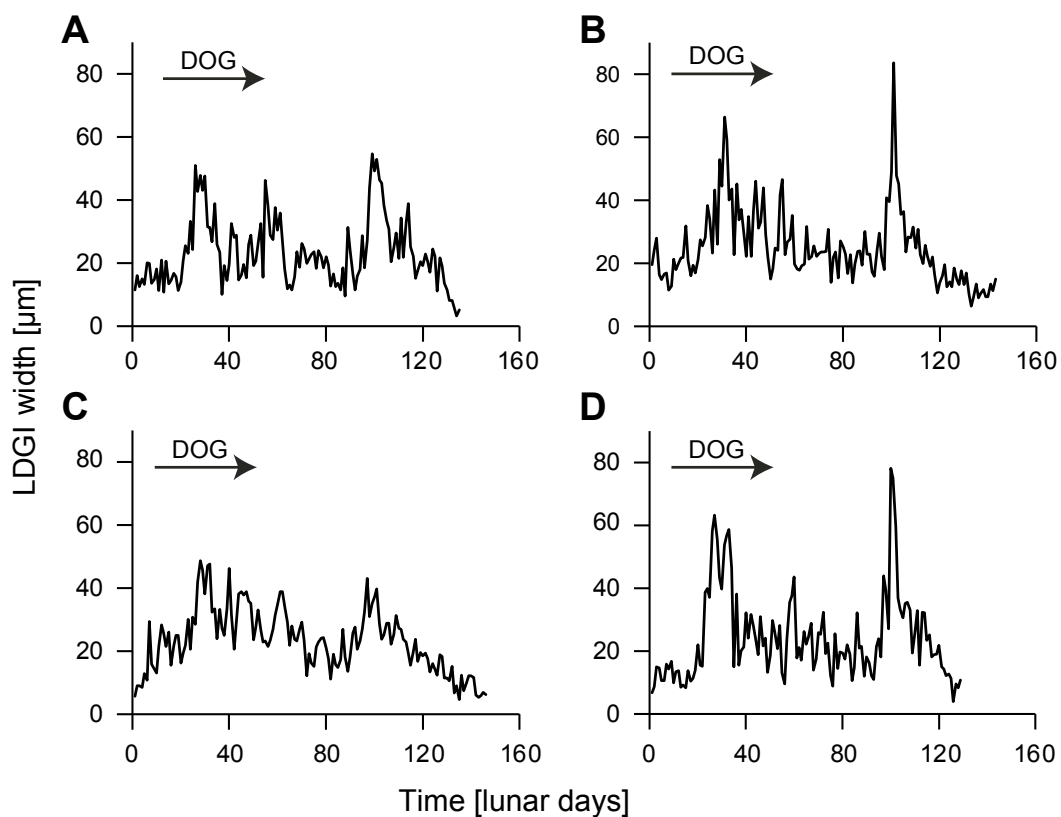


**Fig. 4.** Lunar daily growth increment (LDGI) width chronologies of the four studied *C. edule* specimens. (A) A1, (B) A6, (C) A24 and (D) A28. DOG = direction of growth.

To constrain the timing of seasonal shell growth, the advance of shell growth was studied in the field by visual examination of the newly formed shell material almost every month. On 16 September 2013, the dark annual growth line was about to form in the majority of specimens indicating the main growing season recently ended. Considering the number of daily increments in shells that lived during 2013,

this places the start of the growing season to the middle/end of April (19 April 2013  $\pm$  7 days; Fig. 4). Further verification for the correct temporal alignment comes from the comparison of the shell growth patterns, in particular the alternating lengths of the fortnightly increments, with the tide calendar (Fig. 5; compare Hallmann et al., 2009). The full-to-new moon period (apogee) covers 15 lunar days, whereas the new-to-full moon period (perigee) is 1.5 lunar days shorter. The estimated dating uncertainty is ca. two weeks and results from the difficulty to identify the narrow circalunidian and circatidal increments near the annual growth lines.

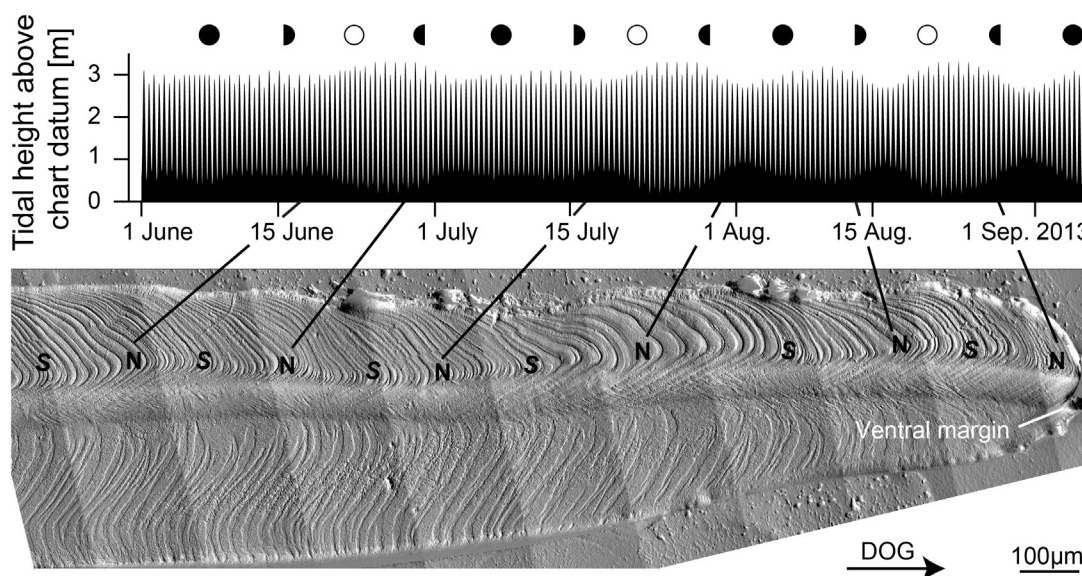


**Fig. 5.** Tidal cycle at the study locality between June and September 2013 and corresponding shell portion of specimen A28. Spring tides occur during full and new moon (open and full circles, respectively), whereas neap tides correspond to half-moon phases (half circles). Full-to-new moon period (apogee) covers 15 lunar days, whereas new-to-full moon period (perigee) covers 13.5 lunar days. The varying length of the fortnightly increment can be utilized for verification of the temporal alignment of the shell record. Broader increments and faint growth lines are laid down during neap tides (N), and narrower increments delimited by more distinct growth lines during spring tides (S). DOG = direction of growth.

During the growing season (19 April  $\pm$  7 days to 16 September  $\pm$  7 days; Fig. 4; Table 1), the bivalves experienced a temperature and salinity range of 16.3 °C (8.2 °C to 22.7 °C) and 35.0 PSU (32.8 to 37.7 PSU), respectively (Fig. 3; Table 3). During the same time interval,  $\text{Sr}/\text{Ca}_{\text{water}}$  fluctuated between 8.10 and 8.66 mmol/mol,  $\text{Li}/\text{Ca}_{\text{water}}$  between 2.51 and 3.15 mmol/mmol and  $\delta^{18}\text{O}_{\text{water}}$  between -1.18‰ and 0.54‰ (Fig. 3; Table 3; see supplementary data for complete dataset).

**Table 3** Oxygen isotope ratios and corresponding temperature reconstructions of the four studied shells

Sample no.	Corresponding time interval	$\delta^{18}\text{O}_{\text{shell}}$ [‰]	$T_{\delta^{18}\text{O}}$ [°C]
A1			
1	15.5. – 12.6.	0.67	14.9
2	13.6. – 22.6.	-0.15	18.5
3	23.6. – 24.7.	-0.69	20.8
4	25.7. – 7.8.	-1.27	23.4
5	13.8. – 31.8.	-0.99	22.1
Mean		-0.49	19.9
Min		-1.27	14.9
Max		0.67	23.4
A6			
1	6.5. – 19.5.	-0.02	17.9
2	20.5. – 15.6.	-0.3	19.1
3	16.6. – 22.7.	-0.56	20.3
4	23.7. – 7.8.	-1.03	22.3
5	8.8. – 8.9.	-0.74	21
Mean		-0.53	20.1
Min		-1.03	17.9
Max		-0.02	22.3
A24			
1	10.5. – 30.5.	0.05	17.6
2	31.5. – 6.7.	-0.81	21.3
3	7.7. – 3.8.	-1.26	23.3
4	4.8. – 20.8.	-1.22	23.1
5	21.8. – 10.9.	-0.68	20.8
Mean		-0.78	21.2
Min		-1.26	17.6
Max		0.05	23.3
A28			
1	10.5. – 30.5.	-0.22	18.8
2	31.5. – 6.7.	-0.44	19.7
3	7.7. – 3.8.	-0.85	21.5
4	4.8. – 20.8.	-1.35	23.7
5	21.8. – 10.9.	-1	22.2
Mean		-0.77	21.2
Min		-1.35	18.8
Max		-0.22	23.7

### 4.3 Oxygen isotope values of shell carbonate and reconstructed temperatures

On average, each sample represented ca.  $22 \pm 8$  lunar days of growth. Average  $\delta^{18}\text{O}_{\text{shell}}$  of the four shells varied between  $-0.49$  and  $-0.78\text{‰}$ . Minimum values ranging from  $-1.35$  to  $-1.03\text{‰}$  and maxima ranging from  $-0.22$  to  $0.67\text{‰}$ , delineated a seasonal cycle with highest amplitudes during the cold season and lowest amplitudes during summer (Table 4).

These values translated into average water temperatures of  $19.9\text{ °C}$  to  $21.2\text{ °C}$ . Reconstructed seasonal temperature minima ranged between  $14.9\text{ °C}$  and  $18.8\text{ °C}$ , maxima between  $22.3\text{ °C}$  and  $23.7\text{ °C}$  (Fig. 6; Table 4). Reconstructed temperatures exceeded instrumental temperatures, on average, by more than  $3\text{ °C}$ . Notably, the offset was typically largest early in the growing season.

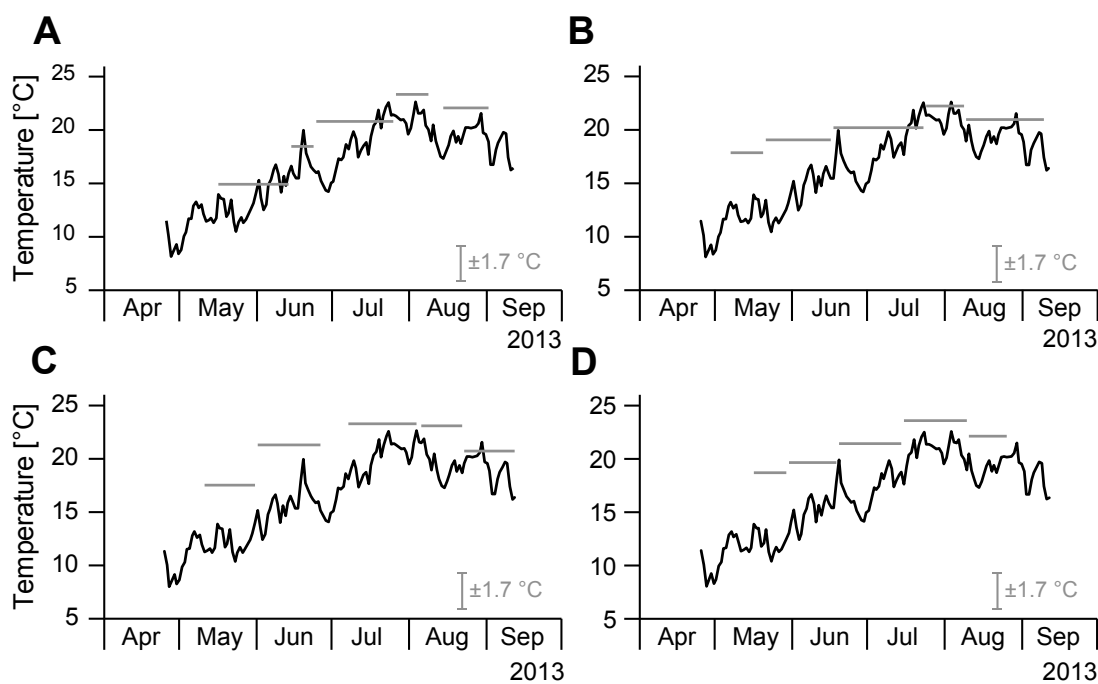


**Fig. 6.** Time-series of measured (black line) and reconstructed water temperature (gray bars). Reconstructed values are based on oxygen isotope values of four shells (A = A1, B = A6, C = A24 and D = A28). Error bars represent potential reconstruction inaccuracies of  $\pm 1.7\text{ °C}$ , derived from 1SD variance ( $0.39\text{‰}$ ) of the seasonal average of  $\delta^{18}\text{O}_{\text{water}}$ .

### 4.4 Element chemistry of shell carbonate and environmental variables

Molar  $\text{Sr}/\text{Ca}_{\text{shell}}$ ,  $\text{Li}/\text{Ca}_{\text{shell}}$  and  $\text{Sr}/\text{Li}_{\text{shell}}$  ratios of four *C. edule* specimens were computed and temporally contextualized by means of sclerochronological analysis (Fig. 7). Chemical data corresponding to the first and last ca. five to ten lunar daily increments were precluded from further analysis due to unclear temporal alignment in these shell portions. Average  $\text{Sr}/\text{Ca}_{\text{shell}}$  of all four specimens were very similar to each other and



measured  $1.67 \pm 0.03$  mmol/mol. Maxima ranged between 2.13 and 2.42 mmol/mol and minima between 1.23 and 1.37 mmol/mol (Table 5).  $\text{Sr}/\text{Ca}_{\text{shell}}$  ratios were typically highest immediately after the annual winter line of 2012/13 and decreased toward summer (Figs. 7A–D). In specimens A6 and A28, values increased toward the end of the growing season of 2013. A weak correlation existed between the  $\text{Sr}/\text{Ca}_{\text{shell}}$  records of specimens A1, A6 and A24 ( $0.23 < r < 0.38$ ;  $p < 0.01$ ). Exceptionally high  $\text{Sr}/\text{Ca}_{\text{shell}}$  ratios of more than 4 mmol/mol were observed in specimen A28 at the beginning of the growing season 2013 (Fig. 7D). Close examination revealed that these data points were derived from the oOSL instead of the iOSL. Hence, these data points were precluded from further interpretation.  $\text{Sr}/\text{Ca}_{\text{shell}}$  ratios were not significantly correlated with either shell growth rate or salinity (Fig. 8; Table 5). However, a weak but statistically significant negative linear correlation ( $-0.29 < r < -0.65$ ;  $p < 0.01$ ) was observed between  $\text{Sr}/\text{Ca}_{\text{shell}}$  and water temperature (Fig. 8G; Table 5).

$\text{Li}/\text{Ca}_{\text{shell}}$  ratios were substantially lower than  $\text{Sr}/\text{Ca}_{\text{shell}}$  (Figs. 7A–D; Table 5). Except for specimen A28 ( $27 \mu\text{mol}/\text{mol}$ ), average  $\text{Li}/\text{Ca}_{\text{shell}}$  values of the studied specimens were nearly identical and equaled  $19 \pm 2 \mu\text{mol}/\text{mol}$ .  $\text{Li}/\text{Ca}_{\text{shell}}$  curves of the studied specimens were closely correlated to each other ( $0.78 < r < 0.94$ ;  $p < 0.01$ ). In all studied specimens,  $\text{Li}/\text{Ca}_{\text{shell}}$  ratios increased exponentially toward summer and then decreased toward the end of the growing season (Aug/Sep; Figs. 7A–D). Similar to  $\text{Sr}/\text{Ca}_{\text{shell}}$ ,  $\text{Li}/\text{Ca}_{\text{shell}}$  ratios were neither correlated to salinity or shell growth rate (Figs. 8A+E, Table 5). However, 56 to 73% of  $\text{Li}/\text{Ca}_{\text{shell}}$  variations were explained by water temperature (Fig. 8H; Table 5).

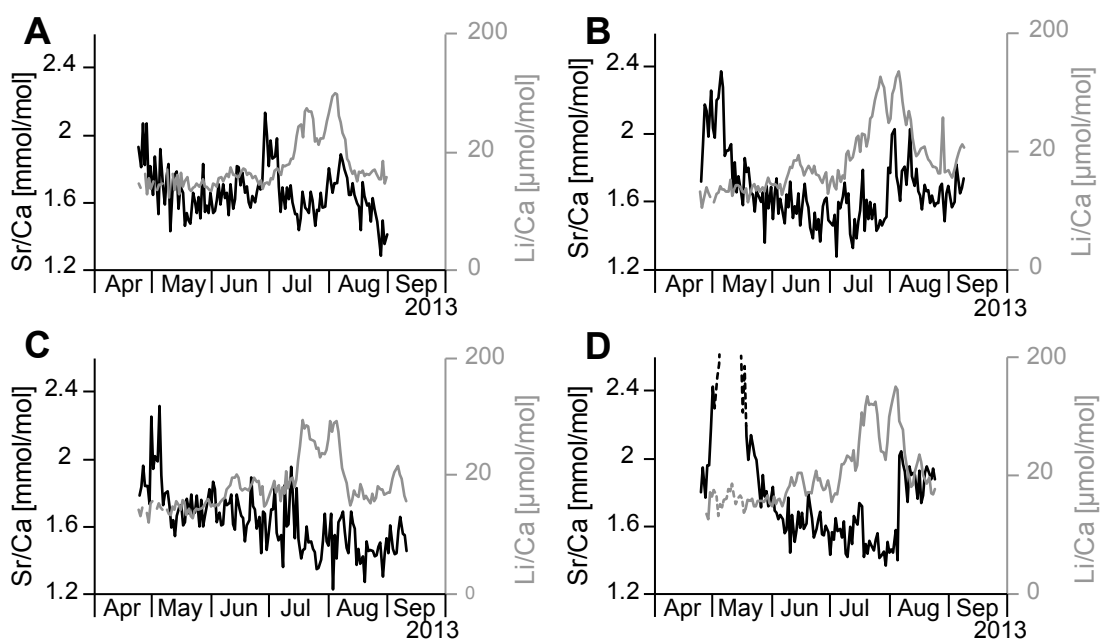


**Fig. 7.**  $\text{Sr}/\text{Ca}_{\text{shell}}$  (black) and  $\text{Li}/\text{Ca}_{\text{shell}}$  (gray) time-series of the oOSL of the four studied shells (A = A1, B = A6, C = A24 and D = A28). Dashed line in D stands for data measured in the iOSL.

**Table 5** Relationship between geochemical properties of the studied shells of *Cerastoderma edule* and environmental parameters during main growing season of 2013.

Shell ID	A1			A6			A24			A28			Average		
	Sr/Ca	Li/Ca	Sr/Li	Sr/Ca	Li/Ca	Sr/Li	Sr/Ca	Li/Ca	Sr/Li	Sr/Ca	Li/Ca	Sr/Li	Sr/Ca	Li/Ca	Sr/Li
Unit	[mmol/ mol]	[ $\mu$ mol/ mol]	[mmol/ mmol]	[mmol/ mol]	[ $\mu$ mol/ mol]	[mmol/ mmol]	[mmol/ mol]	[ $\mu$ mol/ mol]	[mmol/ mmol]	[mmol/ mol]	[ $\mu$ mol/ mol]	[mmol/ mmol]	[mmol/ mol]	[ $\mu$ mol/ mol]	[mmol/ mmol]
N	121	125	121	132	133	132	132	135	132	102	104	102	135	135	135
Average $\pm$ 1SD	$1.66 \pm 0.15$	$18 \pm 12$	$119 \pm 45$	$1.67 \pm 0.20$	$21 \pm 18$	$118 \pm 62$	$1.63 \pm 0.18$	$19 \pm 12$	$110 \pm 46$	$1.71 \pm 0.22$	$27 \pm 23$	$95 \pm 50$	$1.66 \pm 0.13$	$20 \pm 15$	$115 \pm 50$
Min.	1.29	8	28	1.28	7	18	1.23	8	24	1.37	8	14	1.43	9	21
Max.	2.13	62	231	2.37	96	284	2.32	59	213	2.42	109	231	2.13	79	247
	Linear regressions: Element-to-element ratio of shell vs. lunar daily growth increment width														
r	0.04	0.24	-0.15	0.01	0.13	0	0.14	-0.03	0.16	0	0.11	-0.03	0.05	0.18	-0.04
r <sup>2</sup>	0	0.06	0.02	0	0.02	0	0.02	0	0.03	0	0.01	0	0	0.03	0
p	0.69	<0.01	0.09	0.87	0.14	0.99	0.1	0.75	0.07	0.97	0.28	0.77	0.57	0.04	0.67
	Linear regressions: Element-to-element ratio of shell vs. chlorophyll a														
r	-0.07	-0.32	0.26	-0.33	-0.28	0.05	0.14	-0.22	0.1	-0.19	-0.4	0.26	-0.15	-0.27	0.09
r <sup>2</sup>	0	0.1	0.07	0.11	0.08	0	0.02	0.05	0.01	0.04	0.16	0.07	0.02	0.07	0.01
p	0.44	<0.01	<0.01	<0.01	<0.01	0.57	0.1	0.01	0.25	0.06	<0.01	<0.01	0.09	<0.01	0.28
	Linear regressions: Element-to-element ratio of shell vs. Element-to-element ratio of respective water value														
r	0.3	-0.23	-0.1	-0.08	-0.38	-0.04	0.47	-0.12	0.05	-0.09	-0.24	0.04	0.25	-0.23	0.02
r <sup>2</sup>	0.09	0.05	0.01	0.01	0.15	0	0.22	0.01	0	0.01	0.06	0	0.06	0.05	0
p	<0.01	0.01	0.28	0.36	<0.01	0.61	<0.01	0.17	0.55	0.23	0.01	0.66	<0.01	<0.01	0.81
	Linear regressions: Element-to-element ratio of shell vs. salinity														
r	-0.26	-0.06	0.1	-0.24	-0.33	0.19	0.21	-0.04	0.18	-0.09	-0.08	0.23	-0.12	-0.14	0.14
r <sup>2</sup>	0.07	0	0.01	0.06	0.11	0.04	0.04	0	0.03	0.01	0.01	0.05	0.01	0.02	0.02
p	<0.01	0.53	0.3	<0.01	<0.01	0.03	0.02	0.61	0.04	0.37	0.43	0.02	0.18	0.11	0.09
	Linear regressions: Sr/Ca <sub>shell</sub> , Sr/Li <sub>shell</sub> vs. temperature; exponential regressions Li/Ca <sub>shell</sub> vs. temperature														
r	-0.29	0.81	-0.8	-0.42	0.75	-0.87	-0.66	0.84	-0.88	-0.53	0.85	-0.84	-0.66	0.85	-0.9
r <sup>2</sup>	0.08	0.65	0.64	0.18	0.56	0.76	0.44	0.7	0.77	0.28	0.73	0.71	0.44	0.72	0.81
p	<0.01	<0.01	<0.01	<0.01	<0.01	<0.01	<0.01	<0.01	<0.01	<0.01	<0.01	<0.01	<0.01	<0.01	<0.01

Average  $\text{Sr}/\text{Ca}_{\text{shell}}$  and  $\text{Li}/\text{Ca}_{\text{shell}}$  ratios remained ca. five and 150 times below corresponding values in the water during the growing season, respectively ( $\text{Sr}/\text{Ca}_{\text{water}} = 8.44 \pm 0.15$  mmol/mol;  $\text{Li}/\text{Ca}_{\text{water}} = 2.81 \pm 0.18$  mmol/mol). Both element-to-calcium ratios were uncorrelated to variations of respective values in the ambient water (Figs. 8A+F; Table 5) and exhibited two to fourfold larger seasonal ranges (Figs. 8A+F; compare Tables 3+5). Partition coefficients of both elements were well below one ( $K_{\text{Sr/Ca}}^D = \text{Sr}/\text{Ca}_{\text{shell}} / \text{Sr}/\text{Ca}_{\text{water}} = 0.20 \pm 0.02$ , min = 0.17, max = 0.25;  $K_{\text{Li/Ca}}^D = \text{Li}/\text{Ca}_{\text{shell}} / \text{Li}/\text{Ca}_{\text{water}} = 0.007 \pm 0.005$ , min = 0.003, max = 0.30).

$\text{Sr}/\text{Li}_{\text{shell}}$  ratios of the studied specimens varied between  $21 \pm 6$  mmol/mol and  $240 \pm 31$  mmol/mmol. Average  $\text{Sr}/\text{Li}_{\text{shell}}$  ratios ( $111 \pm 12$  mmol/mmol) were up to 40 times larger than respective values in the water ( $3.02 \pm 0.16$  mmol/mmol) (Figs. 9A-D, I; Tables 3+5).  $\text{Sr}/\text{Li}_{\text{shell}}$  curves of the four specimens were strongly correlated to each other ( $0.61 < r^2 < 0.82$ ;  $p < 0.01$ ). Furthermore,  $\text{Sr}/\text{Li}_{\text{shell}}$  values were strongly and inversely correlated to water temperature ( $-0.80 < r < -0.88$ ;  $0.64 < r^2 < 0.77$ ;  $p < 0.01$ ; Figs. 9E–H+J; Table 5).

A linear regression model was constructed from  $\text{Sr}/\text{Li}_{\text{shell}}$  data of three specimens (A1, A6 and A28) and daily water temperature ( $n = 355$ ;  $r = -0.82$ ;  $r^2 = 0.68$ ;  $p < 0.01$ ; Fig. 10A):

$$\text{Sr}/\text{Li} [\text{mmol}/\text{mmol}] = -12.4 (\pm 0.5) \cdot T [^\circ\text{C}] + 320 (\pm 8), \quad (3)$$

where errors are given as 1 standard error. To evaluate how well ambient water temperature can be reconstructed from  $\text{Sr}/\text{Li}_{\text{shell}}$ , this model was solved for temperature

$$T [^\circ\text{C}] = ((\text{Sr}/\text{Li}) [\text{mmol}/\text{mmol}] - 320 (\pm 8)) / -12.4 (\pm 0.5) \quad (4)$$

and then applied to specimen A24 (Fig. 10B). Reconstructed average ( $17.0 \pm 3.7$  °C), minimum ( $8.7$  °C) and maximum water temperatures ( $23.9$  °C) agreed well with instrumental recordings (average =  $16.3 \pm 3.6$  °C; minimum =  $8.2$  °C; maximum =  $22.7$  °C). The average difference between reconstructed and measured water temperature was less than  $\pm 1.5$  °C.

## 5 Discussion

Reconstructed water temperatures based on oxygen isotopes of *Cerastoderma edule* almost consistently overestimated logged temperatures (Fig. 6). Such a constant offset can be explained by an inaccurate  $\delta^{18}\text{O}_{\text{water}}$  value applied for the reconstruction. Temperature estimates would be much more accurate, if a lower  $\delta^{18}\text{O}_{\text{water}}$  value of -1‰ was applied. The difference between best-suited and measured  $\delta^{18}\text{O}_{\text{water}}$  value is likely explained by the timing of sample collection (low tide). Stronger evapotranspiration (Craig and Gordon, 1965) during neap tide results in a more positive  $\delta^{18}\text{O}_{\text{water}}$  value. Consequently, the measured  $\delta^{18}\text{O}_{\text{water}}$  value inaccurately reflects the  $\delta^{18}\text{O}_{\text{water}}$  during high tide, i.e., the time during which intertidal bivalves produce their shell. Moreover, freshwater influxes from two large rivers nearby (Weser and Elbe estuaries) can further modify the  $\delta^{18}\text{O}_{\text{water}}$  value during high tide. As a result, it becomes a challenging task to reconstruct accurate temperatures from  $\delta^{18}\text{O}_{\text{shell}}$  values of recent or fossil *C. edule* specimens inhabiting intertidal zones.

In contrast, temperatures reconstructed from  $\text{Sr}/\text{Li}_{\text{shell}}$  closely resembled logged temperatures. Up to 81% of the variability in  $\text{Sr}/\text{Li}_{\text{shell}}$  was explained by temperature. Even without considering  $\text{Sr}/\text{Li}_{\text{water}}$  in the equation, calculated and logged daily temperatures differed, on average, by only  $\pm 1.5$  °C. This suggests that  $\text{Sr}/\text{Li}_{\text{shell}}$  ratios function as a potential new paleotemperature, especially in nearshore environments.  $\Delta_{47}$  based temperature reconstructions can theoretically be nearly as precise as  $\text{Sr}/\text{Li}_{\text{shell}}$  based temperature predictions but on the expense of sampling (and hence temporal) resolution. Sr and Li concentrations can be obtained quickly by in-situ chemical analyses, e.g., with a quadrupole LA-ICP-MS system. This analytical technique also provides a sampling resolution of tens of micrometers representing shell portions that formed within a few days.

### 5.1 Vital effects

As in other bivalves (Gillikin et al., 2005; Surge and Walker, 2006), the incorporation of trace elements, here, Sr and Li into shells of *Cerastoderma edule*, is under strong biological control. This is firstly indicated by vastly different concentrations of these elements (and element-to-calcium ratios) in microstructurally different shell portions. For example, higher Sr levels were determined in the oOSL (composite prismatic microstructure) than in the iOSL (simple crossed-lamellar microstructure). These observations are in agreement with data reported previously for this species, for example, by Hallam and Price (1968) who demonstrated that the inner shell layer

(complex crossed lamellar) contains, on average, 54% more Sr than the outer shell layer. Similar findings were also reported for trace and minor elements in shells of other bivalve species (e.g., Shirai et al., 2008, 2014; Schöne et al., 2013; Auzoux-Bordenave et al., 2015; Poulain et al., 2015). If the amount of impurities was solely controlled by thermodynamics, Sr and Li levels in contemporaneous shell portions with different skeletal architectures should be similar. Furthermore, the distribution coefficients of both elements not only remained significantly below one (average  $K_{\text{Sr/Ca}}^D = 0.20$ ;  $K_{\text{Li/Ca}}^D = 0.007$ ), but were also different than those expected for or determined in synthetic aragonite ( $K_{\text{Sr/Ca}}^D \approx 1$ , Kinsman and Holland, 1969; Kitano et al., 1971; Gaetani and Cohen, 2006;  $K_{\text{Li/Ca}}^D \approx 0.003$ , Marriott et al., 2004a). These findings substantiate the hypothesis that vital effects govern the incorporation of Sr and Li into shells of *C. edule*.

Although the exact mechanisms controlling the amount of trace impurities in shells are not well understood, the formation of shell material occurs from a fluid (extrapallial fluid, EPF) that should have almost the same ionic composition and ionic strength as the ambient water (Wada and Fujinuki, 1976). This is because bivalves are osmoconformers (Stewart, 1984) and ions can passively move through ion channels (Carré et al., 2006) of the mantle epithelia which separate the EPF from the body fluids and the outer environment. For the main inorganic building blocks of shell formation,  $\text{Ca}^{2+}$  and  $\text{HCO}_3^-$ , active transmembrane enzymatic transport systems are in operation (see further below), and these elements are therefore enriched in the EPF (e.g., Crenshaw, 1972). Since the EPF is nearly isosmotic with the ambient environment with regard to minor and trace elements, the shell should have the same ionic composition as seawater. Evidently, this is not the case. It is assumed that organic macromolecules in the EPF and in the form of organic templates at the crystallization front are responsible for which and how much trace elements are incorporated into the biomineral and which skeletal architecture is produced at specific sites of the shell (Marin et al., 2012; Shirai et al., 2014). In fact, these macromolecules cannot only function as nuclei for the formation of new crystals, they can also inhibit growth when attached to certain crystal planes (Marin et al., 2007) and slightly alter the crystal structure (Pokroy et al., 2004, 2007). Furthermore, Stephanson et al. (2008) showed that concentrations of certain peptides in the calcifying fluid can significantly change the amount of magnesium incorporated into abiogenic calcite. This is of particular importance, because a seasonal variation of the concentration of organic macromolecules with specific binding properties in the EPF has also been demonstrated (Moura et al., 2000). In consequence, the distribution of trace elements between the EPF and the mineral formed under biological control can deviate from expectations based on abiogenic precipitation experiments (see comparison of  $K^D$  values above).

## 5.2 Growth rate and crystal kinetic effects

The incorporation of trace and minor elements into the shell of *C. edule* could potentially be influenced by growth rate, as it has been demonstrated in some other bivalve species (Vander Putten et al., 2000; Gillikin et al., 2005). At higher growth rates, some elements may be deposited away from thermodynamic equilibrium because the demand for these elements exceeds the supply rate which is accomplished through transmembrane diffusion. For example, Thébault et al. (2009) demonstrated a strong covariation of  $\text{Li}/\text{Ca}_{\text{shell}}$  and shell growth rate of *Arctica islandica*. In the case of *C. edule*, however, such growth rate effects do not seem to influence the lithium content of the shells, because shell growth and  $\text{Li}/\text{Ca}_{\text{shell}}$  were uncorrelated (Figs. 8A+C; Table 5).

Growth rate can reportedly also control the incorporation of  $\text{Sr}^{2+}$  in bivalve shells. To avoid any shortage of the main building materials for shell production,  $\text{Ca}^{2+}$  and  $\text{HCO}_3^-$  reach the EPF also in the form of membrane-coated, amorphous calcium carbonate-rich (ACC) vesicles (Jacob et al., 2011) and in particular, through transmembrane pumps (Gillikin et al., 2005; McConnaughey and Gillikin, 2008; Marin et al., 2012). For example,  $\text{Ca}^{2+}$ -ATPase enzymes pump  $\text{Ca}^{2+}$  to the site of calcification and, in exchange for each calcium ion, two  $\text{H}^+$  ions away from the EPF (Wheeler, 1992). Active removal of protons also maintains alkaline conditions near the calcifying front. Support for the existence of such active transport mechanisms has recently been provided by pH measurements according to which the pH increases from the growing edge ( $\text{H}^+$  produced during calcification) toward the outer mantle epithelium (Stemmer et al., in press). Since the ionic radius of  $\text{Sr}^{2+}$  (1.31 Å; Shannon, 1976) is similar to that of  $\text{Ca}^{2+}$  (1.18 Å; Shannon, 1976), strontium can occasionally reach the EPF through these  $\text{Ca}^{2+}$ -ATPase pumps as well (Carré et al., 2006). Faster shell growth should therefore not only result in elevated  $\text{Ca}^{2+}$ -ATPase activity and an enrichment of  $\text{Ca}^{2+}$  in the EPF, but also in a relative depletion of  $\text{Sr}^{2+}$  in the EPF. Some authors therefore suggested that higher precipitation rates are associated with lower  $\text{Sr}/\text{Ca}_{\text{shell}}$  ratios (e.g., Carré et al., 2006). However, shell growth rate and strontium levels of *C. edule* were not correlated (Figs. 8A+C). Therefore, growth rate effects do not explain the variability of strontium in the shell of this species. These findings suggest that a growth rate control of trace and minor element incorporation in bivalve shells likely is a species-specific phenomenon.

Moreover, crystal kinetic effects in the form of precipitation rate have been shown to exert control on the distribution coefficient of trace elements in synthetic calcium carbonate (Busenberg and Plummer, 1985; Gaetani and Cohen, 2006; Gabitov et al., 2011). Two independent explanations for this correlation were proposed:

(a) The growth entrapment model, according to which particularly fast growth prevents equilibration of a newly formed, enriched layer on the surface of the crystal with the surrounding fluid, resulting in the entrapment of large amounts of certain elements (Watson and Liang, 1995, Gaetani and Cohen, 2006; Gabitov et al., 2011), (b) The incorporation of certain monovalent ions at interstitial sites, i.e., at sites which are known to increase in calcite with higher growth rates (Busenberg and Plummer, 1985). Consequently, the distribution coefficients of  $\text{Sr}^{2+}$ ,  $\text{Li}^+$  and  $\text{Sr/Li}$  ( $K^D_{\text{Sr/Li}}$ ) of *C. edule* can change as function of kinetic effects. A verification of these effects in calcium carbonate formed under biological control remains challenging, because the final composition of the biomineral is influenced by additional factors. If, for example, growth rate is used as a proxy for crystal precipitation rate, results must be interpreted carefully, because growth rate also exerts control on the composition of the calcifying fluid (see above). Since faster shell growth is inevitably associated with increased precipitation rate, at least a weak relationship should exist between shell growth rate and the trace element composition, if one of the aforementioned effects exerts a major control on the distribution coefficient of trace elements in shells of *C. edule*. As this is clearly not the case, both models seem to be inapplicable to explain the variations observed here. In the case of the growth entrapment model, this might be caused by the full biological control under which crystallization is proceeding, with organic material at least partly surrounding growing crystals (Marin et al., 2007, 2012) and thus regulating processes occurring at the crystal surface. A deviation from the correlation between the number interstitial sites and the concentration of monovalent ions in calcite demonstrated by Busenberg and Plummer (1985) is not surprising, because *C. edule* produces only the  $\text{CaCO}_3$  polymorph aragonite, for which precipitation experiments demonstrated the incorporation of monovalent ions by substitution into the crystal lattice and not into interstitial sites (Okumura and Kitano, 1986).

### 5.3 Rayleigh fractionation

In the case of foraminifera (Elderfield et al., 1996; Bryan and Marchitto, 2008) and corals (Gagnon et al., 2007; Case et al., 2010; Hathrone et al., 2013.), the distribution of trace elements in the skeletons has been explained by Rayleigh fractionation (Albarède, 1996). This model requires formation of a biomineral in a closed or semi-closed system. While the biomineral forms, the calcifying solution becomes depleted in elements that are preferably incorporated into the biomineral, i.e. elements with a distribution coefficient larger than one, and enriched in elements that are preferably excluded from the biomineral, i.e. elements with a  $K^D$  value smaller than one. In turn, the elemental chemistry of the biomineral also evolves and becomes continuously

enriched in compatible elements and depleted in elements that are preferentially excluded from the biomineral. As a consequence, elements that are preferentially excluded from skeletal aragonite and have  $K^D$  values  $\ll 1$  should be strongly positively correlated with each other. However, this is not the case in bivalves. For example, Sr and Li of *C. edule* are uncorrelated although both elements have  $K^D$  values  $\ll 1$ .

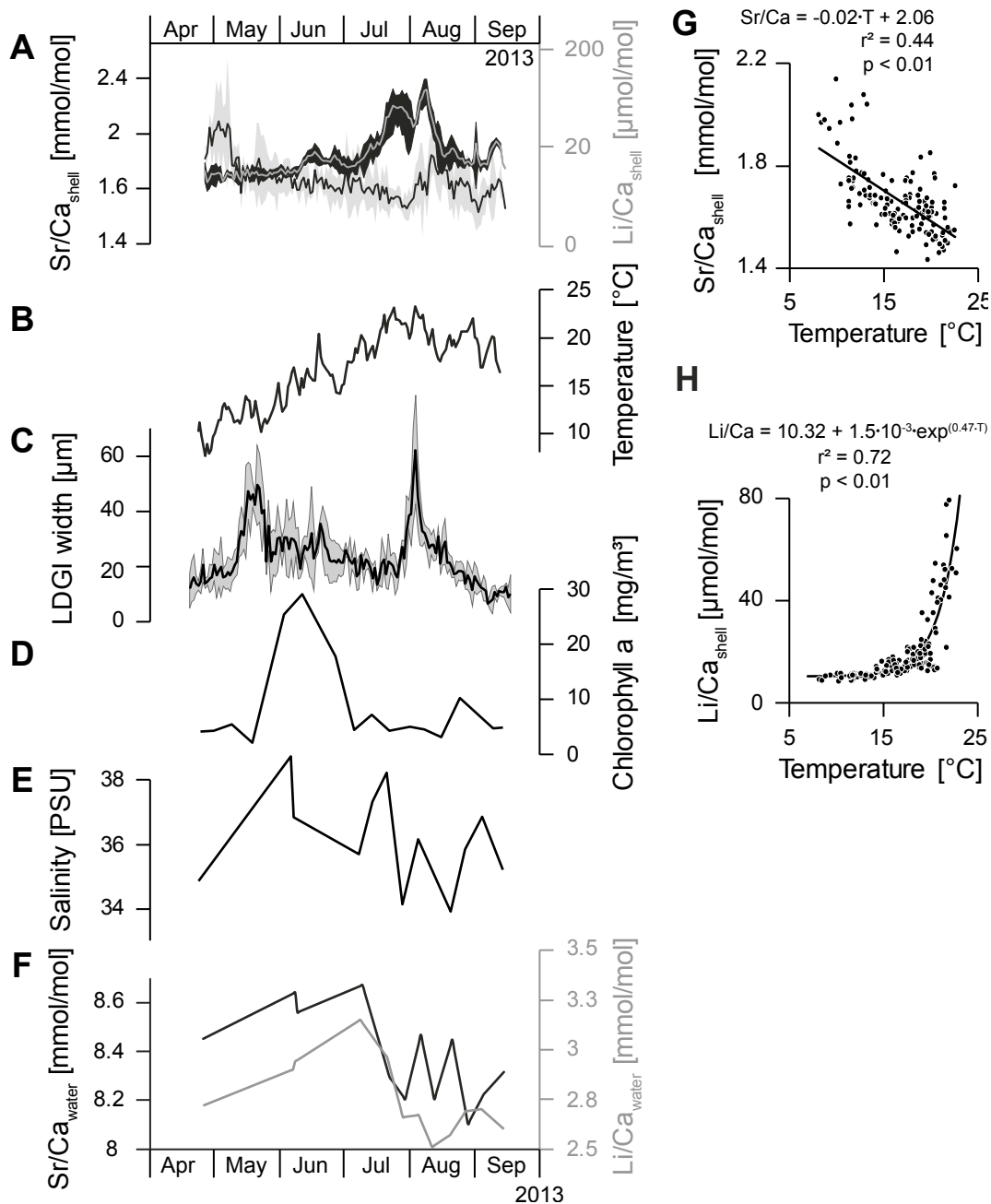


**Fig. 8.** Sclerochronological data of the shell and physico-chemical properties of the ambient water. (A) Average (±1 SD) Sr/Ca<sub>shell</sub> (black) and Li/Ca<sub>shell</sub> (gray) profiles of all four shells. (B) Water temperature; (C) Average (±1 SD) lunar daily growth increment width (LDGI) chronology; (D) Chlorophyll a; (E) Salinity; (F) Sr/Ca<sub>water</sub> and Li/Ca<sub>water</sub> time-series. Regression analysis of water temperature and (G) Sr/Ca<sub>shell</sub> and (H) Li/Ca<sub>shell</sub>.



## 5.4 Salinity and elemental chemistry of the water

The Sr/Ca ratio of biominerals is often considered as a temperature proxy that is largely independent from salinity, because Sr/Ca values in seawater at salinities above 10 remain invariant (Dodd and Crisp, 1982), even on geological longer time scales (Beck et al., 1992). However, a closer look at the data provided in Dodd and Crisp (1982) reveals significant variations. For example, between salinities of 13 (“High Island Beach”) and 35.9 (“Offshore Gulf”), the molar  $\text{Sr/Ca}_{\text{water}}$  values computed from the ion levels given in Dodd and Crisp (1982) fluctuate between 7.5 and 8.8 mmol/mol. Between salinities of 32.7 (“Arkata Boat Ramp”) and 35.9 (“Offshore Gulf”),  $\text{Sr/Ca}_{\text{water}}$  ratios still vary by 0.8 mmol/mol (8 to 8.8 mmol/mol).

The effect of fluctuating  $\text{Sr/Ca}_{\text{water}}$  ratios on temperature estimates based on  $\text{Sr/Ca}_{\text{shell}}$  of *C. edule* can easily be computed from the  $K^D_{\text{Sr/Ca}}$  value (average = 0.20) and the temperature sensitivity (-0.02 mmol/mol/°C) of this species. In the present study,  $\text{Sr/Ca}_{\text{water}}$  varied by ca. 0.6 mmol/mol during the growing season. Corresponding  $\text{Sr/Ca}_{\text{shell}}$  values of *C. edule* would show a seasonal range of ca. 0.12 mmol/mol (if temperature remained invariant). This value corresponds to a temperature range of 6°C. In other words, if the  $\text{Sr/Ca}_{\text{water}}$  variability remains unnoticed, temperature estimates can be off by as much as  $\pm 3$  °C. In the case of  $\text{Sr/Li}_{\text{shell}}$ , the average potential error caused by seasonal changes of the  $\text{Sr/Li}_{\text{water}}$  ratio is only ca.  $\pm 0.8$  °C ( $K^D_{\text{Sr/Li}}$ : Average = 38; 7 to 80 at high and low temperature, respectively; temperature sensitivity of  $\text{Sr/Li}_{\text{shell}} = 12.4$  mmol/mmol/°C; seasonal range of  $\text{Sr/Li}_{\text{water}} = 0.5$  mmol/mmol).

Although our data did not indicate any statistical correlation between  $\text{Sr/Ca}_{\text{shell}}$ ,  $\text{Li/Ca}_{\text{shell}}$  or  $\text{Sr/Li}_{\text{shell}}$  and salinity – an observation which is in line with previous reports on bivalves (Freitas et al., 2006; Wanamaker et al., 2008), cold- and warm-water corals (Hathorne et al., 2013; Raddatz et al., 2013) and inorganic carbonates (Marriott et al., 2004a) – it should be kept in mind that the chemical composition of water in coastal settings can slightly vary, especially on short time-scales, and affect temperature estimates based on variations of trace and minor elements in the shells. On the other hand, the empirically determined average temperature uncertainty based on  $\text{Sr/Li}_{\text{shell}}$  was only  $\pm 1.5$  °C, which justifies to further explore this ratio as a promising new temperature proxy in bivalve shells.

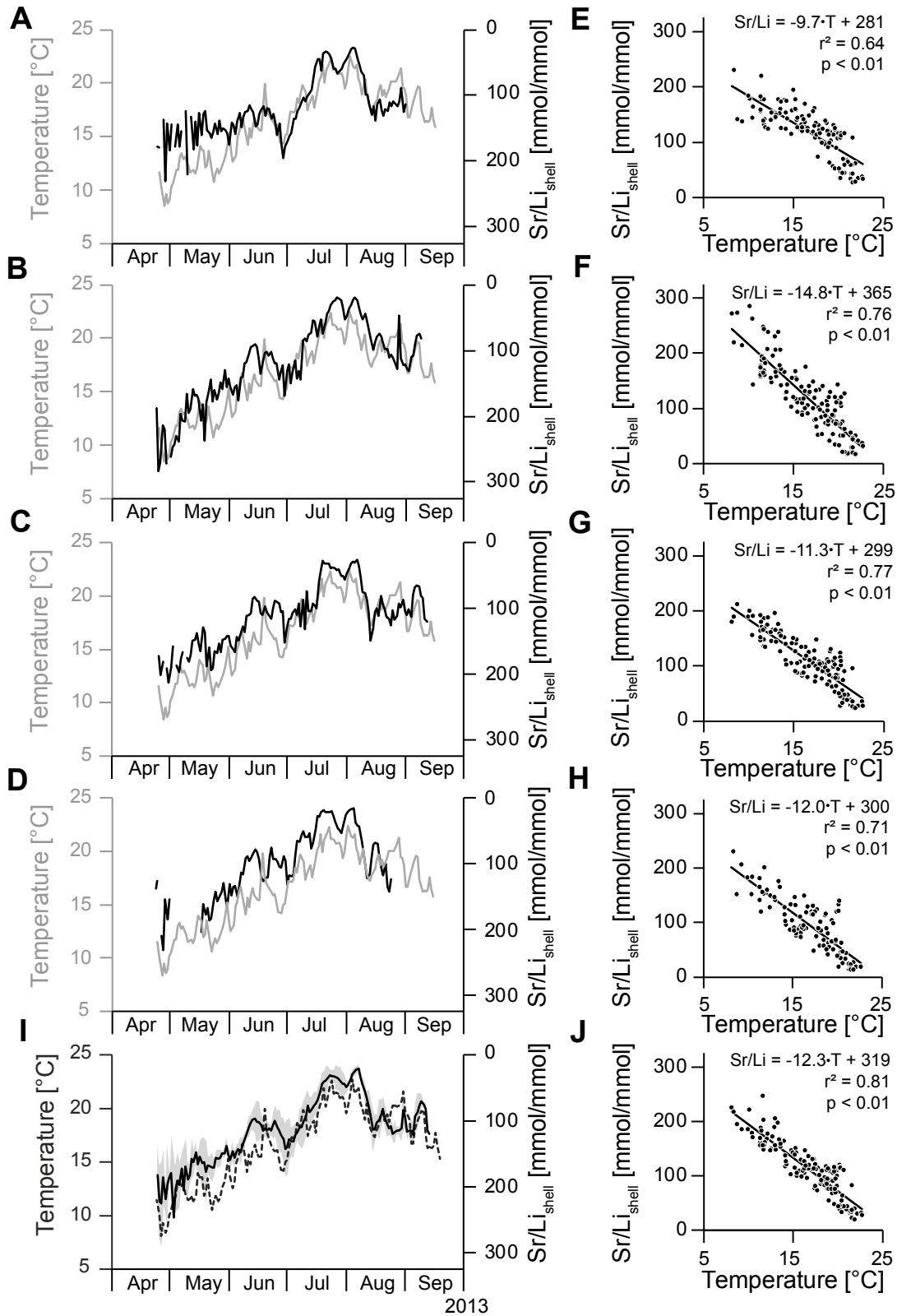


**Fig. 9.** Relationship between geochemical properties of the shell and water temperature. Sr/Li<sub>shell</sub> time-series (black) vs. water temperature (gray) (A = A1, B = A6, C = A24 and D = A28). (E–H) Linear regression analyses of A–D. (I) Average Sr/Li<sub>shell</sub> chronology ( $\pm 1$  SD) of all four specimens (black) vs. water temperature (dashed black). (J) Cross-plot of data shown in (I).

## 5.5 Ocean productivity

In previous studies on bivalves, changes of  $\text{Li}/\text{Ca}_{\text{shell}}$  values were interpreted to reflect changes in ocean productivity (Thébault and Chauvaud, 2013). During diatom blooms, *Pecten maximus* showed elevated  $\text{Li}/\text{Ca}_{\text{shell}}$  values. In the present study, however,  $\text{Li}/\text{Ca}$  peaks of *C. edule* lagged ca. 1.5 months behind the seasonal primary productivity maximum (Figs. 8A+D). In addition,  $\text{Li}/\text{Ca}_{\text{shell}}$  time-series showed a distinct double peak in summer that agreed well with the two temperature maxima, whereas the Chlorophyll a curve only showed a single peak (Figs. 8A+D).

## 5.6 Occurrence of trace and minor elements in bivalve shells

It is still largely unresolved in which form the various different trace and minor elements co-precipitate with calcium carbonate. In coral and synthetic aragonite, for example, the substitution for  $\text{Ca}^{2+}$  in the crystal lattice (Amiel et al., 1973; Okumura and Kitano, 1986) and the absorption to mineral surfaces were shown for certain elements (Watanabe et al., 2001). In abiogenic calcite, lattice defects were demonstrated as another possible incorporation site (Busenberg and Plummer, 1985). In bivalve shells, trace elements were additionally found in the form of separate mineral phases (Odum, 1951; Fritz et al., 1990, 1992) and bound to organics (Foster et al., 2008; Schöne et al., 2010). Following Goldschmidt (1926), strontium as a divalent cation with similar ionic radius ( $\text{Sr}^{2+}$ : 1.31 Å,  $\text{Ca}^{2+}$ : 1.18 Å; Shannon, 1976) can potentially substitute for  $\text{Ca}^{2+}$  in the crystal lattice of aragonite. This has been verified for coral (Finch et al., 2003) and bivalve (Foster et al., 2009) aragonite. Due to the larger difference of the ionic radii and the monovalent character a simple stoichiometric substitution of lithium (0.92 Å; Shannon, 1976) for calcium is unlikely. However, lithium might still substitute for  $\text{Ca}^{2+}$  as long as charge neutrality is ensured, either by vacant lattice sites or by the incorporation of an additional ion (Goldschmidt, 1954; McIntire, 1963; Okumura and Kitano, 1986). Since the coordination of lithium in bivalve shells has not yet been studied, it remains speculative how and in which form lithium is incorporated into these biominerals.

Controversial views also exist on the role of temperature on lithium incorporation into synthetic aragonite. Marriott et al. (2004b) suggest that lithium is easier incorporated into  $\text{CaCO}_3$  at lower temperatures, but more difficult at higher temperature, because the reaction during incorporation is exothermic. On the opposite, Smith et al. (1971) demonstrated that the formation of  $\text{Li}_2\text{CO}_3$  is inversely correlated to temperature. Whereas the solubility of  $\text{Li}_2\text{CO}_3$  increases at lower temperature, its formation is easier at warmer conditions.

### 5.7 Sr/Ca<sub>shell</sub>, Li/Ca<sub>shell</sub>, and Sr/Li<sub>shell</sub> of *C. edule* as temperature proxies

Sr/Ca<sub>shell</sub> and Li/Ca<sub>shell</sub> of *C. edule* covaried statistically significantly with temperature, weakly in the case of strontium and much stronger in the case of lithium (Figs. 8A+B). Similar results have been demonstrated by Hallam and Price (1968), who showed that strontium in shells of *C. edule* is negatively and linearly correlated to temperature. Despite vital effects, this finding compares well with thermodynamic expectations and results obtained from abiogenic precipitation experiments according to which a negative – and quasi-linear – relationship exists between temperature and Sr/Ca in aragonite (Kinsman and Holland, 1969; Gaetani and Cohen, 2006). However, the temperature sensitivity of Sr/Ca<sub>shell</sub> of *C. edule* (-0.02 mmol/mol/°C) was only half as large as in synthetic aragonite (-0.04 mmol/mol/°C; Kinsman and Holland, 1969; Gaetani and Cohen, 2006). For comparison, the temperature sensitivity of coral Sr/Ca is -0.06 mmol/mol/°C (Gagan et al., 2000; Corrège, 2006). In contrast to Sr/Ca<sub>shell</sub>, the Li/Ca<sub>shell</sub> ratios of *C. edule* were positively correlated to temperature, a result again comparing well with theoretic calculations on the temperature dependent incorporation of lithium into abiogenic aragonite and calcite (Hall and Chan, 2004; Hathorne et al., 2013). As yet, no experiments have been conducted to test the temperature effects on Li/Ca in synthetic aragonite.

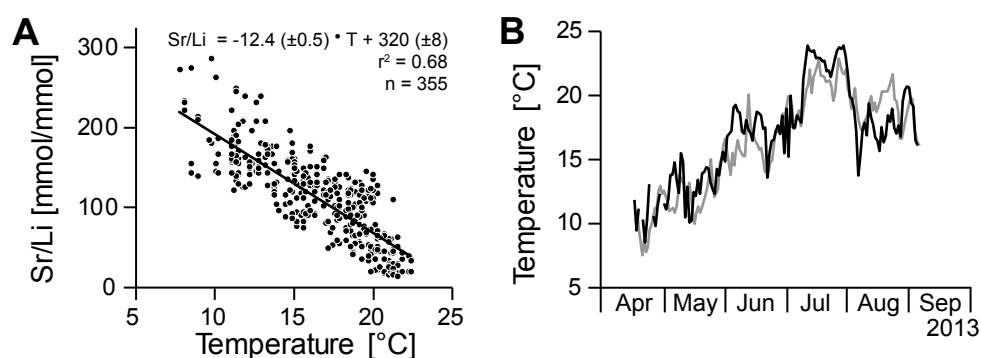


**Fig. 10.** Sr/Li<sub>shell</sub> paleothermometry. (A) Linear regression model constructed from Sr/Li<sub>shell</sub> of specimens A1, A6 and A28. Uncertainty in model represents one standard error (1 SE). (B) Time-series of measured temperature (gray) and temperature reconstructed from Sr/Li<sub>shell</sub> of specimen A24 (black) using model shown in (A).

Findings of the present study further imply that the temperature sensitivity of Sr/Ca<sub>shell</sub> and Li/Ca<sub>shell</sub> of *C. edule* is reinforced by (unknown) biological factors. We hypothesize here that a large portion of vital effects masking the temperature signal are mathematically eliminated by combining the two element-to-calcium ratios. If this hypothesis is true and indexing removes the majority of vital effects, then the incorporation of both elements, Sr and Li is likely controlled by similar mechanisms in *C. edule*. Normalizing Sr/Ca to Li/Ca reduced the scatter and increased the

explained variability (higher  $r^2$  value). The slope of the regression line of  $\text{Sr}/\text{Li}_{\text{shell}}$  vs. temperature is particularly steep (= large temperature sensitivity), because a negative linear regression was combined with a positive exponential regression.

## 6 Summary and conclusions

$\text{Sr}/\text{Li}_{\text{shell}}$  of *Cerastoderma edule* potentially serves as a promising new temperature proxy for aragonitic bivalve shells, specifically in coastal environments where traditional oxygen isotope-based temperature estimates can be erroneous. Up to 81% of the variability of  $\text{Sr}/\text{Li}_{\text{shell}}$  is explained by temperature, i.e. much more than either  $\text{Sr}/\text{Ca}_{\text{shell}}$  or  $\text{Li}/\text{Ca}_{\text{shell}}$  values. The empirically determined precision is on the order of  $\pm 1.5$  °C. Normalizing  $\text{Sr}/\text{Ca}$  to  $\text{Li}/\text{Ca}$  likely eliminates the majority of vital effects that typically challenge  $\text{Sr}/\text{Ca}_{\text{shell}}$ -based temperature predictions. Apparently, growth rate and Rayleigh fractionation do not control the incorporation of Sr or Li in the shell. Future studies are required to test if  $\text{Sr}/\text{Li}_{\text{shell}}$  also serves as a reliable temperature proxy in other bivalve species inhabiting different environments and if a similar relationship also exists in other calcium carbonate polymorphs.

## 7 Acknowledgments

We thank Lena Gaide, Lena Nachreiner, Hans Uhlmann, Ralf Sinning (Nationalpark-Haus Wangerland) as well as Michael Bremer (Jugendherberge Schillighörn) for their help in the field and the regular collection of water samples. We are grateful to Etienne Neuhaus for his help designing Figures 1 and 2. Michael Maus (University of Mainz) is kindly acknowledged for his help with the wet chemical analyses. We thank two anonymous reviewers and the editor, Michael Böttcher, for their comments that helped to significantly improve the manuscript. Financial support for this project was provided by the German Research Foundation, Deutsche Forschungsgemeinschaft (DFG) to BRS (SCH0793/13).

## 8 References

- Albarède, F., 1996. Introduction to geochemical modelling. Cambridge University Press, Cambridge (564 pp.).
- Amiel, A.J., Friedman, G.M., Miller, D.S., 1973. Distribution and nature of incorporation of trace elements in modern aragonitic corals. *Sedimentology*. 20, 47–64.
- Auzoux-Bordenave, S., Brahmi, C., Badou, A., de Rafélis, M., Huchette, S., 2015. Shell growth, microstructure and composition over the development cycle of the European abalone *Haliotis tuberculata*. *Mar. Biol.* 162, 687–697.
- Barlow, M.J., Kingston, P.F., 2001. Observations on the effects of barite on the gill tissues of the suspension feeder *Cerastoderma edule* (Linné) and the deposit feeder *Macoma balthica* (Linné). *Mar. Pollut. Bull.* 42, 71–76.
- Beck, J.W., Edwards, R.L., Ito, E., Taylor, F.W., Recy, J., Rougerie, F., Joannot, P., Henin, C., 1992. Sea-surface temperature from coral skeletal strontium/calcium ratios. *Science* 257, 644–647.
- Bourget, E., Brock, V., 1990. Short-term shell growth in bivalves: individual, regional, and age-related variations in the rhythm of deposition of *Cerastoderma (=Cardium) edule*. *Mar. Biol.* 106, 103–108.
- Bryan, S.P., Marchitto, T.M., 2008. Mg/Ca-temperature proxy in benthic foraminifera: New calibrations from the Florida Straits and a hypothesis regarding Mg/Li. *Paleoceanography* 23, PA2220.
- Burdon, D., Callaway, R., Elliott, M., Smith, T., Wither, A., 2014. Mass mortalities in bivalve populations: A review of the edible cockle *Cerastoderma edule* (L.). *Estuar. Coast. Shelf Sci.* 150, 271–280.
- Busenberg, E., Plummer, N.L., 1985. Kinetic and thermodynamic factors controlling the distribution of  $\text{SO}_4^{2-}$  and  $\text{Na}^+$  in calcites and selected aragonites. *Geochim. Cosmochim. Acta* 49, 713–725.
- Butler, P.G., Richardson, C.A., Scourse, J.D., Wanamaker Jr., A.D., Shammon, T.M., Bennell, J.D., 2010. Marine climate in the Irish Sea: analysis of a 489-year marine master chronology derived from growth increments in the shell of the clam *Arctica islandica*. *Quat. Sci. Rev.* 29, 1614–1632.
- Butler, P.G., Wanamaker Jr., A.D., Scourse, J.D., Richardson, C.A., Reynolds, D.J., 2013. Variability of marine climate on the North Icelandic Shelf in a 1357-year proxy archive based on growth increments in the bivalve *Arctica islandica*. *Palaeogeogr. Palaeoclimatol. Palaeoecol.* 373, 141–151.

- Came, R.E., Eiler, J.M., Veizer, J., Azmy, K., Brand, U., Weidman, C.R., 2007. Coupling of surface temperatures and atmospheric CO<sub>2</sub> concentrations during the Palaeozoic era. *Nature* 449, 198–201.
- Carré, M., Bentaleb, I., Bruguier, O., Ordinola, E., Barrett, N.T., Fontugne, M., 2006. Calcification rate influence on trace element concentrations in aragonitic bivalve shells: Evidences and mechanisms. *Geochim. Cosmochim. Acta* 70, 4906–4920.
- Case, D.H., Robinson, L.F., Auro, M.E., Gagnon, A.C., 2010. Environmental and biological controls on Mg and Li in deep-sea scleractinian corals. *Earth Planet. Sci. Lett.* 300, 215–225.
- Chauvaud, L., Lorrain, A., Dunbar, R.B., Paulet, Y.-M., Thouzeau, G., Jean, F., Guarini, J.-M., Mucciarone, D., 2005. Shell of the Great Scallop *Pecten maximus* as a high-frequency archive of paleoenvironmental changes. *Geochem. Geophys. Geosyst.* 6, Q08001.
- Corrège, T., 2006. Sea surface temperature and salinity reconstruction from coral geochemical tracers. *Palaeogeogr. Palaeoclimatol. Palaeoecol.* 232, 408–428.
- Craig, H., Gordon, L.I., 1965. Deuterium and oxygen 18 variations in the ocean and the marine atmosphere. In: Tongiorgi, E. (Ed.), *Stable Isotopes in Oceanographic Studies and Paleotemperatures*. Consiglio nazionale delle ricerche, Spoleto, pp. 9–130.
- Crenshaw, M.A., 1972. The inorganic composition of molluscan extrapallial fluid. *Biol. Bull.* 143, 506–512.
- Deith, M.R., 1985. The composition of tidally deposited growth lines in the shell of the edible cockle, *Cerastoderma edule*. *J. Mar. Biol. Assoc. U. K.* 65, 573–581.
- Dettman, D.L., Reische, A.K., Lohmann, K.C., 1999. Controls on the stable isotope composition of seasonal growth bands in aragonitic fresh-water bivalves (unionidae). *Geochim. Cosmochim. Acta* 63, 1049–1057.
- Dodd, J.R., 1965. Environmental control of strontium and magnesium in *Mytilus*. *Geochim. Cosmochim. Acta* 29, 385–398.
- Dodd, J.R., Crisp, E.L., 1982. Non-linear variation with salinity of Sr/Ca and Mg/Ca ratios in water and aragonitic bivalve shells and implications for paleosalinity studies. *Palaeogeogr. Palaeoclimatol. Palaeoecol.* 38, 45–56.
- DOE (U.S. Department of Energy), 1994. *Handbook of Methods for the Analysis of the Various Parameters of the Carbon Dioxide System in Sea Water, Version 2*. Dickson, A.G., Goyet, C. (Eds.). ORNL/CDIAC-74.
- Eagle, R.A., Eiler, J.M., Tripathi, A.K., Ries, J.B., Freitas, P.S., Hiebenthal, C., Wanamaker Jr., A.D., Taviani, M., Elliot, M., Marensi, S., Nakamura, K., Ramirez, P., Roy, K., 2013. The influence of temperature and seawater carbonate saturation state on <sup>13</sup>C-<sup>18</sup>O bond ordering in bivalve mollusks. *Biogeosci.* 10, 4591–4606.

- Eiler, J.M., 2011. Paleoclimate reconstruction using carbonate clumped isotope thermometry. *Quat. Sci. Rev.* 30, 3575–3588.
- Elderfield, H., Yu, J., Anand, P., Kiefer, T., Nyland, B., 2006. Calibrations for benthic foraminiferal Mg/Ca paleothermometry and the carbonate ion hypothesis. *Earth Planet. Sci. Lett.* 250, 633–649.
- Epstein, S., Buchsbaum, R., Lowenstam, H.A., Urey, H.C., 1953. Revised carbonate-water isotopic temperature scale. *Geol. Soc. Am. Bull.* 64, 1315–1326.
- Evans, J.W., 1972. Tidal growth increments in the cockle *Clinocardium nuttalli*. *Science* 176, 416–417.
- Farrow, G.E., 1971. Periodicity structures in the bivalve shell: experiments to establish growth controls in *Cerastoderma edule* from the Thames Estuary. *Palaeontology* 14, 571–587.
- Finch, A.A., Allison, N., Sutton, S.R., Newville, M., 2003. Strontium in coral aragonite: 1. Characterization of Sr coordination by extended absorption X-ray fine structure. *Geochim. Cosmochim. Acta* 67, 1189–1194.
- Foster, L.C., Finch, A.A., Allison, N., Andersson, C., Clarke, L.J., 2008. Mg in aragonitic bivalve shells: Seasonal variations and mode of incorporation in *Arctica islandica*. *Chem. Geol.* 254, 113–119.
- Foster, L.C., Allison, N., Finch, A.A., Andersson, C., 2009. Strontium distribution in the shell of the aragonite bivalve *Arctica islandica*. *Geochem. Geophys. Geosyst.* 10, Q03003.
- Freitas, P.S., Clarke, L.J., Kennedy, H., Richardson, C.A., Abrantes, F., 2006. Environmental and biological controls on elemental (Mg/Ca, Sr/Ca and Mn/Ca) ratios in shells of the king scallop *Pecten maximus*. *Geochim. Cosmochim. Acta* 70, 5119–5133.
- Freitas, P.S., Clarke, L.J., Kennedy, H.A., Richardson, C.A., 2008. Inter- and intra-specimen variability masks reliable temperature control on shell Mg/Ca ratios in laboratory- and field-cultured *Mytilus edulis* and *Pecten maximus* (bivalvia). *Biogeosci.* 5, 1245–1258.
- Fritz, L.W., Ragone, L.M., Lutz, R.A., Swapp, S., 1990. Biomineralization of barite in the shell of the freshwater Asiatic clam *Corbicula fluminea* (Mollusca: Bivalvia). *Limnol. Oceanogr.* 35, 756–762.
- Fritz, L.W., Ferrence, G., Jacobsen, T.R., 1992. Induction of barite mineralization in the Asiatic clam *Corbicula fluminea*. *Limnol. Oceanogr.* 37, 442–448.
- Füllenbach, C.S., Schöne, B.R., Branscheid, R., 2014. Microstructures in shells of the freshwater gastropod *Viviparus viviparus*: A potential sensor for temperature change? *Acta Biomater.* 10, 3911–3921.



- Gabitov, R.I., Schmitt, A.K., Rosner, M., McKeegan, K.D., Gaetani, G.A., Cohen, A.L., Watson, E.B., Harrison, T.M., 2011. In situ  $\delta^7\text{Li}$ , Li/Ca, and Mg/Ca analyses of synthetic aragonites. *Geochem. Geophys. Geosyst.* 12, Q03001.
- Gaetani, G.A., Cohen, A.L., 2006. Element partitioning during precipitation of aragonite from seawater: A framework for understanding paleoproxies. *Geochim. Cosmochim. Acta* 70, 4617–4634.
- Gagan, M.K., Ayliffe, L.K., Beck, J.W., Cole, J.E., Druffel, E.R.M., Dunbar, R.B., Schrag, D.P., 2000. New views of tropical paleoclimates from corals. *Quat. Sci. Rev.* 19, 45–64.
- Gagnon, A.C., Adkins, J.F., Fernandez, D.P., Robinson, L.F., 2007. Sr/Ca and Mg/Ca vital effects correlated with skeletal architecture in a scleractinian deep-sea coral and the role of Rayleigh fractionation. *Earth Planet. Sci. Lett.* 261, 280–295.
- Ghosh, P., Adkins, J., Affek, H., Balta, B., Guo, W., Schauble, E.A., Schrag, D., Eiler, J.M., 2006.  $^{13}\text{C}$ – $^{18}\text{O}$  bonds in carbonate minerals: A new kind of paleothermometer. *Geochim. Cosmochim. Acta* 70, 1439–1456.
- Goldschmidt, V.M., 1926. Die Gesetze der Krystallochemie. *Naturwissenschaften* 14, 477–485.
- Goldschmidt, V.M., 1954. *Geochemistry*. Clarendon Press, Oxford, 730 pp.
- Gonfiantini, R., 1978. Standards for stable isotope measurements in natural compounds. *Nature* 271, 534–536.
- Gillikin, D.P., Lorrain, A., Navez, J., Taylor, J.W., André, L., Keppens, E., Baeyens, W., Dehairs, F., 2005. Strong biological controls on Sr/Ca ratios in aragonitic marine bivalve shells. *Geochem. Geophys. Geosyst.* 6, Q05009.
- Grossman, E.L., Ku, T.-L., 1986. Oxygen and carbon isotope fractionation in biogenic aragonite: Temperature effects. *Chem. Geol. Isot. Geosci. Sect.* 59, 59–74.
- Hall, J.M., Chan, L.-H., 2004. Li/Ca in multiple species of benthic and planktonic foraminifera: Thermocline, latitudinal, and glacial-interglacial variation. *Geochim. Cosmochim. Acta* 68, 529–545.
- Hallam, A., Price, N.B., 1968. Environmental and biochemical control of strontium in shells of *Cardium edule*. *Geochim. Cosmochim. Acta* 32, 319–328.
- Hallmann, N., Burchell, M., Schöne, B.R., Irvine, G. V, Maxwell, D., 2009. High-resolution sclerochronological analysis of the bivalve mollusk *Saxidomus gigantea* from Alaska and British Columbia: techniques for revealing environmental archives and archaeological seasonality. *J. Archaeol. Sci.* 36, 2353–2364.

- Hallmann, N., Schöne, B.R., Irvine, G. V, Burchell, M., Cokelet, E.D., Hilton, M.R., 2011. An improved understanding of the Alaska Coastal Current: the application of a bivalve growth-temperature model to reconstruct freshwater-influenced paleoenvironments. *Palaios* 26, 346–363.
- Hathorne, E.C., Felis, T., Suzuki, A., Kawahata, H., Cabioch, G., 2013. Lithium in the aragonite skeletons of massive *Porites* corals: A new tool to reconstruct tropical sea surface temperatures. *Paleoceanography* 28, 143–152.
- Henkes, G.A., Passey, B.H., Wanamaker Jr., A.D., Grossman, E.L., Ambrose Jr., W.G., Carroll, M.L., 2013. Carbonate clumped isotope compositions of modern marine mollusk and brachiopod shells. *Geochim. Cosmochim. Acta* 106, 307–325.
- Holland, H.A., Schöne, B.R., Lipowsky, C., Esper, J., 2014. Decadal climate variability of the North Sea during the last millennium reconstructed from bivalve shells (*Arctica islandica*). *The Holocene* 24, 771–786.
- House, M.R., Farrow, G.E., 1968. Daily growth banding in the shell of the cockle, *Cardium edule*. *Nature* 219, 1384–1386.
- Jacob, D.E., Wirth, R., Soldati, A.L., Wehrmeister, U., Schreiber, A., 2011. Amorphous calcium carbonate in the shells of adult *Unionoida*. *J. Struct. Biol.* 173, 241–249.
- Jochum, K.P., Nohl, U., Herwig, K., Lammel, E., Stoll, B., Hofmann, A.W., 2005. GeoReM: a new geochemical database for reference materials and isotopic standards. *Geostand. Geoanalyt. Res.* 29, 333–338.
- Jochum, K.P., Stoll, B., Herwig, K., Willbold, M., 2007. Validation of LA-ICP-MS trace element analysis of geological glasses using a new solid-state 193 nm Nd:YAG laser and matrix-matched calibration. *J. Anal. At. Spectrom.* 22, 112–121.
- Jochum, K.P., Weis, U., Stoll, B., Kuzmin, D., Yang, Q., Raczek, I., Jacob, D.E., Stracke, A., Birbaum, K., Frick, D.A., Günther, D., Enzweiler, J., 2011. Determination of reference values for NIST SRM 610-617 glasses following ISO guidelines. *Geostand. Geoanalyt. Res.* 35, 397–429.
- Jochum, K.P., Scholz, D., Stoll, B., Weis, U., Wilson, S.A., Yang, Q., Schwalb, A., Börner, N., Jacob, D.E., Andreae, M.O., 2012. Accurate trace element analysis of speleothems and biogenic calcium carbonates by LA-ICP-MS. *Chem. Geol.* 318–319, 31–44.
- Jochum, K.P., Stoll, B., Weis, U., Jacob, D.E., Mertz-Kraus, R., Andreae, M.O., 2014. Non-Matrix-Matched Calibration for the Multi-Element Analysis of Geological and Environmental Samples Using 200 nm Femtosecond LA-ICP-MS: A Comparison with Nanosecond Lasers. *Geostand. Geoanalyt. Res.* 38, 265–292.
- Jones, D.S., 1983. Sclerochronology: reading the record of the molluscan shell. *Am. Sci.* 71, 384–391.

- Jones, D.S., Quitmyer, I.R., 1996. Marking time with bivalve shells: oxygen isotopes and season of annual increment formation. *Palaios* 11, 340–346.
- Kaehler, S., McQuaid, C.D., 1999. Use of the fluorochrome calcein as an in situ growth marker in the brown mussel *Perna perna*. *Mar. Biol.* 133, 455–460.
- Kim, S.-T., Mucci, A., Taylor, B.E., 2007. Phosphoric acid fractionation factors for calcite and aragonite between 25 and 75°C: Revisited. *Chem. Geol.* 246, 135–146.
- Kingston, P., 1974. Some observations on the effects of temperature and salinity upon the growth of *Cardium edule* and *Cardium glaucum* larvae in the laboratory. *J. Mar. Biol. Assoc. U. K.* 54, 309–317.
- Kinsman, D.J.J., Holland, H.D., 1969. The co-precipitation of cations with CaCO<sub>3</sub> - IV. The co-precipitation of Sr<sup>2+</sup> with aragonite between 16° and 96°C. *Geochim. Cosmochim. Acta* 33, 1–17.
- Kitano, Y., Kanamori, N., Oomori, T., 1971. Measurements of distribution coefficients of strontium and barium between carbonate precipitate and solution - Abnormally high values of distribution coefficients measured at early stages of carbonate formation. *Geochem. J.* 4, 183–206.
- Klein, R.T., Lohmann, K.C., Thayer, C.W., 1996. Bivalve skeletons record sea-surface temperature and δ<sup>18</sup>O via Mg/Ca and <sup>18</sup>O/<sup>16</sup>O ratios. *Geology* 24, 415–418.
- Lomovasky, B.J., Brey, T., Morriconi, E., Calvo, J., 2002. Growth and production of the venerid bivalve *Eurhomalea exalbida* in the Beagle Channel, Tierra del Fuego. *J. Sea Res.* 48, 209–216.
- Longerich, H.P., Jackson, S.E., Günther, D., 1996. Laser ablation inductively coupled plasma mass spectrometric transient signal data acquisition and analyte concentration calculation. *J. Anal. At. Spectrom.* 11, 899–904.
- Lønne, O.J., Gray, J.S., 1988. Influence of tides on microgrowth bands in *Cerastoderma edule* from Norway. *Mar. Ecol. Prog. Ser.* 42, 1–7.
- Lorrain, A., Gillikin, D.P., Paulet, Y.-M., Chauvaud, L., Le Mercier, A., Navez, J., André, L., 2005. Strong kinetic effects on Sr/Ca ratios in the calcitic bivalve *Pecten maximus*. *Geology* 33, 965–968.
- Mahé, K., Bellamy, E., Lartaud, F., de Rafélis, M., 2010. Calcein and manganese experiments for marking the shell of the common cockle (*Cerastoderma edule*): tidal rhythm validation of increments formation. *Aquat. Living Resour.* 23, 239–245.
- Malham, S.K., Hutchinson, T.H., Longshaw, M., 2012. A review of the biology of European cockles (*Cerastoderma* spp.). *J. Mar. Biol. Assoc. U. K.* 92, 1563–1577.

- Marchitto Jr., T.M., Jones, G.A., Goodfriend, G.A., Weidman, C.R., 2000. Precise temporal correlation of Holocene mollusk shells using sclerochronology. *Quat. Res.* 53, 236–246.
- Marin, F., Luquet, G., Marie, B., Medakovic, D., 2007. Molluscan shell proteins: Primary structure, origin, and evolution. *Curr. Top. Dev. Biol.* 80, 209–276.
- Marin, F., Le Roy, N., Marie, B., 2012. The formation and mineralization of mollusk shell. *Front. Biosci.* S4, 1099–1125.
- Marriott, C.S., Henderson, G.M., Crompton, R., Staubwasser, M., Shaw, S., 2004a. Effect of mineralogy, salinity, and temperature on Li/Ca and Li isotope composition of calcium carbonate. *Chem. Geol.* 212, 5–15.
- Marriott, C.S., Henderson, G.M., Belshaw, N.S., Tudhope, A.W., 2004b. Temperature dependence of  $\delta^7\text{Li}$ ,  $\delta^{44}\text{Ca}$  and Li/Ca during growth of calcium carbonate. *Earth Planet. Sci. Lett.* 222, 615–624.
- McConnaughey, T.A., Gillikin, D.P., 2008. Carbon isotopes in mollusk shell carbonates. *Geo-Mar. Lett.* 28, 287–299.
- McIntire, W.L., 1963. Trace element partition coefficients—a review of theory and applications to geology. *Geochim. Cosmochim. Acta* 27, 1209–1264.
- McKinney, C.R., McCrea, J.M., Epstein, S., Allen, H.A., Urey, H.C., 1950. Improvements in mass spectrometers for the measurement of small differences in isotope abundance ratios. *Rev. Sci. Instrum.* 21, 724–730.
- Montagna, P., McCulloch, M., Douville, E., López Correa, M., Trotter, J., Rodolfo-Metalpa, R., Dissard, D., Ferrier-Pagès, C., Frank, N., Freiwald, A., Goldstein, S., Mazzoli, C., Reynaud, S., Rüggeberg, A., Russo, S., Taviani, M., 2014. Li/Mg systematics in scleractinian corals: Calibration of the thermometer. *Geochim. Cosmochim. Acta* 132, 288–310.
- Mook, W.G., 1971. Paleotemperatures and chlorinities from stable carbon and oxygen isotopes in shell carbonate. *Palaeogeogr. Palaeoclimatol. Palaeoecol.* 9, 245–263.
- Moran, A.L., 2000. Calcein as a marker in experimental studies newly-hatched gastropods. *Mar. Biol.* 137, 893–898.
- Moura, G., Vilarinho, L., Santos, A.C., Machado, J., 2000. Organic compounds in the extrapalial fluid and haemolymph of *Anodonta cygnea* (L.) with emphasis on the seasonal biomineralization process. *Comp. Biochem. Physiol. B* 125, 293–306.
- Nicol, D., 1951. Recent species of the veneroid pelecypod *Arctica*. *J. Wash. Acad. Sci.* 41, 102–106.
- Odum, H.T., 1951. Notes on the strontium content of sea water, celestite radiolaria, and strontianite snail shells. *Science* 114, 211–213.

- Ohno, T., 1985. Experimentelle Analysen zur Rhythmik des Schalenwachstums einiger Bivalven und ihre palaeobiologische Bedeutung. *Palaeontogr. A* 189, 63–123.
- Okumura, M., Kitano, Y., 1986. Coprecipitation of alkali metal ions with calcium carbonate. *Geochim. Cosmochim. Acta* 50, 49–58.
- Orton, J.H., 1926. On the rate of growth of *Cardium edule*. Part I. Experimental observations. *J. Mar. Biol. Assoc. U. K.* 14, 239–279.
- Pokroy, B., Quintana, J.P., Caspi, E.N., Berner, A., Zolotoyabko, E., 2004. Anisotropic lattice distortions in biogenic aragonite. *Nat. Mater.* 3, 900–902.
- Pokroy, B., Fieramosca, J., Von Dreele, R., Fitch, A.N., Caspi, E.N., Zolotoyabko, E., 2007. Atomic structure of biogenic aragonite. *Chem. Mater.* 19, 3244–3251.
- Ponsero, A., Dabouineau, L., Allain, J., 2009. Modelling of common European cockle *Cerastoderma edule* fishing grounds aimed at sustainable management of traditional harvesting. *Fish. Sci.* 75, 839–850.
- Popov, S. V., 1986. Composite prismatic structure in bivalve shell. *Acta Palaeontol. Pol.* 31, 3–26.
- Poulain, C., Gillikin, D.P., Thébault, J., Munaron, J.M., Bohn, M., Robert, R., Paulet, Y.-M., Lorrain, A., 2015. An evaluation of Mg/Ca, Sr/Ca and Ba/Ca ratios as environmental proxies in aragonite bivalve shells. *Chem. Geol.* 396, 42–50.
- Raddatz, J., Liebetrau, V., Rüggeberg, A., Hathorne, E., Krabbenhöft, A., Eisenhauer, A., Böhm, F., Vollstaedt, H., Fietzke, J., López Correa, M., Freiwald, A., Dullo, W.-C., 2013. Stable Sr-isotope, Sr/Ca, Mg/Ca, Li/Ca and Mg/Li ratios in the scleractinian cold-water coral *Lophelia pertusa*. *Chem. Geol.* 352, 143–152.
- Richardson, C.A., Crisp, D.J., Runham, N.W., 1979. Tidally deposited growth bands in the shell of the common cockle, *Cerastoderma edule* (L.). *Malacologia* 18, 277–290.
- Rollion-Bard, C., Blamart, D., 2015. Possible controls on Li, Na, and Mg incorporation into aragonite coral skeletons. *Chem. Geol.* 396, 98–111.
- Schöne, B.R., Fiebig, J., Pfeiffer, M., Gleß, R., Hickson, J., Johnson, A.L.A., Dreyer, W., Oschmann, W., 2005a. Climate records from a bivalved Methuselah (*Arctica islandica*, Mollusca; Iceland). *Palaeogeogr. Palaeoclimatol. Palaeoecol.* 228, 130–148.
- Schöne, B.R., Pfeiffer, M., Pohlmann, T., Siegismund, F., 2005b. A seasonally resolved bottom-water temperature record for the period AD 1866–2002 based on shells of *Arctica islandica* (Mollusca, North Sea). *Int. J. Climatol.* 25, 947–962.
- Schöne, B.R., Dunca, E., Fiebig, J., Pfeiffer, M., 2005c. Mutvei's solution: An ideal agent for resolving microgrowth structures of biogenic carbonates. *Palaeogeogr. Palaeoclimatol. Palaeoecol.* 228, 146–166.

- Schöne, B.R., Zhang, Z., Jacob, D.E., Gillikin, D.P., Tütken, T., Garbe-Schönberg, D., McConnaughey, T.A., Soldati, A., 2010. Effect of organic matrices on the determination of the trace element chemistry (Mg, Sr, Mg/Ca, Sr/Ca) of aragonitic bivalve shells (*Arctica islandica*) - Comparison of ICP-OES and LA-ICP-MS data. *Geochem. J.* 44, 23–37.
- Schöne, B.R., Zhang, Z., Radermacher, P., Thébault, J., Jacob, D.E., Nunn, E.V., Maurer, A.-F., 2011. Sr/Ca and Mg/Ca ratios of ontogenetically old, long-lived bivalve shells (*Arctica islandica*) and their function as paleotemperature proxies. *Palaeogeogr. Palaeoclimatol. Palaeoecol.* 302, 52–64.
- Schöne, B.R., Radermacher, P., Zhang, Z., Jacob, D.E., 2013. Crystal fabrics and element impurities (Sr/Ca, Mg/Ca, and Ba/Ca) in shells of *Arctica islandica* - Implications for paleoclimate reconstructions. *Palaeogeogr. Palaeoclimatol. Palaeoecol.* 373, 50–59.
- Shannon, R.D., 1976. Revised effective ionic radii and systematic studies of interatomic distances in halides and chalcogenides. *Acta Crystallogr. A* 32, 751–767.
- Shirai, K., Takahata, N., Yamamoto, H., Omata, T., Sasaki, T., Sano, Y., 2008. Novel analytical approach to bivalve shell biogeochemistry: A case study of hydrothermal mussel shell. *Geochem. J.* 42, 413–420.
- Shirai, K., Schöne, B.R., Miyaji, T., Radermacher, P., Krause Jr, R.A., Tanabe, K., 2014. Assessment of the mechanism of elemental incorporation into bivalve shells (*Arctica islandica*) based on elemental distribution at the microstructural scale. *Geochim. Cosmochim. Acta* 126, 307–320.
- Smith Jr., S.H., Williams, D.D., Miller, R.R., 1971. Solubility of lithium carbonate at elevated temperatures. *J. Chem. Eng. Datas* 16, 16–17.
- Stemmer, K., Brey, T., Glas, M., Beutler, M., Schalkhauser, B., de Beer, D., 2015. In situ measurements of pH, Ca<sup>2+</sup> and DIC dynamics within the extrapallial fluid of the ocean quahog *Arctica islandica*. *J. Exp. Mar. Biol. Ecol.* (accepted for publication).
- Stephenson, A.E., DeYoreo, J.J., Wu, L., Wu, K.J., Hoyer, J., Dove, P.M., 2008. Peptides enhance magnesium signature in calcite: insights into origins of vital effects. *Science* 322, 724–727.
- Stewart, M.G., 1984. Permeability and epidermal transport. In: Bereiter-Hahn, J. Matoltsy, A.G., Richards, K.S. (Eds.), *Biology of the Integument. 1 Invertebrates*. Springer, Berlin, pp. 486–501.
- Surge, D., Walker, K.J., 2006. Geochemical variation in microstructural shell layers of the southern quahog (*Mercenaria campechiensis*): Implications for reconstructing seasonality. *Palaeogeogr. Palaeoclimatol. Palaeoecol.* 237, 182–190.

- Swan, E.F., 1956. The meaning of strontium-calcium ratios. *Deep-Sea Res.* 4, 71.
- Takesue, R.K., van Geen, A., 2004. Mg/Ca, Sr/Ca, and stable isotopes in modern and Holocene *Protothaca staminea* shells from a northern California coastal upwelling region. *Geochim. Cosmochim. Acta* 68, 3845–3861.
- Thébault, J., Schöne, B.R., Hallmann, N., Barth, M., Nunn, E.V., 2009. Investigation of Li/Ca variations in aragonitic shells of the ocean quahog *Arctica islandica*, northeast Iceland. *Geochem. Geophys. Geosyst.* 10, Q12008.
- Thébault, J., Chauvaud, L., 2013. Li/Ca enrichments in great scallop shells (*Pecten maximus*) and their relationship with phytoplankton blooms. *Palaeogeogr. Palaeoclimatol. Palaeoecol.* 373, 108–122.
- Vander Putten, E., Dehairs, F., Keppens, E., Baeyens, W., 2000. High resolution distribution of trace elements in the calcite shell layer of modern *Mytilus edulis*: Environmental and biological controls. *Geochim. Cosmochim. Acta* 64, 997–1011.
- Wada, K., Fujinuki, T., 1976. Biomineralization in bivalve molluscs with emphasis on the chemical composition of the extrapallial fluid. In: Bryan, N.M., Wilbur, K.M. (Eds.), *Mechanisms of Mineralization in the Invertebrates and Plants*. University of South Carolina Press, Georgetown, pp. 175–190.
- Wanamaker Jr., A.D., Kreutz, K.J., Wilson, T., Borns Jr, H.W., Introne, D.S., Feindel, S., 2008. Experimentally determined Mg/Ca and Sr/Ca ratios in juvenile bivalve calcite for *Mytilus edulis*: implications for paleotemperature reconstructions. *Geo-Mar. Lett.* 28, 359–368.
- Wanamaker Jr., A.D., Kreutz, K.J., Schöne, B.R., Introne, D.S., 2011. Gulf of Maine shells reveal changes in seawater temperature seasonality during the Medieval Climate Anomaly and the Little Ice Age. *Palaeogeogr. Palaeoclimatol. Palaeoecol.* 302, 43–51.
- Watanabe, T., Minagawa, M., Oba, T., Winter, A., 2001. Pretreatment of coral aragonite for Mg and Sr analysis: Implications for coral thermometers. *Geochem. J.* 35, 265–269.
- Watson, E.B., Liang, Y., 1995. A simple model for sector zoning in slowly grown crystals: implications for growth rate and lattice diffusion, with emphasis on accessory minerals in crustal rocks. *Am. Mineral.* 80, 1179–1187.
- Wefer, G., Berger, W.H., 1991. Isotope paleontology: growth and composition of extant calcareous species. *Mar. Geol.* 100, 207–248.
- Wheeler, A.P., 1992. Mechanisms of molluscan shell formation. In: Bonucci, E. (Ed.), *Calcification in Biological Systems*. CRC Press, Boca Raton, pp. 77–83.
- Williams, D.F., Arthur, M.A., Jones, D.S., Healy-Williams, N., 1982. Seasonality and mean annual sea surface temperatures from isotopic and sclerochronological records. *Nature* 256, 432–434.

- Wisshak, M., López Correa, M., Gofas, S., Salas, C., Taviani, M., Jakobsen, J., Freiwald, A., 2009. Shell architecture, element composition, and stable isotope signature of the giant deep-sea oyster *Neopycnodonte zibrowii* sp. n. from the NE Atlantic. *Deep-Sea Res. I* 56, 374–407.
- Witbaard, R., Duineveld, G.C.A., De Wilde, P.A.W.J., 1997. A long-term growth record derived from *Arctica Islandica* (Mollusca, Bivalvia) from the Fladen Ground (northern North Sea). *J. Mar. Biol. Assoc. U. K.* 77, 801–816.
- Yan, H., Soon, W., Wang, Y., 2015. A composite sea surface temperature record of the northern South China Sea for the past 2500 years: A unique look into seasonality and seasonal climate changes during warm and cold periods. *Earth-Sci. Rev.* 141, 122–135.



## Manuscript III

### Minute co-variations of Sr/Ca ratios and microstructures in the aragonitic shell of *Cerastoderma edule* (Bivalvia)

—

### Are geochemical variations at the ultra-scale masking potential environmental signals?

Submitted to *Geochimica Cosmochimica Acta*

Christoph S. Füllenbach<sup>1</sup>, Bernd R. Schöne<sup>1</sup>, Kotaro Shirai<sup>2</sup>, Naoto Takahata<sup>2</sup>, Akizumi Ishida<sup>2</sup>, Yuji Sano<sup>2</sup>

<sup>1</sup>Institute of Geosciences, University of Mainz,  
Johann-Joachim-Becher-Weg 21, 55128 Mainz, Germany

<sup>2</sup>Atmosphere and Ocean Research Institute,  
University of Tokyo, 1-5-1, Kashiwanoha, Kashiwa, Chiba 277-8564, Japan

#### Authors contribution

Concept: CSF

Execution: CSF

Analyses: Growth patterns: CSF; SEM: CSF; NanoSIMS: KS, NT, AI;

EPMA: CSF, Stephan Buhre, Nora Groschopf

Data analysis: CSF, KS

Writing: CSF, BRS, KS

## Abstract

It remains a challenging task to reconstruct water temperatures from Sr/Ca ratios of bivalve shells. Although in many aragonitic species Sr/Ca is negatively correlated to temperature – which is expected from abiogenic precipitation experiments –, the incorporation of Sr into the shell of bivalves is strongly controlled by physiological processes and occurs away from predicted thermodynamic equilibrium. Strontium-to-calcium ratios of aragonitic shells remain far below that of the ambient water. Moreover, Sr levels vary considerably among shell portions displaying different microstructures and / or organic contents. Values observed at annual growth lines and portions between them (= annual growth increments) deviate much stronger from each other than expected from temperature or  $\text{Sr/Ca}_{\text{water}}$  change. As demonstrated here by ultra-high resolution analysis (electron microprobe, NanoSIMS) of Sr in shells of *Cerastoderma edule*, Sr levels are also heterogeneously distributed at the lower micrometer scale. In the outer shell portion of the outer shell layer for example, Sr/Ca ratios were significantly higher at circatidal growth lines (irregular simple prismatic structure;  $2.9 \pm 0.4$  mmol/mol) and lower within circatidal increments (nondenticular prismatic structure;  $2.5 \pm 0.2$  mmol/mol).  $\text{S/Ca}_{\text{shell}}$ , measured to approximate the organic concentration of the analyzed microstructure, showed the opposite pattern, i.e., high values in circatidal increments ( $2.4 \pm 0.3$  mmol/mol), low values at circatidal growth lines ( $2.1 \pm 0.5$  mmol/mol). Maximum values of  $\text{Sr/Ca}_{\text{shell}}$  (4 mmol/mol) and  $\text{S/Ca}_{\text{shell}}$  (4.6 mmol/mol), however, were typically associated with annual growth lines. The intimate link between  $\text{Sr/Ca}_{\text{shell}}$ ,  $\text{S/Ca}_{\text{shell}}$  and shell architecture may indicate that microstructures or the processes controlling their formation exert a strong control over the incorporation of strontium into shells of *C. edule*. Analytical techniques with lower sampling resolution, e.g., LA-ICP-MS, cannot resolve such fine-scale Sr variations. As a result, the signal-to-noise ratio decreases and the data generated by such techniques do not seem to provide useful paleotemperature data. Future studies should therefore employ a combined analysis of  $\text{Sr/Ca}_{\text{shell}}$  and shell microstructures.  $\text{Sr/Ca}_{\text{shell}}$  values of shell portions consisting of different microstructures should be interpreted separately.

## 1 Introduction

Strontium-to-calcium ratios of many biogenic carbonates can provide robust temperature estimates (Beck et al., 1992). Unlike  $\delta^{18}\text{O}$  values, the Sr/Ca thermometer functions well in fully marine as well as brackish waters, because  $\text{Sr}/\text{Ca}_{\text{water}}$  remains nearly invariant in seawater above 10 PSU (Dodd and Crisp, 1982). Thus, changes in Sr/Ca ratio of the  $\text{CaCO}_3$  predominantly reflect changes in temperature, but not salinity and freshwater influx. The Sr/Ca thermometer is routinely used in tropical, shallow-marine corals (Corrège, 2006), because the incorporation of  $\text{Sr}^{2+}$  into their aragonitic skeletons is close to predicted thermodynamic equilibrium and similar to that of abiogenic aragonite (Kinsman and Holland, 1969; Dietzel et al., 2004; Gaetani and Cohen, 2006). At 25 °C the distribution coefficient,  $K^D_{\text{Sr}/\text{Ca}}$ , of synthetic aragonite is 1.19 (Dietzel et al., 2004) and that of Porites 1.06 (Shen et al., 1996). With increasing water temperature, decreasing levels of Sr substitute for Ca in the crystal lattice. The temperature sensitivity of corals is, on average, -0.06 mmol/mol Sr/Ca per 1 °C (Corrège, 2006) and therefore slightly higher than that of synthetic aragonite (-0.04 mmol/mol Sr/Ca per 1 °C; Gaetani and Cohen, 2006).

Interpreting Sr/Ca ratios of aragonitic bivalve shells, however, remains a challenging task. Several authors found a negative correlation between  $\text{Sr}/\text{Ca}_{\text{shell}}$  and water temperature (Dodd, 1965; Hallam and Price, 1968; Schöne et al., 2011; Yan et al., 2013) and reported temperature sensitivities ranging between -0.02 mmol/mol/°C in *Cerastoderma edule* (Füllenbach et al., 2015) and *Corbicula fluminea* (Zhao et al., 2016) and -0.06 to -0.07 mmol/mol/°C in *Tridacna* spp. (Yan et al., 2013). Others found a positive correlation (Stecher et al., 1996; Hart and Blusztajn, 1998; Toland et al., 2000; Wannamaker et al., 2008) or none at all (Vander Putten et al., 2000; Carré et al., 2006). Furthermore, various authors noticed a correlation between  $\text{Sr}/\text{Ca}_{\text{shell}}$  and growth rate (Swan, 1956; Stecher et al., 1996; Takesue and van Geen, 2004; Gillikin et al., 2005; Lorrain et al., 2005) and ontogenetic age (Swan, 1956). What existing studies have in common is  $K^D_{\text{Sr}/\text{Ca}}$  values of only 0.2 to 0.3 between temperatures of ca. 0 and 30 °C (Gillikin et al., 2005; Füllenbach et al., 2015; Zhao et al., 2016) indicating a strong discrimination against Sr. However, when studied in more detail, it becomes apparent that Sr is heterogeneously distributed in the biomineral. Firstly, when measured by means of laser ablation inductively coupled plasma mass spectrometry (LA-ICP-MS) and 50  $\mu\text{m}$  resolution in line scan mode, shell portions between consecutive annual growth lines (= annual increments) of *Arctica islandica* reveal considerable temporal fluctuations of alternating high and low  $\text{Sr}/\text{Ca}_{\text{shell}}$  values (Schöne et al., 2013). This intra-annual  $\text{Sr}/\text{Ca}_{\text{shell}}$  noise of up to  $\pm 0.5$  mmol/mol that can hardly be explained by short-term changes in water temperature or  $\text{Sr}/\text{Ca}_{\text{water}}$ . In the absence of higher resolution Sr mapping, it currently remains unresolved why  $\text{Sr}/\text{Ca}_{\text{shell}}$  varies on

intra-annual time-scales and to what degree the actual variability is attenuated by time-averaged sampling. Secondly, depending on species, Sr is either strongly enriched (Foster et al., 2009; Schöne et al., 2011, 2013; Shirai et al., 2014) or strongly depleted at the annual growth lines (Stecher et al., 1996; Takesue and van Geen, 2004). In the veneroid *Mercenaria mercenaria*, for example, Stecher et al. (1996) documented  $\text{Sr}/\text{Ca}_{\text{shell}}$  values of up to 2.6 mmol/mol in annual increments, but only 1 to 1.2 mmol/mol in annual (winter) growth lines. On the contrary, Schöne et al. (2013) reported values of 0.84 and 2.47 mmol/mol from annual increments and annual growth lines (formed between November and January) of *A. islandica*, respectively. Likewise, Füllenbach et al. (2015) measured elevated Sr levels near annual (winter) lines of *Cerastoderma edule*. In all three species, the abrupt  $\text{Sr}/\text{Ca}_{\text{shell}}$  shifts cannot be explained by changes of  $\text{Sr}/\text{Ca}_{\text{water}}$  or water temperature (Stecher et al., 1996; Schöne et al., 2013, Füllenbach et al., 2015). However, the abrupt changes in Sr content at the annual growth lines are clearly associated with modifications of the shell microstructure (Schöne et al., 2013; Shirai et al., 2014). In the light of these findings it is still surprising that whole shell (Hallam and Price, 1968), low-pass filtered (Füllenbach et al., 2015) or annually averaged (Schöne et al., 2011)  $\text{Sr}/\text{Ca}_{\text{shell}}$  data are often statistically significantly – though not particularly strongly – correlated with water temperature.

Here, we studied the distribution of strontium, calcium, and sulfur (representing organics) in a shell of the common cockle *C. edule* by means of ultra-high-resolution in-situ analytical techniques, i.e., quantitatively by electron microprobe and semi-quantitatively by NanoSIMS. Special attention was paid to relationships between  $\text{Sr}/\text{Ca}_{\text{shell}}$  and  $\text{S}/\text{Ca}_{\text{shell}}$  values, growth patterns and microstructures. Specifically, we addressed the following questions: (i) How variable is the Sr content of the shell at the sub/micrometer-scale? (ii) What explains the enrichment of Sr at the annual growth lines? (iii) Which sampling strategies should be applied in future studies  $\text{Sr}/\text{Ca}_{\text{shell}}$  studies? The ultimate goals of this study were to better understand the variability and trends of  $\text{Sr}/\text{Ca}_{\text{shell}}$  data taken with lower spatial resolution and to investigate if higher sampling resolution can resolve issues that currently impede the routine use of  $\text{Sr}/\text{Ca}$  as a temperature proxy in bivalve shells.

## 2 Material and Methods

This manuscript focuses on the geochemical heterogeneity in *C. edule* on the ultra-scale. Because analytical techniques which allow for such a high spatial resolution are extremely time-consuming, we did not measure different specimens, but tested

the reproducibility of our findings by repeated analyses within different areas of the same specimen.

## 2.1 *Cerastoderma edule*

*C. edule* is a common inhabitant of the intertidal zone along the European coastline (Malham et al., 2012). The growing season of this short-lived, fast-growing species typically lasts from early spring to late fall (Bourget and Brock, 1990). Annual growth lines are visible as notches on the outer shell surface and as distinct lines in cross-sections (Orton, 1926; House and Farrow, 1968; Farrow, 1971; Bourget and Brock, 1990; Ponsoero et al., 2009). Intra-annual growth patterns including circatidal (semi-diurnal), circa-lunidian (lunar daily) and fortnightly growth increments and lines (Deith, 1985) are particularly well developed in the second and third ontogenetic year. Circatidal growth lines form during low tide and circatidal growth increments during immersion at high tide (Richardson et al., 1979; Ohno, 1985; Lønne and Gray, 1988; Mahé et al., 2010). In later ontogenetic years, microgrowth patterns are difficult to discern because the shell growth rate is strongly reduced (Bourget and Brock, 1990). The fully aragonitic shell (tested by Raman spectroscopy) can be subdivided into an inner (= ISL) and outer shell layer (= OSL). The OSL consists of an inner (= iOSL) and outer portion (= oOSL), separated by a transition zone (= TZ; Fig. 1).

## 2.2 Biomineralization

Shell formation in *C. edule* and other bivalves occurs in two fluid- or gel-filled reaction compartments, so-called extrapallial spaces (EPS) which are separated from the hemolymph (blood) and ambient water by the mantle epithelia. The ISL forms in the inner extrapallial space (iEPS), the OSL in the outer extrapallial space (oEPS). According to the prevalent opinion, mantle epithelial cells produce an organic template (Wilbur and Jodrey, 1955; Bevelander and Nakahara, 1969) that acts as a (water-insoluble) matrix which orchestrates the formation of the biomineral including its architecture, chemical composition and the polymorph of CaCO<sub>3</sub>. These organic constituents become part of the biomineral as an intercrystalline matrix (Marin et al. 2012) that enwraps individual microstructural units (= nanocrystal assemblages). Other organic macromolecules, in particular acidic glycoproteins, become incorporated into the shell as intracrystalline organic matrix (Marin et al., 2012). Trace and minor elements, however, can substitute for Ca<sup>2+</sup> in the crystal lattice (Carriker et al., 1980), be adsorbed to mineral surfaces (Carriker et al., 1980), bound to organics (Lingard et

al, 1992; Schöne et al., 2010), or be incorporated as separate mineral phases (Carriker et al., 1982; Fritz et al., 1990). How these ions are transported to the site of calcification will be discussed in the following.

The calcifying fluid in the EPS of marine bivalves is nearly isosmotic with the ambient water with regard to trace and minor elements (Wada and Fujinuki, 1976), because ions can passively move across the mantle epithelia via intercellular diffusion (Wilbur and Saleuddin, 1983) and intracellular ion channels (e.g. Carré et al., 2006). To meet the high demand of the main building materials of shell formation, a large proportion of  $\text{Ca}^{2+}$  and  $\text{HCO}_3^-$  ions are also actively transported to the EPS through enzymatic pumps such as  $\text{Ca}^{2+}$ -ATPase (Wilbur and Saleuddin, 1983). A fourth transmembrane ion transport mechanism possibly involves membrane-coated vesicles (granules) containing amorphous calcium carbonate (ACC; Han and Aizenberg, 2008; Jacob et al., 2011; for a review also see Addadi et al., 2003; Cartwright et al., 2012) that are released by the mantle epithelium into the EPS, where ACC becomes destabilized and then converted into a crystalline polymorph of  $\text{CaCO}_3$ . Although the calcifying fluid in the EPS has nearly the same chemical composition as the ambient water, the shell is depleted in many elements including Sr. Presumably, organic macromolecules synthesized by mantle epithelial cells and released into the EPS control the amount and type of trace elements that are incorporated into the shell (compare Stephenson et al., 2008), as well as the crystal morphology, size and orientation. Organic macromolecules not only control the formation of specific microstructures and  $\text{CaCO}_3$  polymorphs (Marin et al., 2004), they also trigger and inhibit the formation of new nanocrystal assemblages (Marin et al., 2007). As illustrated by this brief review, bivalve shell formation is under strong biological control. The concentration of many trace and minor elements in the shell is thus much lower than expected from abiogenic precipitation experiments.

## 2.3 Sample locality and shell preparation

On 11 March 2014, one specimen of *C. edule* (SNS-11Mar14-A20) was collected alive from the high intertidal zone of the North Sea near the village of Schillig, Germany (53°42′45.68″N, 008°01′14.88″E). After removing the soft tissues and cleaning the shell from adherent sediment, the left valve was mounted on a plexiglass cube. To prevent damage during sawing, the valve was covered with a thin layer of quick-drying epoxy resin (JB KWIK). Then, a 2-millimeter-thick section was cut along the axis of maximum growth, embedded in epoxy resin (Struers EPOFix) and stored under vacuum for three hours to remove air-bubbles from the resin. For NanoSIMS analyses,

the sample was ground on SiC disks (P320, P600, P1200, P2400). Polishing was performed with a 3  $\mu\text{m}$  poly-diamond solution followed by three hour fine-polishing on a Buehler VibroMet using 1  $\mu\text{m}$   $\text{Al}_2\text{O}_3$  powder. To prevent any contamination, the sample was ultrasonically cleaned in Milli-Q water between each preparation step. Then, the sample was coated with a  $\sim 10$ -nanometer thick Pt-Pd-layer and analyzed by means of NanoSIMS. Subsequently, element concentrations of the same sample were determined by means of electron microprobe analysis. For this purpose, the sample was ground and polished again with a Struers Tegramin 25/30 system using diamond discs and poly-diamond solutions of various grit sizes. Between each grinding step, the sample was ultrasonically cleaned in a mixture of alcohol and water. Before coating the sample with a 20-nanometer thick layer of carbon, the sample was dried overnight in a vacuum oven (70 °C) to remove any extant water from the sample surface.

## 2.4 Shell microstructures and growth patterns

Shell microstructures and growth patterns were analyzed with a LOT Quantum Design FEI Phenom (2<sup>nd</sup> edition) electron microscope at 4100 to 48,000  $\times$  magnification. Microgrowth patterns were analyzed within the third ontogenetic year (Figs. 1A+B). Images for microstructural analyses were taken in shell portions that formed during the last four ontogenetic years, i.e., during age three to six.

## 2.5 Semi-quantitative mapping using NanoSIMS

Ion maps of  $^{44}\text{Ca}^+$  and  $^{88}\text{Sr}^+$  were obtained using a NanoSIMS 50 (AMETEK, Inc., CAMECA SAS) housed at the Atmosphere and Ocean Research Institute, University of Tokyo. A 100 pA primary  $^{16}\text{O}^-$  beam with diameter of  $\sim 2$   $\mu\text{m}$  was used at an accelerating voltage of 8 kV. Secondary ions were detected simultaneously using a multi-collector electron multiplier system. The mass resolution power was 4000 at 10% peak height. Maps of 50 x 50  $\mu\text{m}$  were measured with a raster size of 256 x 256 pixels, and a total of 30 flames were taken on each map. The collecting time was 65 seconds per flame. After pre-sputtering, which was included within the 30 flames, clear ion images were obtained (usually between 15<sup>th</sup> and 29<sup>th</sup> flame). Because carbonate is easily charged, it is difficult to define the exact pre-sputtering time through each session. From corrected images, ion maps of  $^{88}\text{Sr}^+ / ^{44}\text{Ca}^+$  were calculated and expressed as  $^{88}\text{Sr}^+ / ^{44}\text{Ca}^+ \times 10,000$ . Ion images were analyzed using the free image processing software ImageJ including the openmims plugin (<http://imagej.nih.gov/ij/>; <http://nrims.harvard.edu/software/openmims>; last checked on 17 March 2016).

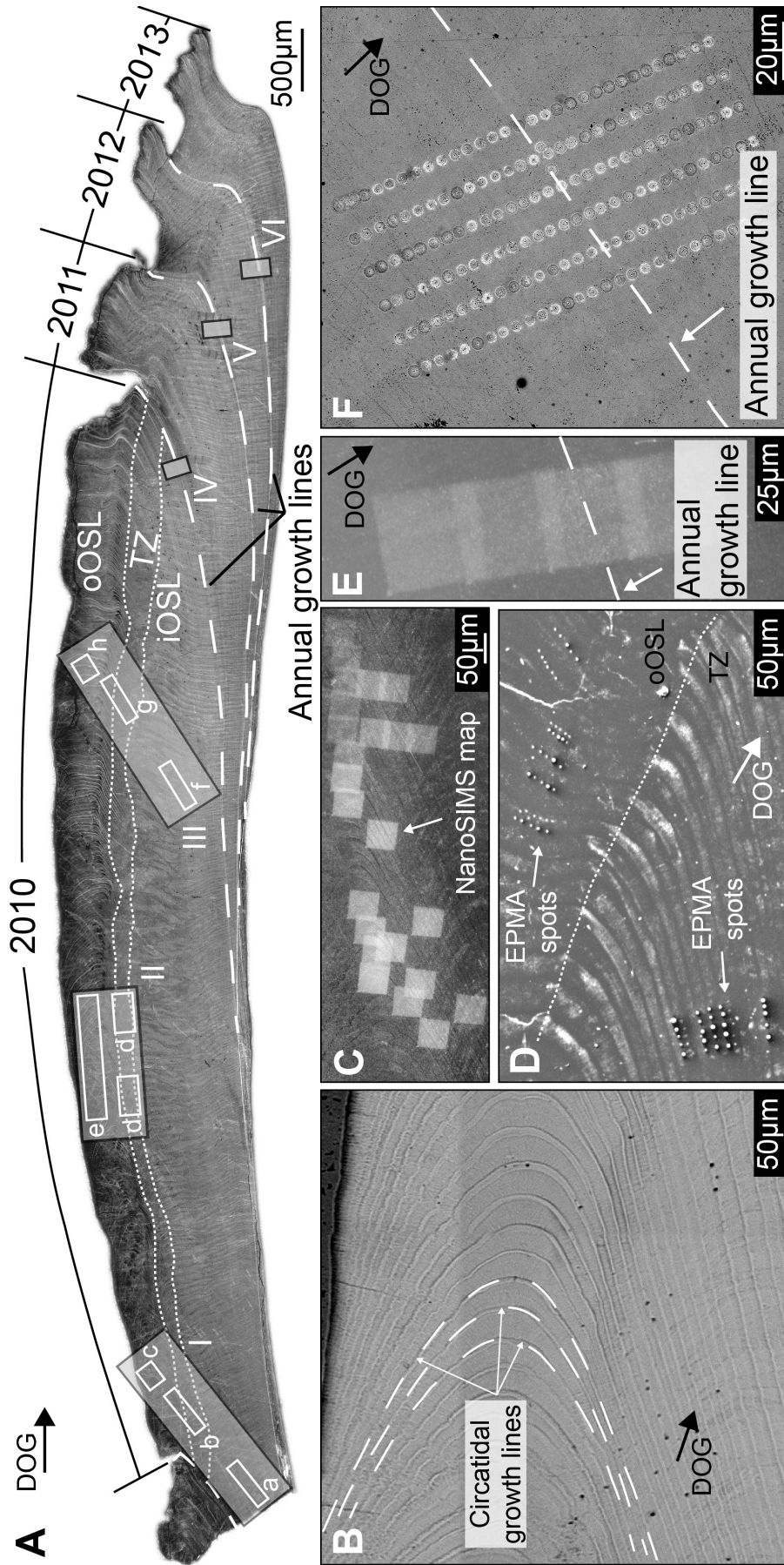




**Fig. 1.** Synopsis of sampled shell regions and applied sample techniques. (A) Light-microscopy image of analyzed shell thick-section. Annual growth lines are indicated by dashed white lines. White dotted lines denote limits of the different shell layers (iOSL = inner outer shell layer; TZ = transition zone; oOSL = outer outer shell layer). Roman numerals (I–VI) indicate shell regions analyzed with EPMA. Regions I–III are further divided into sub-regions (a–h) corresponding to transects of the same sequence of consecutive circatidal increments and lines measured within different shell layers. (B) Close-up of oOSL and TZ focused on circatidal growths patterns. Dashed lines represent circatidal growth lines. A couplet of two circatidal growth increments forms each lunar day (~24.8 h). (C) NanoSIMS-maps acquired in oOSL and TZ. Mapped areas are approximately located between region II and III. (D) EPMA measurements on consecutively formed circatidal growth lines and increments. The geochemical composition of each growth structure is inferred from the arithmetical mean of 5 spot analyses. (E) NanoSIMS-maps across an annual growth line (region IV). (F) EPMA-grit across an annual growth line (region IV). DOG = direction of growth.

## 2.6. Quantitative spot measurements using electron probe microanalyzer

Quantitative concentrations of strontium, sulfur and calcium were determined with an electron probe microanalyzer (JEOL JXA 8200) in spot mode (WDS; 15 kV accelerating voltage; 8 nA beam current; 1  $\mu\text{m}$  beam diameter; 2–3  $\mu\text{m}$  excitation radius) at the Institute of Geosciences, University of Mainz. Measurements were completed in six different regions (I–VI; Fig. 1A). Element levels measured in region I (= early growing season of 2010; ontogenetic year three), II (= main part of the growing season) and III (= towards the end of the growing season 2010) focused on geochemical variations of circatidal growth patterns. Each of the three regions was further subdivided into two (= region II, sub-region d–e) to three (= region I, sub-region a–c; region III, sub-region f–h) sub-regions, respectively, which covered approximately the same time interval within the oOSL, TZ and iOSL (Figs. 1A+D). Each data point represents the arithmetic mean of five spots measured in close proximity (ca. 5  $\mu\text{m}$  distance between each spot; Fig. 1D).

Regions IV–VI correspond to grids (= 6 x 25, 6 x 30, and 8 x 25 spots; spot-to-spot distance ca. 12 to 15  $\mu\text{m}$  lateral and 5  $\mu\text{m}$  vertical) measured across annual growth lines (IV = 2010/11; V = 2011/12, VI = 2012/13; Figs. 1A+F). Within each grid, data of spots arranged in rows parallel to the annual growth lines were arithmetically averaged. Because of the complex orientation of annual growth lines in the TZ and in the oOSL, electron microprobe measurements were only completed in the iOSL. In total, the concentration of Sr, S and Ca was measured in 1226 single spots.

Synthetic strontiumsulfate ( $\text{SrSO}_4$ ), bariumsulfate ( $\text{BaSO}_4$ ) and calcite ( $\text{CaCO}_3$ ) minerals were analyzed as standards for strontium, sulfur and calcium concentrations, respectively. Average concentrations of repeated measurements agree within 2.3% with reference values and the relative standard deviations (1 RSD) are < 2.7%. Strontium and sulfur concentrations were normalized to calcium and reported as  $\text{Sr}/\text{Ca}_{\text{shell}}$  and  $\text{S}/\text{Ca}_{\text{shell}}$  ratios, respectively.

### 3 Results

The studied specimen of *C. edule* was six years-old when collected. The last annual increment formed during 2013; the growing season of 2014 had not yet started when the bivalve was collected. As expected, the broadest annual increments were deposited during age one to three. Thereafter, growth rates decreased strongly. Tide-controlled microgrowth patterns such as circatidal, circalunidian, and fortnightly growth increments and lines were particularly well developed in ontogenetic years two and three.

#### 3.1 Shell microstructure

Each shell portion was characterized by a specific microstructure (Fig. 2). Nondenticular composite prismatic microstructures (= CP) predominated in the oOSL (Fig. 2B), crossed-acicular structures (= CA) in the TZ (Fig. 2C) and crossed-lamellar structures (= XLM) in the iOSL (Fig. 2D). Microstructures were disrupted by growth lines that stretched parabolically-shaped from the oOSL to the iOSL and ultimately approached the inner shell layer at a very low angle (Figs. 1A+B). Circatidal growth lines were broadest (ca. 3 – 8  $\mu\text{m}$ ) in the oOSL and became gradually narrower toward the myostracum (ca. 0.2 – 1  $\mu\text{m}$ ). Within the oOSL, growth lines consisted of irregular simple prisms (= ISP; Fig. 2B2) and as such differed structurally from the adjacent increments (= CP; Fig. 2B1). Within the circatidal lines, the longest axes of the prisms were aligned parallel to the direction of growth (Fig. 2B). Transitions between the microstructures of the growth increments and lines were abrupt. Within a single growth line, prisms gradually broadened in the direction of growth and were typically larger than structural units of the adjacent increments (Fig. 2B2). Within the TZ, growth lines also consisted of ISP and differed from the adjacent microstructure (= CA; Fig. 2C). In the iOSL, growth lines and increments consisted of the same microstructure (= XLM; Fig. 2D) and were only distinguishable from each other by larger 3<sup>rd</sup>-order lamellae in the circatidal growth lines (Fig. 2D2). The transition between larger and smaller 3<sup>rd</sup>-order lamellae in circatidal growth lines and increments was abrupt. Consequently, in each shell layer the same (contemporaneously formed) growth line differed microstructurally.

Annual growth lines showed the same sequence of microstructures as observed for intra-annual lines, i.e., ISP in the oOSL and TZ, and XLM in the iOSL. Widths of annual growth lines measured between ca. 1 and 5  $\mu\text{m}$ . Transitions between the microstructures of the annual growth increments and lines were abrupt in the oOSL and TZ, but gradual in the iOSL (Figs. 2E+E1).

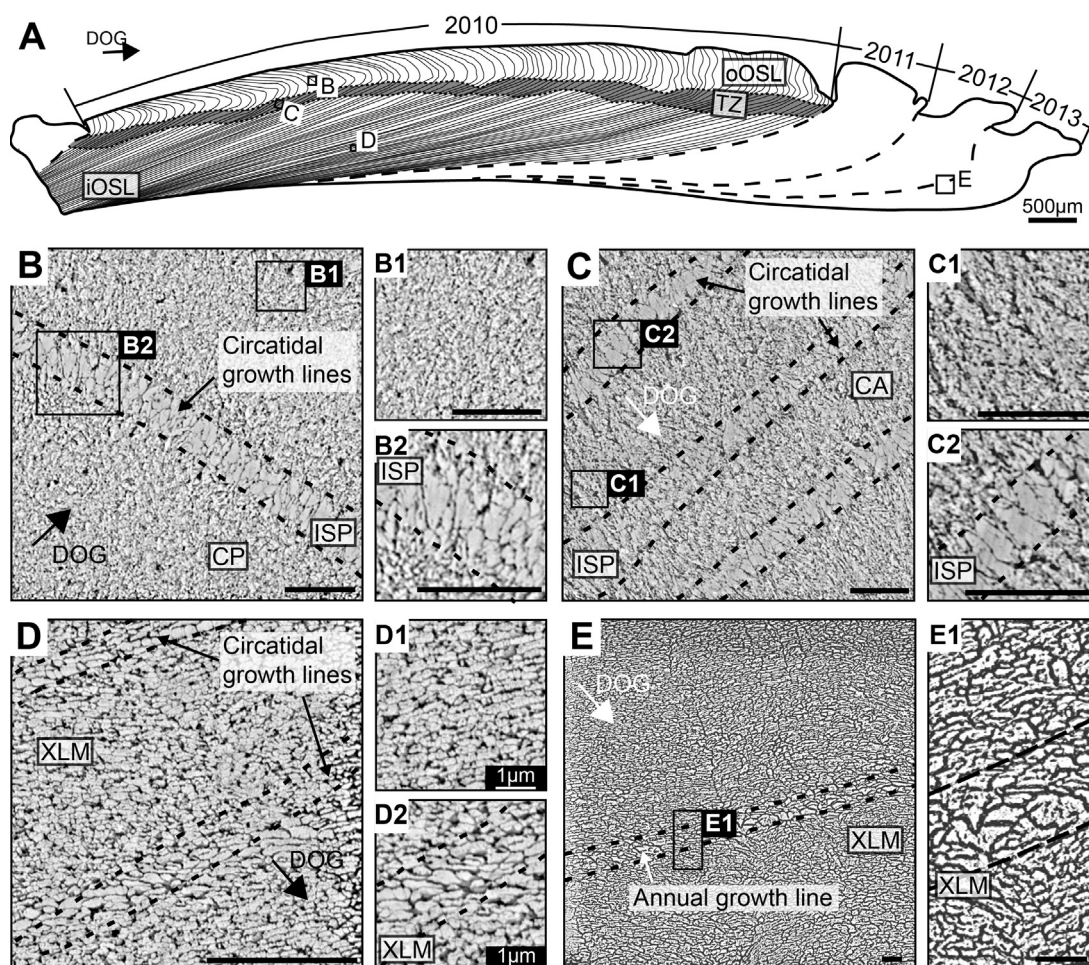


**Fig. 2.** SEM images of microstructures of *C. edule* within circatidal and annual growth patterns. (A) Schematic illustration of circatidal (thin black parabolic lines) and annual (thick black dashed lines) growth patterns and shell layers (inner outer shell layer = iOSSL; transition zone = TZ; outer outer shell layer = oOSSL; subdivided by fine dashed line) of the last four growing season (2010–2013). (B) Microstructures of the oOSSL with nondenticular composite prismatic structures (= CP) in circatidal increments (B1) and irregular simple prisms (= ISP) in circatidal growth lines (B2). Note the abrupt change between both structures. (C) Microstructures of the TZ with circatidal increments formed by crossed-acicular structures (= CA; C1) and circatidal growth lines characterized by irregular simple prisms (= ISP; C2). (D) Microstructures of the iOSSL, with circatidal increments and growth lines both formed by crossed-lamellar structures (= XLM). Note the difference in size between smallest units (3<sup>rd</sup>-order lamellae) in the increments (D1) and within the growth line (D2). (E) Crossed-lamellar structures within the iOSSL along an annual growth line. Third-order lamellae are slightly enlarged at the annual line (E1). In all images (B–E) dashed lines indicate transitions between growth line and increment. Scale bar if not otherwise indicated represents 5 μm. DOG = Direction of growth.

### 3.2 Intra-annual Sr/Ca<sub>shell</sub> and S/Ca<sub>shell</sub> variations

Semi-quantitative element maps determined by NanoSIMS revealed distinct Sr/Ca<sub>shell</sub> enrichments at circatidal growth lines (Fig. 3A). Within the oOSSL and the TZ, the transition between enriched and depleted domains was abrupt and associated with a change in microstructure (Figs. 3B+C). In contrast, within the iOSSL, the difference of Sr concentration in lines and increments was smaller and the transition between the two growth structures less abrupt (Fig. 3D).

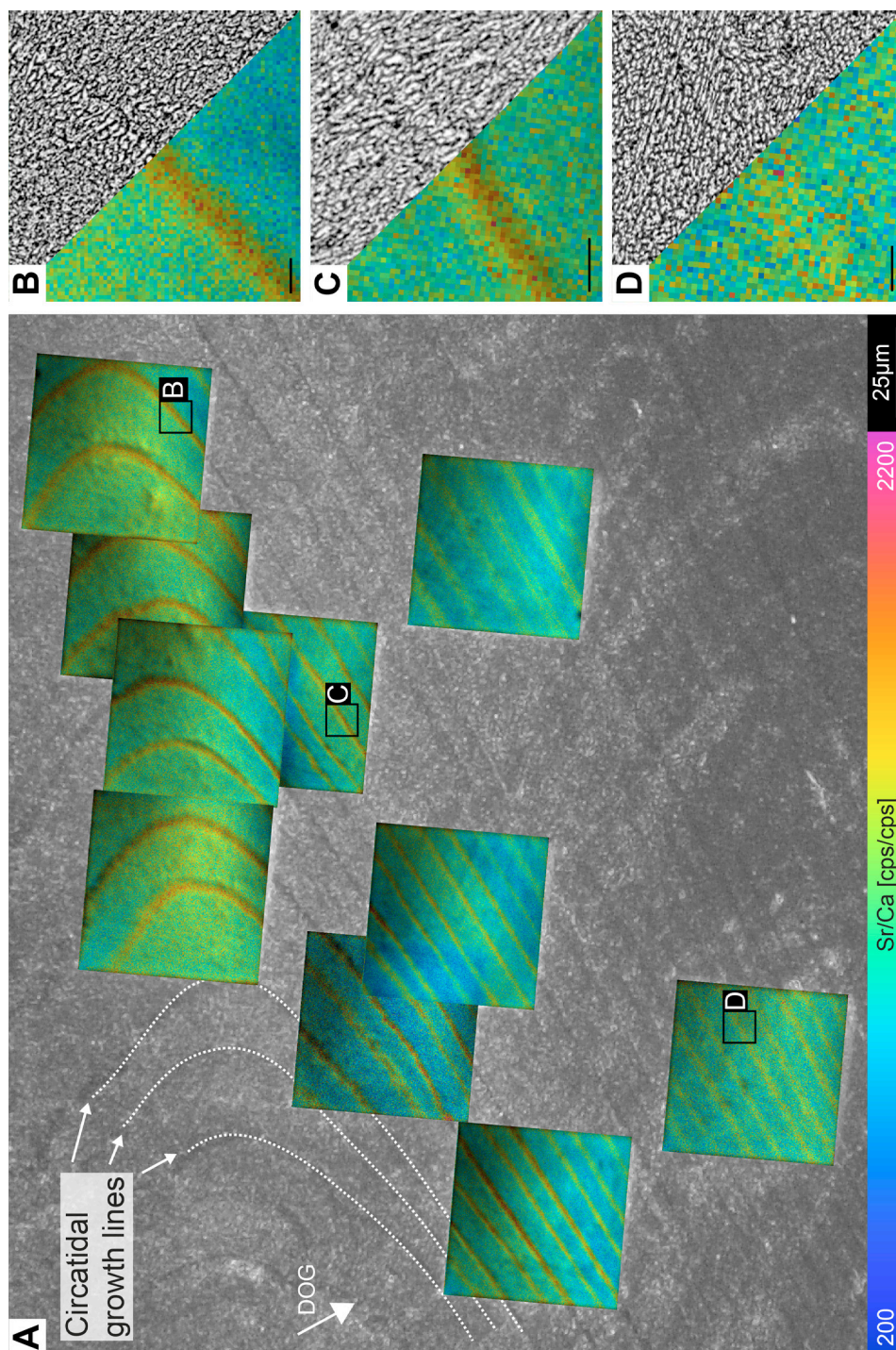


**Fig. 3.**  $\text{Sr}/\text{Ca}_{\text{shell}}$  ratios and microstructures along circatidal growth patterns in the oOSL and TZ of ontogenetic year three. (A) Semi-quantitative  $\text{Sr}/\text{Ca}_{\text{shell}}$  maps superimposed on a light microscope image. Signal intensity ( $^{88}\text{Sr}^{+}/^{44}\text{Ca}^{+} \times 10,000$ ) is given in color code. Circatidal growth lines are indicated by white dashed lines. (B–D) Contextualization of microstructure and semi-quantitative  $\text{Sr}/\text{Ca}_{\text{shell}}$  maps across circatidal growth lines in (B) the oOSL, (C) the TZ and (D) the iOSL. Note the exact match of varied microstructures and enriched  $\text{Sr}/\text{Ca}_{\text{shell}}$  ratios. DOG = direction of growth. Scale bar if not otherwise indicated represents 1  $\mu\text{m}$ .

As revealed by electron microprobe,  $\text{Sr}/\text{Ca}_{\text{shell}}$  ratios in ontogenetic year three measured, on average (all values averaged),  $2.5 \pm 0.4$  mmol/mol. Circatidal growth lines contained, on average, 15% more Sr than circatidal increments. The arithmetic mean of all studied circatidal growth lines equaled  $2.7 \pm 0.4$  mmol/mol, whereas the mean of all studied circatidal increments was  $2.3 \pm 0.3$  mmol/mol (Table 1). The same distribution pattern of Sr-enriched circatidal lines and Sr-depleted increments persisted in each portion of the OSL, i.e., the oOSL, TZ and iOSL (Fig. 1A), and was particularly well observed in sub-region ‘e’ (Fig. 4A). The largest difference between lines and increments was 0.6 mmol/mol in the oOSL (Table 1). Furthermore, along contemporaneously formed shell portions,  $\text{Sr}/\text{Ca}_{\text{shell}}$  increased from the iOSL to oOSL (Table 1). In one studied transect, however, this trend was not present (Table 1).

Sulfur-to-calcium ratios ( $\text{S}/\text{Ca}_{\text{shell}}$ ) of ontogenetic year three measured on average  $2.2 \pm 0.4$  mmol/mol. Contrasting findings of  $\text{Sr}/\text{Ca}_{\text{shell}}$  ratios,  $\text{S}/\text{Ca}_{\text{shell}}$  was depleted at circatidal growth lines (mean of all studied circatidal growth lines:  $2.1 \pm 0.5$  mmol/mol) and enriched within circatidal increments were (mean of all studied circatidal increments:  $2.3 \pm 0.3$  mmol/mol). When the studied portions of the iOSL-oOSL-transects were individually analyzed,  $\text{S}/\text{Ca}_{\text{shell}}$  ratios were enriched in increments by up to 0.5 mmol/mol (= 30%) in eight out of nine cases (Table 1). In comparison with  $\text{Sr}/\text{Ca}_{\text{shell}}$  the distribution pattern of enriched circatidal increments and depleted circatidal growth lines was less distinct (Fig. 4B). No significant correlation was found between  $\text{S}/\text{Ca}_{\text{shell}}$  and  $\text{Sr}/\text{Ca}_{\text{shell}}$  in any of the studied shell portions (compare Figs. 4A and B).

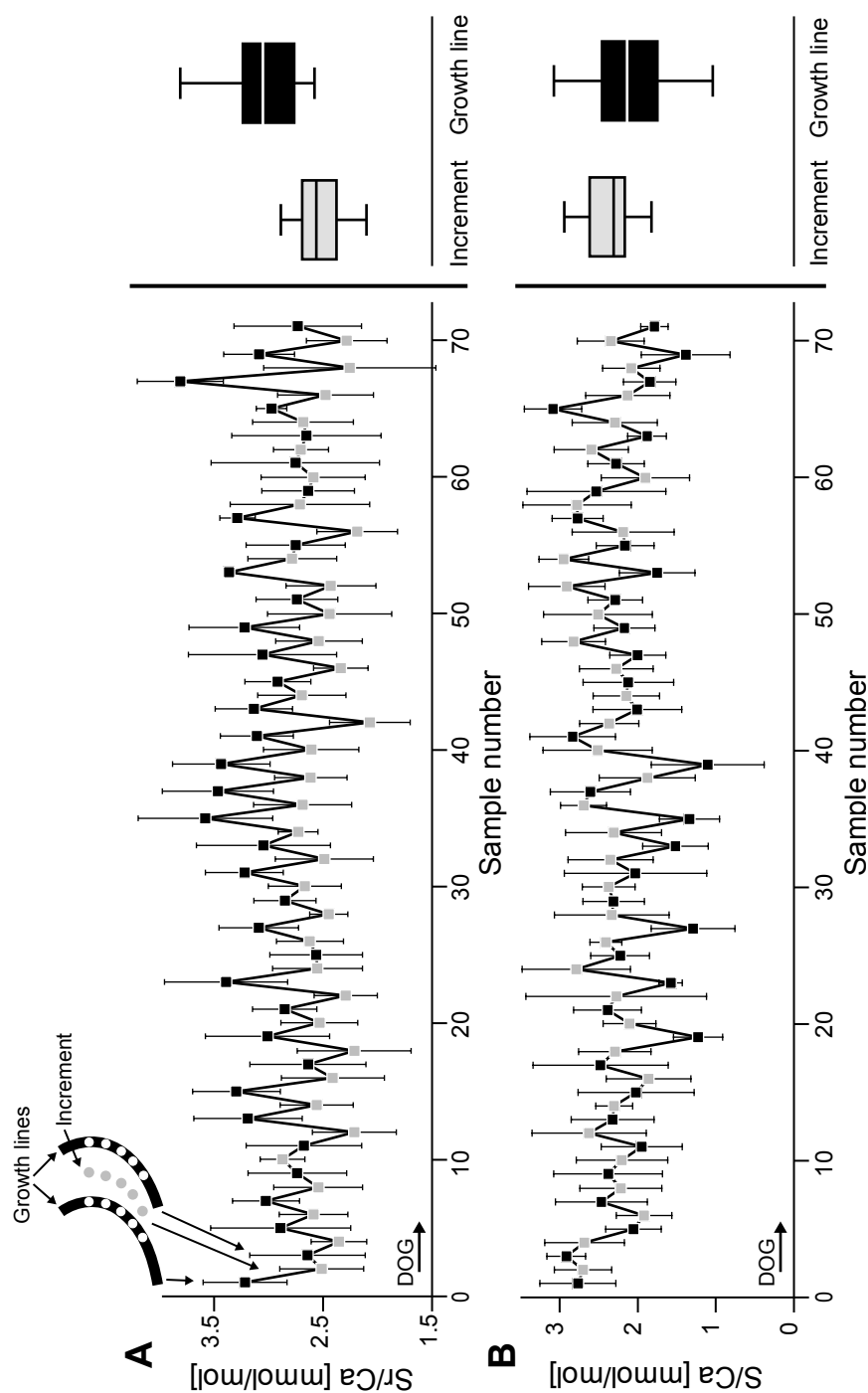


**Fig. 4.** Quantitative (A)  $\text{Sr}/\text{Ca}_{\text{shell}}$  and (B)  $\text{S}/\text{Ca}_{\text{shell}}$  ratios of 71 consecutively measured circatidal growth lines (= black squares) and growth increments (= grey squares) of sub-region 'e'. Each data point represents the arithmetical mean of 5 EPMA spot measurements (see sketch). Error bars represent  $1\sigma$  standard deviation. Data is plotted in direction of growth (= DOG). Boxplots show median, 25% and 75% quantiles of averaged data of circatidal increments and growth lines.

**Table 1.** Quantitative  $\text{Sr}/\text{Ca}_{\text{shell}}$  and  $\text{S}/\text{Ca}_{\text{shell}}$  ratios of circatidal growth structures measured within the growing season of 2010. Absolute (= Abs) and relative (= Rel) differences between circatidal growth lines (= GL) and increments (= Inc) are calculated for regions and corresponding sub-regions. Grey background if higher ratios were measured in growth lines; no background color if ratios were higher in increments. Asterisk marks statistical significant (2-way t-test) differences.

Region	n	Sr/Ca Average $\pm$ 1SD [mmol/mol]	S/Ca Average $\pm$ 1SD [mmol/mol]	Sub- region	n	Sr/Ca Average $\pm$ 1SD [mmol/mol]	S/Ca Average $\pm$ 1SD [mmol/mol]		
I	All	$2.3 \pm 0.4$	$2.4 \pm 0.2$	a	All	9	$1.9 \pm 0.2$	$2.1 \pm 0.4$	
					GL	4	$2.0 \pm 0.2$	$2.0 \pm 0.3$	
					Inc	5	$1.8 \pm 0.2$	$2.2 \pm 0.4$	
					Abs. difference		0.1	0.2	
					Rel. difference		7%	8%	
					All	9	$2.4 \pm 0.4$	$2.4 \pm 0.5$	
	GL	15	$2.4 \pm 0.4$	$2.3 \pm 0.2$	b	GL	4	$2.6 \pm 0.2$	$2.3 \pm 0.5$
						Inc	5	$2.2 \pm 0.2$	$2.6 \pm 0.2$
						Abs. difference		0.5	0.4
	Rel. difference		17%	17%					
	All	$2.3 \pm 0.3$	$2.3 \pm 0.1$	c	All	9	$2.5 \pm 0.3$	$2.6 \pm 0.6$	
					GL	4	$2.7 \pm 0.1$	$2.5 \pm 0.3$	
					Inc	5	$2.2 \pm 0.2$	$2.6 \pm 0.2$	
					Abs. difference		0.5*	0.2	
					Rel. difference		17%	6%	
All					16	$2.3 \pm 0.3$	$2.3 \pm 0.3$		
II	All	$2.5 \pm 0.3$	$2.3 \pm 0.1$	d	GL	5	$2.4 \pm 0.3$	$2.3 \pm 0.3$	
					Inc	5	$2.2 \pm 0.3$	$2.3 \pm 0.2$	
					Abs. difference		0.3	0.01	
					Rel. difference		10%	1%	
					All	71	$2.8 \pm 0.4$	$2.2 \pm 0.4$	
					GL	44	$2.7 \pm 0.4$	$2.2 \pm 0.4$	e
	Inc	36	$2.5 \pm 0.2$	$2.4 \pm 0.3$					
	Abs. difference		0.5*	0.3*					
	Rel. difference		17%	13%					
	III	All	$2.3 \pm 0.3$	$1.9 \pm 0.1$	f	All	8	$2.0 \pm 0.3$	$2.1 \pm 0.4$
						GL	5	$2.2 \pm 0.1$	$2.1 \pm 0.5$
						Inc	3	$1.8 \pm 0.3$	$2.0 \pm 0.2$
Abs. difference							0.4*	0.1	
Rel. difference							18%	3%	
All						8	$2.6 \pm 0.4$	$1.9 \pm 0.2$	
GL		15	$2.5 \pm 0.3$	$1.9 \pm 0.2$	g	GL	5	$2.8 \pm 0.2$	$1.9 \pm 0.2$
						Inc	3	$2.2 \pm 0.2$	$1.9 \pm 0.2$
						Abs. difference		0.6*	0.1
Rel. difference			20%	3%					
All		$2.3 \pm 0.3$	$1.9 \pm 0.1$	h	All	8	$2.3 \pm 0.3$	$1.8 \pm 0.4$	
					GL	5	$2.4 \pm 0.3$	$1.6 \pm 0.3$	
	Inc				3	$2.2 \pm 0.3$	$2.1 \pm 0.4$		
	Abs. difference					0.2	0.5		
	Rel. difference					9%	30%		
	All				24	$2.3 \pm 0.3$	$1.9 \pm 0.1$		

### 3.3 Sr/Ca<sub>shell</sub> and S/Ca<sub>shell</sub> ratios at annual growth lines

In the vicinity of annual growth lines studied in the iOSL, semi-quantitative element maps revealed strong Sr/Ca<sub>shell</sub> enrichments (Fig. 5). Highest values were associated with minor microstructural changes, i.e., larger 3<sup>rd</sup>-order lamellae (Figs. 5B+C). Sr/Ca<sub>shell</sub> ratios at annual growth lines measured between 3.1 and 4.0 mmol/mol and thus consistently exceeded ratios determined at circatidal growth lines (Table 2). Lowest values (1.3 – 1.4 mmol/mol) were measured shortly after the annual growth line confirming qualitative observations (Figs. 5+6). In contrast to circatidal growth lines, S/Ca<sub>shell</sub> values were typically highest near the annual growth lines (3.8 – 4.8 mmol/mol) and considerably lower in the adjacent shell portions (Figs. 5+6). As in the case of Sr/Ca<sub>shell</sub>, highest S/Ca<sub>shell</sub> ratios occurred without a major change of the predominant microstructure. Variations of Sr/Ca<sub>shell</sub> and S/Ca<sub>shell</sub> at annual growth lines were significantly positively correlated ( $0.34 < r^2 < 0.75$ ;  $p < 0.01$ ; Fig. 6).



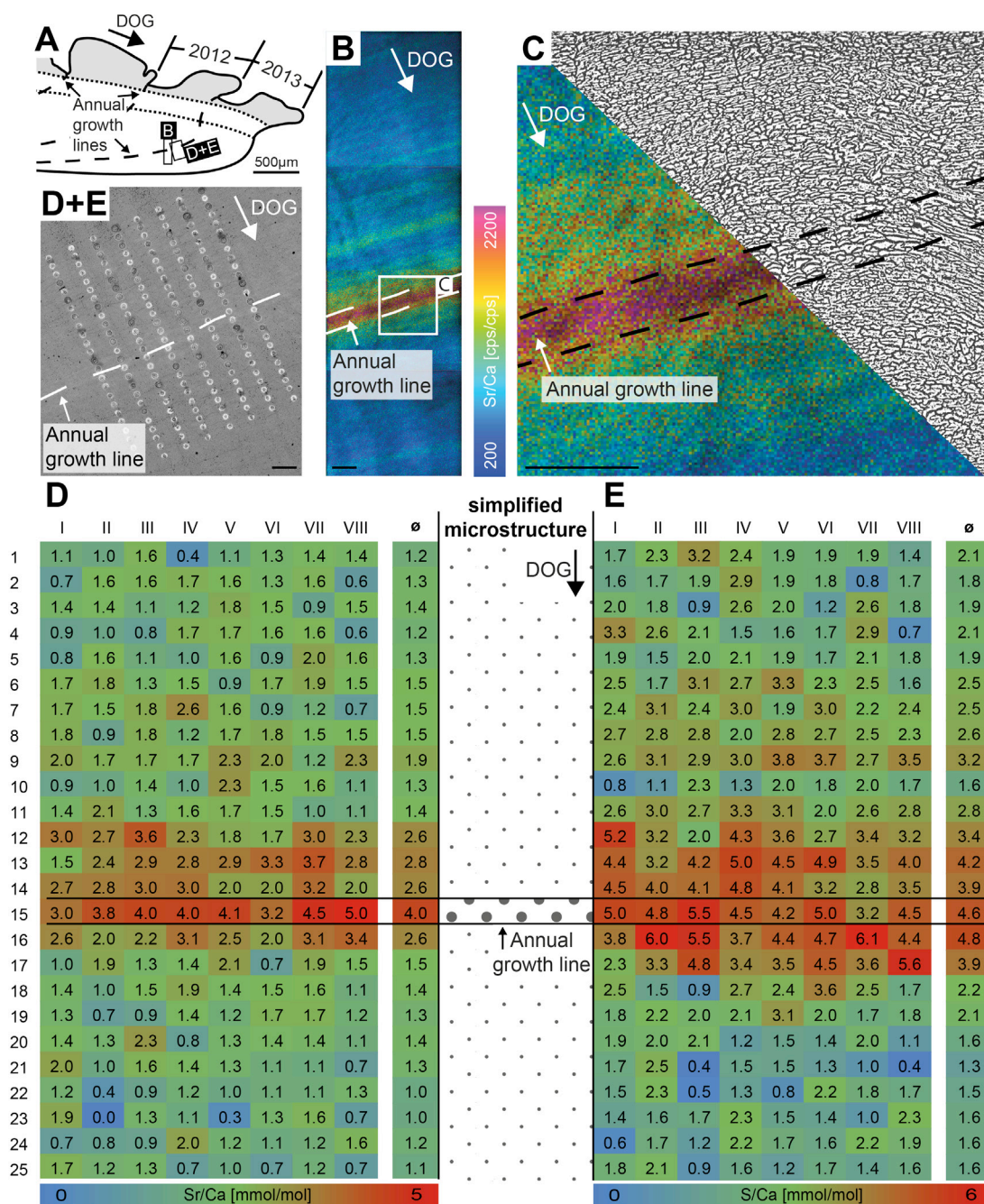


**Fig. 5.** Semi-quantitative and quantitative  $\text{Sr}/\text{Ca}_{\text{shell}}$  and  $\text{S}/\text{Ca}_{\text{shell}}$  ratios across the annual growth line of winter 2012/2013. (A) Schematic illustration of shell layers, annual growth layers and the sampled region. Annual growth lines are indicated by dashed black lines, transitions between the different shell layers by black dotted lines. (B) Semi-quantitative  $\text{Sr}/\text{Ca}_{\text{shell}}$  maps. Annual growth line is indicated by white dashed line. Signal intensity ( $^{88}\text{Sr}^{+}/^{44}\text{Ca}^{+} \times 10,000$ ) is given in color code. (C) Contextualization of microstructure and  $\text{Sr}/\text{Ca}_{\text{shell}}$  ratios across annual growth line. (D+E) Microprobe spots measured across annual growth line. Quantitative  $\text{Sr}/\text{Ca}_{\text{shell}}$  (D) and  $\text{S}/\text{Ca}_{\text{shell}}$  ratio (E) of each spot is listed in tabular form. DOG = direction of growth. Scale bar if not otherwise indicated represents 5  $\mu\text{m}$ .

**Table 2.** Quantitative Sr/Ca<sub>shell</sub> and S/Ca<sub>shell</sub> ratios across annual growth lines of 2010/2011 (= region IV), 2011/2012 (= region V) and 2012/2013 (= region VI), respectively. Each sample number represents the arithmetic mean of 6 to 8 EPMA spot measurements arranged in a line approximately parallel to the annual growth line, i.e. perpendicular to the direction of growth (see Figs. 1A+F and Figs. 5D+E for orientation). Sample numbers increase with direction of growth. Approximate position of the annual growth line is depicted by grey background.

Sample number	Region IV		Sample number	Region V		Sample number	Region VI	
	2010/2011			2011/2012			2012/2013	
	Sr/Ca	S/Ca		Sr/Ca	S/Ca		Sr/Ca	S/Ca
	Average ± 1SD			Average ± 1SD			Average ± 1SD	
	[mmol/mol]			[mmol/mol]			[mmol/mol]	
1	1.6 ± 0.1	2.6 ± 0.6	1	1.8 ± 0.2	2.7 ± 0.8	1	1.2 ± 0.4	2.1 ± 0.5
2	1.7 ± 0.5	2.6 ± 0.4	2	1.8 ± 0.3	2.6 ± 0.6	2	1.3 ± 0.4	1.8 ± 0.6
3	1.9 ± 0.4	3.1 ± 0.6	3	1.9 ± 0.6	3.1 ± 0.8	3	1.4 ± 0.3	1.9 ± 0.6
4	1.8 ± 0.6	2.9 ± 0.5	4	2.2 ± 0.4	3.1 ± 0.7	4	1.2 ± 0.4	2.1 ± 0.8
5	2.2 ± 0.8	3.8 ± 0.9	5	2.0 ± .4	3.8 ± 0.3	5	1.3 ± 0.4	1.9 ± 0.2
6	3.3 ± 0.7	3.5 ± 0.3	6	2.0 ± 0.2	3.5 ± 0.4	6	1.5 ± 0.3	2.5 ± 0.6
7	1.7 ± 0.5	3.5 ± 0.7	7	2.3 ± 0.6	4.1 ± 0.9	7	1.5 ± 0.6	2.5 ± 0.4
8	2.2 ± 0.5	3.8 ± 1.0	8	1.5 ± 0.5	2.7 ± 0.3	8	1.5 ± 0.3	2.6 ± 0.3
9	1.7 ± 0.4	3.0 ± 0.9	9	1.6 ± 0.5	3.3 ± 1.0	9	1.9 ± 0.4	3.2 ± 0.4
10	1.8 ± 0.6	3.5 ± 0.7	10	1.5 ± 0.5	3.2 ± 0.9	10	1.3 ± 0.5	1.6 ± 0.5
11	2.8 ± 0.6	3.2 ± 0.5	11	2.4 ± 0.7	4.0 ± 0.7	11	1.4 ± 0.3	2.8 ± 0.4
12	1.9 ± 0.2	3.3 ± 0.6	12	1.7 ± 0.2	3.3 ± 0.4	12	2.6 ± 0.6	3.4 ± 1.0
13	1.4 ± 0.5	2.6 ± 0.9	13	1.4 ± 0.3	3.1 ± 0.7	13	2.8 ± 0.6	4.2 ± 0.6
14	1.6 ± 0.5	3.1 ± 0.3	14	1.4 ± 0.4	2.9 ± 0.8	14	2.6 ± 0.5	3.9 ± 0.7
15	1.8 ± 0.5	3.1 ± 0.4	15	2.4 ± 0.9	3.3 ± 0.5	15	4.0 ± 0.6	4.6 ± 0.7
16	1.5 ± 0.3	3.0 ± 0.8	16	1.9 ± 0.5	3.7 ± 0.7	16	2.6 ± 0.5	4.8 ± 0.9
17	1.6 ± 0.3	2.3 ± 0.5	17	1.3 ± 0.4	3.0 ± 0.3	17	1.5 ± 0.5	3.9 ± 1.0
18	1.8 ± 0.2	2.8 ± 0.3	18	1.9 ± 0.5	3.0 ± 0.5	18	1.4 ± 0.3	2.2 ± 0.8
19	1.6 ± 0.3	2.8 ± 0.5	19	1.7 ± 0.5	3.3 ± 0.7	19	1.3 ± 0.3	2.1 ± 0.4
20	1.8 ± 0.4	2.9 ± 0.9	20	1.8 ± 0.6	3.6 ± 0.6	20	1.4 ± 0.4	1.6 ± 0.4
21	1.7 ± 0.3	3.0 ± 0.8	21	2.4 ± 0.5	3.9 ± 0.5	21	1.3 ± 0.4	1.3 ± 0.7
22	1.6 ± 0.5	2.5 ± 0.4	22	3.1 ± 0.6	3.8 ± 0.9	22	1.0 ± 0.3	1.5 ± 0.6
23	1.7 ± 0.2	2.5 ± 0.7	23	2.3 ± 0.4	3.6 ± 1.0	23	1.0 ± 0.6	1.6 ± 0.4
24	1.4 ± 0.3	2.0 ± 0.7	24	2.9 ± 0.8	3.9 ± 0.5	24	1.2 ± 0.4	1.6 ± 0.5
			25	2.2 ± 0.8	4.1 ± 1.1	25	1.1 ± 0.4	1.6 ± 0.4
			26	1.6 ± 0.2	3.1 ± 0.9			
			27	1.3 ± 0.2	2.4 ± 0.5			

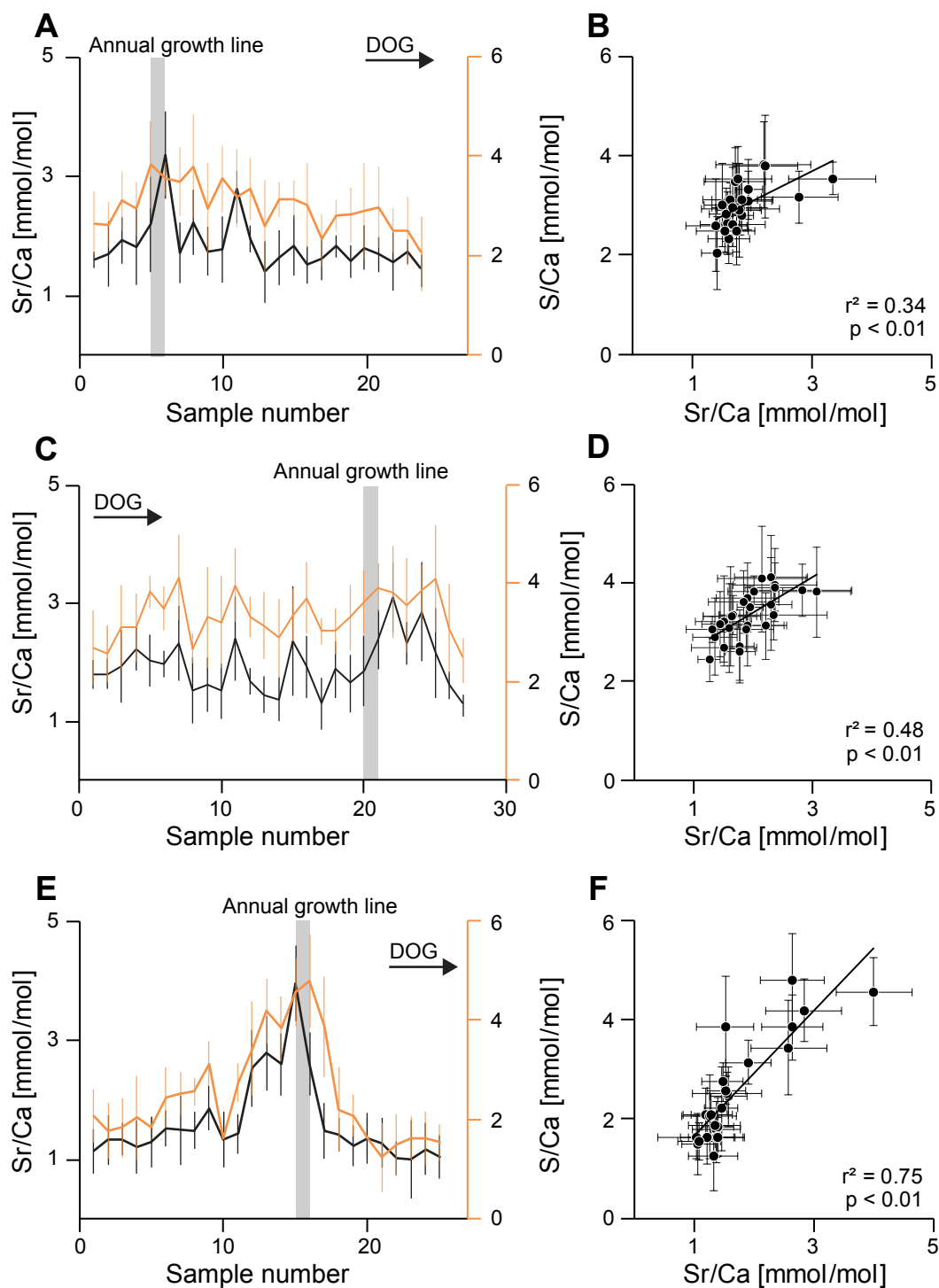


**Fig. 6.** Sr/Ca<sub>shell</sub> and S/Ca<sub>shell</sub> variations across annual growth lines (A = 2010/2011; B = 2011/2012; C = 2012/2013). Each sample number represents the arithmetic mean of 6 to 8 spots arranged in a line approximately parallel to the annual growth line (see Figs. 1A+F and Figs. 5D+E for orientation). Mean values are plotted with direction of growth (= DOG; perpendicular to the growth line). Error bars represent 1 $\sigma$  standard deviation. Grey bar indicates approximate position of annual growth line (= AGL). (B, D, F) Cross-plots of data shown in (A, C, E).

## 4 Discussion

Results of this study clearly demonstrated that Sr – on the lower micrometer-scale – was heterogeneously distributed in the shell of *C. edule*. Strontium was strongly enriched at the circatidal and annual growth lines and depleted in growth increments. Such changes were clearly linked to the shell architecture. Sulfur-to-calcium ratios of the shell also showed microstructure-related fluctuations. Lowest  $S/Ca_{\text{shell}}$  values were generally determined at circatidal growth lines, highest values at annual growth lines. Similar links between microstructure and trace chemistry have also been reported from corals (Meibom et al., 2008) and other bivalve species (Lazareth et al., 2003; Schöne et al., 2013; Shirai et al., 2014). With a coarser sampling resolution (e.g., LA-ICP-MS or wet chemical analysis of micromilled shell portions), the sharp geochemical variations at the micrometer-scale would have remained unnoticed. Yet, knowing the  $Sr/Ca_{\text{shell}}$  distribution patterns and their causes is an important prerequisite for establishing Sr/Ca as a temperature proxy in bivalves. It can also help to devise new sampling strategies.

### 4.1. Controls on the distribution of $Sr/Ca_{\text{shell}}$ at growth lines and increments

#### 4.1.1 Water temperature and $Sr/Ca_{\text{water}}$

The abrupt and strong increase of  $Sr/Ca_{\text{shell}}$  at the circatidal growth lines, specifically in the oOSL, can certainly not be explained by changes of temperature or  $Sr/Ca_{\text{water}}$ . Since Sr/Ca of the shell and water are positively correlated (Chen et al., 2015; Zhao et al., 2016) and the distribution coefficients for  $Sr/Ca_{\text{shell}}$  of *C. edule* and other bivalve species are typically low, i.e.,  $K^D_{Sr/Ca} = 0.2$  (Gillikin et al., 2005; Füllenbach et al., 2015), the observed average change of  $Sr/Ca_{\text{shell}}$  by 0.4 mmol/mol would require a concurrent rise of  $Sr/Ca_{\text{water}}$  by 2 mmol/mol ( $= 0.4 / 0.2$  mmol/mol) – within one tidal cycle. However, at the study site  $Sr/Ca_{\text{water}}$  values varied by less than ca. 0.6 mmol/mol during a one year-long monitoring experiment (Füllenbach et al., 2015). Furthermore, according to Dodd and Crisp (1982),  $Sr/Ca_{\text{water}}$  typically remains fairly conservative over long time-scales above a salinity of 10, and the salinity at the study site rarely dropped below 28 (Füllenbach et al., 2015). Thus, it is impossible to explain the strong  $Sr/Ca_{\text{shell}}$  variations by short-term changes of the water chemistry.

Likewise, required temperature changes would be unrealistically large. Given a negative correlation between temperature and  $Sr/Ca_{\text{shell}}$  in *C. edule* (Hallam and Price, 1968) and a temperature sensitivity of  $-0.02$  mmol/mol/°C (Füllenbach et al.,

2015), the average 0.4 mmol/mol shift in  $\text{Sr}/\text{Ca}_{\text{shell}}$  at the circatidal increments would imply a temperature drop during low tide by 20 °C. Even larger changes in  $\text{Sr}/\text{Ca}_{\text{water}}$  and/or water temperature were needed to produce the  $\text{Sr}/\text{Ca}_{\text{shell}}$  increase at the winter lines.

#### 4.1.2. Crystal kinetics and shell growth rate

Kinetic effects may serve as another explanation for the strong Sr-enrichment at the growth lines. For example, Gaetani and Cohen (2006) reported a positive correlation between crystal precipitation rate and the incorporation of  $\text{Sr}^{2+}$  into abiogenic aragonite. Since crystal kinetics of *C. edule* shells have not been determined, shell growth rate may serve as a proxy for kinetic effects. If Sr levels were controlled by kinetic effects, shell portions formed during fastest growth would contain the highest  $\text{Sr}/\text{Ca}_{\text{shell}}$  values. Evidently, this is not the case (Figs. 3A+4A). Circatidal growth increments (= period of fast growth) contain less Sr than circatidal growth lines (periods of slow growth) (Figs. 3A+4A). Furthermore, due to the shell curvature and the shape of the ventral margin, shell portions of the iOSL and TZ grow slower than contemporaneous portions of the oOSL. Therefore, one would expect gradually rising Sr levels along isochronous shell portions from the myostracum toward the outer shell surface. However, this was only the case in two of the three studied transects (Table 1).

#### 4.1.3. Biomineralization processes and shell microstructures

Sano et al. (2012) and Hori et al. (2015) also found distinct changes of Sr levels on the intra-annual time-scale in the giant clam, *Tridacna derasa*. Microgrowth lines that were formed during night showed ca. 0.4 to 0.7 mmol/mol higher  $\text{Sr}/\text{Ca}_{\text{shell}}$  values than fast-growing microgrowth increments precipitated during daytime. Sano et al. (2012) explained this finding with the variable activity of  $\text{Ca}^{2+}$ -ATPase. During periods of rapid biomineralization and higher metabolic rate, increased enzyme-mediated transmembrane transport of  $\text{Ca}^{2+}$  ions toward the EPS diluted the  $\text{Sr}^{2+}$  concentration in the calcifying fluids, therefore  $\text{Sr}/\text{Ca}_{\text{shell}}$  values can be used as proxy for daily light cycle. However, during night, the  $\text{Ca}^{2+}$ -ATPase activity was strongly reduced resulting in a relative increase of  $\text{Sr}^{2+}$  in the calcifying fluid and thus in the shell portions formed during that time. A similar mechanism may also account for the chemical variation observed in the shell of *C. edule*.

However, considering the changes in  $\text{S}/\text{Ca}_{\text{shell}}$  and the close coupling between  $\text{Sr}/\text{Ca}_{\text{shell}}$  and microstructure we favor an alternative model. The amount and type of trace impurities incorporated into the shell is primarily controlled by organic

macromolecules, and to a lesser extent by the concentration of these ions in the calcifying fluid. For example, peptides have been demonstrated to increase the concentration of magnesium in abiogenically precipitated calcite by lowering the dehydration enthalpy of the  $Mg^{2+}$  which facilitated the uptake of this cation (Stephenson et al., 2008). The strong biological control over element uptake and incorporation into the shell also becomes evident when the chemical compositions of the shell, the fluid in the EPS and ambient water are compared. The fluid in the EPS of marine bivalves reportedly has nearly the same composition with regard to trace and minor elements as the ambient seawater, but the chemistry of the shell differs significantly from that of the seawater and EPS (Klein et al., 1996; Gillikin et al., 2005; Poulain et al., 2015).  $Sr^{2+}$  is depleted in the shell, although much larger proportions of this element could potentially be accommodated in the crystal lattice of aragonite as demonstrated by abiogenic precipitation experiments (Gaetani and Cohen, 2006). Higher strontium levels at the growth lines could therefore indicate that the biological control mechanisms tailed off permitting more  $Sr^{2+}$  ions being incorporated into the biomineral during periods of slow growth. The bivalve may achieve this by synthesizing organic substances with different relative concentrations. Seasonal changes of the organochemical composition of the calcifying fluid have been documented, for example, for the bivalve *Anodonta cygnea* (Moura et al., 2000), and ontogenetic changes in *A. islandica* (Goodfriend and Weidman, 2001). Likely, such changes also occur on a sub-daily basis. Support for the assumption of a modified biochemical composition in the EPS during times of growth line formation and overall lower metabolic rates comes from concurrent changes in shell sulfur content. Sulfur is an important constituent of some of the organic macromolecules in the EPS (e.g. polysaccharides Dauphin, 2002) and can therefore serve as a proxy for organics (Dauphin et al., 2003).

It may also be possible that organic macromolecules in the EPS exert an indirect control over the incorporation of strontium into the shell. Proteins are known to control the formation of specific shell microstructures (Marin et al., 2012) whose units most likely possess different crystallographic orientations. In turn, the crystallographic orientation of the microstructural units affects the amount of trace elements that can be adhesively bound to mineral phase because different crystal faces can accommodate different amounts of foreign ions (Rimstidt et al., 1998). In the studied shell, portions with more distinct changes of the microstructure, i.e., the oOSL and TZ, showed more abrupt shifts of the Sr content than portions with weaker microstructural modifications, i.e., the iOSL. Noteworthy, the elevated  $Sr/Ca_{shell}$  levels in the shell were always associated with larger microstructural units (Figs. 3+5).

Furthermore, the organic phase of the EPS may affect the incorporation of  $Sr^{2+}$  into aragonite without interfering with the ions themselves. Since the incorporation

of small amounts of organics are known to alter the crystal lattice of biologically formed aragonite (Pokroy et al., 2004; Zolotoyabko and Pokroy, 2007; Younis et al., 2012), a slight variation of the crystallographic unit cell may change the amount of co-precipitated strontium. Potentially, some macromolecules of the EPS which are produced during the formation of the growth lines facilitate the incorporation of  $\text{Sr}^{2+}$  ions by modifying the crystal lattice.

## 4.2 $\text{Sr}/\text{Ca}_{\text{shell}}$ enrichment at circatidal and annual growth lines

On average,  $\text{Sr}/\text{Ca}_{\text{shell}}$  values at the annual growth lines were 30% higher than at circatidal growth lines (compare Table 1 and 2). At first glance, this is surprising because an annual growth line consists of a series of densely crowded circatidal growth increments and lines, i.e., a mixture of Sr-enriched and Sr-depleted shell portions. One would therefore expect a  $\text{Sr}/\text{Ca}_{\text{shell}}$  value at the annual growth line plotting somewhere between the average values measured at circatidal growth lines and increments. Apparently, the biomineralization processes change seasonally as previously noted for *A. cygnea* by Moura et al. (2000). Circatidal and annual growth lines not only differ in respect to Sr content, but also in their  $\text{S}/\text{Ca}_{\text{shell}}$  values (compare Table 1 and 2). While  $\text{S}/\text{Ca}_{\text{shell}}$  ratios at circatidal growth lines were low compared to the adjacent circatidal increments, sulfur concentrations near the annual growth lines were strongly enriched, even more than circatidal increments. Most likely, the organic composition of the EPS underwent significant changes during winter and contained a relative larger amount of sulfur-bearing substances that facilitated directly or indirectly the incorporation of  $\text{Sr}^{2+}$  in the inorganic phase of the biomineral.

## 4.3 Implications for future analysis of $\text{Sr}/\text{Ca}_{\text{shell}}$

Micrometer-scale, shell architecture-related variations of trace impurities in relation to sub-annual growth patterns have so far not been considered – to our knowledge – in any bivalve sclerochronological study. The intra-annual  $\text{Sr}/\text{Ca}_{\text{shell}}$  scatter of  $\pm 0.5$  mmol/mol reported Schöne et al. (2013) can at least to some degree be attributed to changing Sr levels at growth lines and increments. Analyses of sample spots covering a larger number of circatidal (or daily) growth lines would return higher  $\text{Sr}/\text{Ca}_{\text{shell}}$  values than those covering more circatidal (or daily) growth increments. The error induced by averaging chemical data from portions with different microstructures may partly explain why the correlation between temperature and  $\text{Sr}/\text{Ca}_{\text{shell}}$  was quite low in many existing studies ( $\sim R^2 < 0.4$ ; Takesue and van Geen, 2004; Carré et al, 2006; Füllenbach et al., 2015).

A stronger correlation between  $\text{Sr}/\text{Ca}_{\text{shell}}$  and temperature can likely be identified in shells with less microstructural variability. In fact, Zhao et al. (2016) recently presented such data for *C. fluminea* specimens that were reared under laboratory conditions. These authors reported an explained variability of nearly 50%. The microstructure of the shell portions that formed under artificial conditions deviated significantly from those formed in nature. Growth lines were only faintly developed and the shell microstructure (crossed-lamellar structures) hence nearly invariant. Similar observations were reported by Richardson et al. (1980) for artificially grown *C. edule* specimens. Presumably, the stronger correlation was a result of a more homogeneous microstructure and more homogeneous distribution of Sr.

Considering the findings herein, subsequent studies should (i) complete chemical measurements within the same shell layer and the same overall microstructure, i.e., the oOSL, TZ or iOSL of *C. edule*. (ii) The sampling resolution should be adapted to the size of the microgrowth structures so that  $\text{Sr}/\text{Ca}_{\text{shell}}$  levels in circatidal increments and lines are determined separately. (iii) To study the relationship with temperature and determine the temperature sensitivity,  $\text{Sr}/\text{Ca}_{\text{shell}}$  values of circatidal increments and lines as well as annual growth lines should then be plotted separately. (iv) If the temperature sensitivities of  $\text{Sr}/\text{Ca}_{\text{shell}}$  from circatidal increments, circatidal and annual growth lines are the same, it is possible to compute a mathematical model that can be used to correct data which were taken with lower sampling resolution and which cover different fractions of Sr-enriched lines and increments. If the temperature sensitivities of the different growth structures differ from each other, a lower sampling resolution is not advised. The data from the three growth structures must be then be treated separately and the chemical composition measured with the appropriate spatial resolution. To apply these strategies to other species, subsequent studies are required which determine the chemical heterogeneity of other bivalve species.

## 5 Summary and Conclusions

The  $\text{Sr}/\text{Ca}_{\text{shell}}$  levels of *C. edule* were strongly linked to the shell microstructure. Since the latter varied on small spatial scales,  $\text{Sr}/\text{Ca}_{\text{shell}}$  ratios were heterogeneously distributed across the shell. Sr was strongly enriched at circatidal growth lines and depleted in circatidal growth increments. Highest Sr levels occurred at annual growth lines. Near the outer shell surface, the Sr levels increased abruptly at the growth lines. Further inside of the shell near the myostracum, however, the Sr content fluctuated more gradually and microstructural changes at the growth lines were less pronounced. As a



general feature of elevated Sr concentration at growth lines was larger microstructural units. The distribution of sulfur was also inhomogeneous. Lowest  $S/Ca_{shell}$  levels were recorded at circatidal growth lines and highest at annual growth lines. The close link between  $Sr/Ca_{shell}$ , shell architecture and  $S/Ca_{shell}$  (as an indicator of composition and / or concentration of the organic matrix) suggests that microstructures or mechanisms in charge of their formation control the incorporation of strontium into the shells of this species.

It is therefore advised to measure the strontium content in the same shell layer and same overall microstructure and interpret the data from different growth structures separately.  $Sr/Ca_{shell}$  data from annual growth lines should not be combined with those determined at circatidal (or daily) increments and lines. Subsequent studies need to determine how the temperature sensitivity of  $Sr/Ca_{shell}$  from circatidal growth lines compares with  $Sr/Ca_{shell}$  from circatidal growth increments and annual growth lines, respectively. If the slopes of the regression lines agree with each other, a mathematical model can be constructed to correct  $Sr/Ca_{shell}$  data which were taken with lower sampling resolution and which cover different fractions of Sr-enriched lines and increments. Otherwise, the chemical data from different growth structures should be interpreted separately from each other.

Given that previous studies already found a statistically significant relationship between  $Sr/Ca_{shell}$  and water temperature by applying whole (Hallam and Price, 1968) and in-situ (= LA-ICP-MS) analyses (Füllenbach et al, 2015), it seems very likely that  $Sr/Ca_{shell}$ -based temperature reconstructions with shells of this species can be further improved by modifying the sampling strategies. Subsequent studies should test if similar sampling strategies could also help to establish the element-to-calcium-based paleothermometry using shells of other bivalve species.

## 6 Acknowledgments

Stephan Buhre and Nora Groschopf (University of Mainz) are kindly acknowledged for their help with EPMA measurements. Financial support for this project was provided by the German Research Foundation, Deutsche Forschungsgemeinschaft (DFG) to BRS (SCHO793/13) and by Grant-in-Aid for Scientific Research(S) JSPS KAKENHI Grant Number 24221002.

## 8 References

- Addadi, L., Raz, S., Weiner, S., 2003. Taking advantage of disorder: Amorphous calcium carbonate and its roles in biomineralization. *Adv. Mater.* 15, 959–970.
- Beck, J.W., Edwards, R.L., Ito, E., Taylor, F.W., Recy, J., Rougerie, F., Joannot, P., Henin, C., 1992. Sea-surface temperature from coral skeletal strontium/calcium ratios. *Science* 257, 644–647.
- Bevelander, G., Nakahara, H., 1969. An electron microscope study of the formation of the nacreous layer in the shell of certain bivalve molluscs. *Calc. Tiss. Res.* 3, 84–92.
- Bourget, E., Brock, V., 1990. Short-term shell growth in bivalves: individual, regional, and age-related variations in the rhythm of deposition of *Cerastoderma* (= *Cardium*) *edule*. *Mar. Biol.* 106, 103–108.
- Carré, M., Bentaleb, I., Bruguier, O., Ordinola, E., Barrett, N.T., Fontugne, M., 2006. Calcification rate influence on trace element concentrations in aragonitic bivalve shells: Evidences and mechanisms. *Geochim. Cosmochim. Acta* 70, 4906–4920.
- Carriker, M.R., Palmer, R.E., Sick, L.V., Johnson, C.C., 1980. Interaction of mineral elements in sea water and shell of oysters (*Crassostrea virginica* (Gmelin)) cultured in controlled and natural systems. *J. Exp. Mar. Biol. Ecol.* 46, 279–296.
- Carriker, M.R., Swann, C.P., Ewart, J.W., 1982. An exploratory study with the proton microprobe of the ontogenetic distribution of 16 elements in the shell of living oysters (*Crassostrea virginica*). *Mar. Biol.* 69, 235–246.
- Cartwright, J.H.E., Checa, A.G., Gale, J.D., Gebauer, D., Sainz-Díaz, C.I., 2012. Calcium carbonate polymorphism and its role in biomineralization: How many amorphous calcium carbonates are there? *Angew. Chem. Int. Edit.* 51, 11960–11970.
- Chen, F., Feng, J.-L., Hu, H.-P., 2015. Relationship between the shell geochemistry of the modern aquatic gastropod *Radix* and water chemistry of lakes of the Tibetan Plateau. *Hydrobiologia*. doi:10.1007/s10750-015-2634-1
- Corrège, T., 2006. Sea surface temperature and salinity reconstruction from coral geochemical tracers. *Palaeogeogr. Palaeoclimatol. Palaeoecol.* 232, 408–428.
- Dauphin, Y., 2002. Comparison of the soluble matrices of the calcitic prismatic layer of *Pinna nobilis* (Mollusca, Bivalvia, Pteriomorpha). *Comp. Biochem. Physiol. A* 132, 577–590.
- Dauphin, Y., Cuif, J.-P., Doucet, J., Salomé, M., Susini, J., Williams, C.T., 2003. In situ mapping of growth lines in the calcitic prismatic layers of mollusc shells using X-ray absorption near-edge structure (XANES) spectroscopy at the sulphur K-edge. *Mar. Biol.* 142, 299–304.

- Deith, M.R., 1985. The composition of tidally deposited growth lines in the shell of the edible cockle, *Cerastoderma edule*. J. Mar. Biol. Assoc. U. K. 65, 573–581.
- Dietzel, M., Gussone, N., Eisenhauer, A., 2004. Co-precipitation of Sr<sup>2+</sup> and Ba<sup>2+</sup> with aragonite by membrane diffusion of CO<sub>2</sub> between 10 and 50 °C. Chem. Geol. 203, 139–151.
- Dodd, J.R., 1965. Environmental control of strontium and magnesium in *Mytilus*. Geochim. Cosmochim. Acta 29, 385–398.
- Dodd, J.R., Crisp, E.L., 1982. Non-linear variation with salinity of Sr/Ca and Mg/Ca ratios in water and aragonitic bivalve shells and implications for paleosalinity studies. Palaeogeogr. Palaeoclimatol. Palaeoecol. 38, 45–56.
- Farrow, G.E., 1971. Periodicity structures in the bivalve shell: experiments to establish growth controls in *Cerastoderma edule* from the Thames Estuary. Palaeontology 14, 571–587.
- Foster, L.C., Allison, N., Finch, A.A., Andersson, C., 2009. Strontium distribution in the shell of the aragonite bivalve *Arctica islandica*. Geochem. Geophys. Geosyst. 10, Q03003. doi:10.1029/2007GC001915
- Fritz, L.W., Ragone, L.M., Lutz, R.A., 1990. Biomineralization of barite in the shell of the freshwater Asiatic clam *Corbicula fluminea* (Mollusca: Bivalvia). Limnol. Oceanogr. 35, 756–762.
- Füllenbach, C.S., Schöne, B.R., Mertz-Kraus, R., 2015. Strontium/lithium ratio in aragonitic shells of *Cerastoderma edule* (Bivalvia) — A new potential temperature proxy for brackish environments. Chem. Geol. 417, 341–355.
- Gaetani, G.A., Cohen, A.L., 2006. Element partitioning during precipitation of aragonite from seawater: A framework for understanding paleoproxies. Geochim. Cosmochim. Acta 70, 4617–4634.
- Gillikin, D.P., Lorrain, A., Navez, J., Taylor, J.W., André, L., Keppens, E., Baeyens, W., Dehairs, F., 2005. Strong biological controls on Sr/Ca ratios in aragonitic marine bivalve shells. Geochem. Geophys. Geosyst. 6, Q05009.
- Goodfriend, G.A., Weidman, C.R., 2001. Ontogenetic trends in aspartic acid racemization and amino acid composition within modern and fossil shells of the bivalve *Arctica*. Geochim. Cosmochim. Acta 65, 1921–1932.
- Han, T.Y.J., Aizenberg, J., 2008. Calcium carbonate storage in amorphous form and its template-induced crystallization. Chem. Mater. 20, 1064–1068.
- Hallam, A., Price, N.B., 1968. Environmental and biochemical control of strontium in shells of *Cardium edule*. Geochim. Cosmochim. Acta 32, 319–328.
- Hart, S.R., Blusztajn, J., 1998. Clams as recorders of ocean ridge volcanism. Science 280, 883–886.

- Hori, M., Sano, Y., Ishida, A., Takahata, N., Shirai, K., Watanabe, T., 2015. Middle Holocene daily light cycle reconstructed from the strontium/calcium ratios of a fossil giant clam shell. *Sci. Rep.* 5, 8734.
- House, M.R., Farrow, G.E., 1968. Daily growth banding in the shell of the cockle, *Cardium edule*. *Nature* 219, 1384–1386.
- Jacob, D.E., Wirth, R., Soldati, A.L., Wehrmeister, U., Schreiber, A., 2011. Amorphous calcium carbonate in the shells of adult *Unionoida*. *J. Struct. Biol.* 173, 241–249.
- Kinsman, D.J.J., Holland, H.D., 1969. The co-precipitation of cations with CaCO<sub>3</sub> - IV. The co-precipitation of Sr<sup>2+</sup> with aragonite between 16° and 96 °C. *Geochim. Cosmochim. Acta* 33, 1–17.
- Klein, R.T., Lohmann, K.C., Thayer, C.W., 1996. Sr/Ca and <sup>13</sup>C/<sup>12</sup>C ratios in skeletal calcite of *Mytilus trossulus*: Covariation with metabolic rate, salinity, and carbon isotopic composition of seawater. *Geochim. Cosmochim. Acta* 60, 4207–4221.
- Lazareth, C.E., Vander Putten, E., André, L., Dehairs, F., 2003. High-resolution trace element profiles in shells of the mangrove bivalve *Isognomon ephippium*: a record of environmental spatiotemporal variations? *Estuar. Coastal Shelf Sci.* 57, 1103–1114.
- Lingard, S.M., Evans, D., Bourgoin, B.P., 1992. Method for the estimation of organic-bound and crystal-bound metal concentrations in bivalve shells. *Bull. Environ. Contam. Toxicol.* 48, 179–184.
- Lønne, O.J., Gray, J.S., 1988. Influence of tides on microgrowth bands in *Cerastoderma edule* from Norway. *Mar. Ecol. Prog. Ser.* 42, 1–7.
- Lorrain, A., Gillikin, D.P., Paulet, Y.-M., Chauvaud, L., Le Mercier, A., Navez, J., André, L., 2005. Strong kinetic effects on Sr/Ca ratios in the calcitic bivalve *Pecten maximus*. *Geology* 33, 965–968.
- Mahé, K., Bellamy, E., Lartaud, F., de Rafélis, M., 2010. Calcein and manganese experiments for marking the shell of the common cockle (*Cerastoderma edule*): tidal rhythm validation of increments formation. *Aquat. Living Resour.* 23, 239–245.
- Malham, S.K., Hutchinson, T.H., Longshaw, M., 2012. A review of the biology of European cockles (*Cerastoderma* spp.). *J. Mar. Biol. Assoc. U.K.* 92, 1563–1577.
- Marin, F., Luquet, G., 2004. Molluscan shell proteins. *Comptes Rendus Palevol* 3, 469–492.
- Marin, F., Luquet, G., Marie, B., Medakovic, D., 2007. Molluscan Shell Proteins: Primary Structure, Origin, and Evolution. *Curr. Top. Dev. Biol.* 80, 209–276.
- Marin, F., Le Roy, N., Marie, B., 2012. The formation and mineralization of mollusk shell. *Front. Biosci.* S4, 1099–1125.

- Meibom, A., Cuif, J.-P., Houlbreque, F., Mostefaoui, S., Dauphin, Y., Meibom, K.L., Dunbar, R.B., 2008. Compositional variations at ultra-structure length scales in coral skeleton. *Geochim. Cosmochim. Acta* 72, 1555–1569.
- Moura, G., Vilarinho, L., Santos, A.C., Machado, J., 2000. Organic compounds in the extrapalial fluid and haemolymph of *Anodonta cygnea* (L.) with emphasis on the seasonal biomineralization process. *Comp. Biochem. Physiol. B.* 125, 293–306.
- Ohno, T., 1985. Experimentelle Analysen zur Rhythmik des Schalenwachstums einiger Bivalven und ihre palaeobiologische Bedeutung. *Palaeontogr. A* 189, 63–123.
- Orton, J.H., 1926. On the rate of growth of *Cardium edule*. Part I. Experimental observations. *J. Mar. Biol. Assoc. U.K.* 14, 239–279.
- Pokroy, B., Quintana, J.P., Caspi, E.N., Berner, A., Zolotoyabko, E., 2004. Anisotropic lattice distortions in biogenic aragonite. *Nat. Mater.* 3, 900–902.
- Ponsero, A., Dabouineau, L., Allain, J., 2009. Modelling of common European cockle *Cerastoderma edule* fishing grounds aimed at sustainable management of traditional harvesting. *Fish. Sci.* 75, 839–850.
- Poulain, C., Gillikin, D.P., Thébault, J., Munaron, J.M., Bohn, M., Robert, R., Paulet, Y.-M., Lorrain, A., 2015. An evaluation of Mg/Ca, Sr/Ca and Ba/Ca ratios as environmental proxies in aragonite bivalve shells. *Chem. Geol.* 396, 42–50.
- Richardson, C.A., Crisp, D.J., Runham, N.W., 1979. Tidally deposited growth bands in the shell of the common cockle, *Cerastoderma edule* (L.). *Malacologia* 18, 277–290.
- Richardson, C.A., Crisp, D.J., Runham, N.W., 1980. An endogenous rhythm in shell deposition in *Cerastoderma edule*. *J. Mar. Biol. Assoc. U. K.* 60, 991–1004.
- Rimstidt, J.D., Balog, A., Webb, J., 1998. Distribution of trace elements between carbonate minerals and aqueous solutions. *Geochim. Cosmochim. Acta* 62, 1851–1863.
- Sano, Y., Kobayashi, S., Shirai, K., Takahata, N., Matsumoto, K., Watanabe, T., Sowa, K., Iwai, K., 2012. Past daily light cycle recorded in the strontium/calcium ratios of giant clam shells. *Nat. Commun.* 3, 761.
- Schöne, B.R., Zhang, Z., Jacob, D.E., Gillikin, D.P., Tütken, T., Garbe-Schönberg, D., McConnaughey, T.A., Soldati, A.L., 2010. Effect of organic matrices on the determination of the trace element chemistry (Mg, Sr, Mg/Ca, Sr/Ca) of aragonitic bivalve shells (*Arctica islandica*) - Comparison of ICP-OES and LA-ICP-MS data. *Geochem. J.* 44, 23–37.
- Schöne, B.R., Zhang, Z., Radermacher, P., Thébault, J., Jacob, D.E., Nunn, E.V., Maurer, A.-F., 2011. Sr/Ca and Mg/Ca ratios of ontogenetically old, long-lived bivalve shells (*Arctica islandica*) and their function as paleotemperature proxies. *Palaeogeogr. Palaeoclimatol. Palaeoecol.* 302, 52–64.

- Schöne, B.R., Radermacher, P., Zhang, Z., Jacob, D.E., 2013. Crystal fabrics and element impurities (Sr/Ca, Mg/Ca, and Ba/Ca) in shells of *Arctica islandica* - Implications for paleoclimate reconstructions. *Palaeogeogr. Palaeoclimatol. Palaeoecol.* 373, 50–59.
- Shen, C.C., Lee, T., Chen, C.Y., Wang, C.H., Dai, C.F., Li, L.A., 1996. The calibration of D[Sr/Ca] versus sea surface temperature relationship for *Porites* corals. *Geochim. Cosmochim. Acta* 60, 3849–3858.
- Shirai, K., Schöne, B.R., Miyaji, T., Radermacher, P., Krause Jr, R.A., Tanabe, K., 2014. Assessment of the mechanism of elemental incorporation into bivalve shells (*Arctica islandica*) based on elemental distribution at the microstructural scale. *Geochim. Cosmochim. Acta* 126, 307–320.
- Stecher, H.A., Krantz, D.E., Lord, C.J., Luther, G.W., Bock, K.W., 1996. Profiles of strontium and barium in *Mercenaria mercenaria* and *Spisula solidissima* shells. *Geochim. Cosmochim. Acta* 60, 3445–3455.
- Stephenson, A.E., DeYoreo, J.J., Wu, L., Wu, K.J., Hoyer, J., Dove, P.M., 2008. Peptides enhance magnesium signature in calcite: insights into origins of vital effects. *Science* 322, 724–727.
- Swan, E.F., 1956. The meaning of strontium-calcium ratios. *Deep-Sea Res.* 4, 71.
- Takesue, R.K., van Geen, A., 2004. Mg/Ca, Sr/Ca, and stable isotopes in modern and Holocene *Protothaca staminea* shells from a northern California coastal upwelling region. *Geochim. Cosmochim. Acta* 68, 3845–3861.
- Toland, H., Perkins, B., Pearce, N.J.G., Keenan, F., Leng, M.J., 2000. A study of sclerochronology by laser ablation ICP-MS. *J. Anal. At. Spectrom.* 15, 1143–1148.
- Vander Putten, E., Dehairs, F., Keppens, E., Baeyens, W., 2000. High resolution distribution of trace elements in the calcite shell layer of modern *Mytilus edulis*: Environmental and biological controls. *Geochim. Cosmochim. Acta* 64, 997–1011.
- Wada, K., Fujinuki, T., 1976. Biomineralization in bivalve molluscs with emphasis on the chemical composition of the extrapallial fluid. In: Bryan, N.M., Wilbur, K.M. (Eds.), *Mechanisms of Mineralization in the Invertebrates and Plants*. University of South Carolina Press, Georgetown, pp. 175–190.
- Wanamaker Jr, A.D., Kreutz, K.J., Wilson, T., Borns, H.W., Introne, D.S., Feindel, S., 2008. Experimentally determined Mg/Ca and Sr/Ca ratios in juvenile bivalve calcite for *Mytilus edulis*: implications for paleotemperature reconstructions. *Geo-Mar. Lett.* 28, 359–368.
- Wilbur, K.M., Jodrey, L.H., 1955. Studies on shell formation. V. The inhibition of shell formation by carbonic anhydrase inhibitors. *Biol. Bull.* 108, 359–365.
- Wilbur, K.M., Saleuddin, A.S.M., 1983. Shell formation. In: Saleuddin, A.S.M., Wilbur, K.M. (Eds.), *The Mollusca. Physiology, Part 1, 4*. Academic Press, New York, pp. 235–287.

- Yan, H., Shao, D., Wang, Y., Sun, L., 2013. Sr/Ca profile of long-lived *Tridacna gigas* bivalves from South China Sea: A new high-resolution SST proxy. *Geochim. Cosmochim. Acta* 112, 52–65.
- Younis, S., Kauffmann, Y., Pokroy, B., Zolotoyabko, E., 2012. Atomic structure and ultrastructure of the *Murex troscheli* shell. *J. Struct. Biol.* 180, 539–45.
- Zhao, L., Schöne, B.R., Mertz-Kraus, R., 2016. Controls on strontium and barium incorporation into freshwater bivalve shells (*Corbicula fluminea*). *Palaeogeogr. Palaeoclimatol. Palaeoecol.* (article in press).
- Zolotoyabko, E., Pokroy, B., 2007. Biomineralization of calcium carbonate: structural aspects. *CrystEngComm* 9, 1156–1161.





# **Chapter 3**

---

## **Summary & future perspectives**

### 3.1 Summary & Conclusions

This thesis presents novel approaches to advance temperature reconstructions using mollusk shells. Based on detailed studies of shell microstructures (manuscript I) and Sr/Li<sub>shell</sub> ratios (manuscript II), two new potential temperature proxies were proposed. Moreover, findings suggest a link between strontium levels and shell microstructures. Chemical data should only be compared when they were determined in the same microstructure. This strategy may help to improve the reliability of Sr/Ca<sub>shell</sub>-based temperature reconstructions (manuscript III). In the following, the central statement and a brief summary of the major results are presented for each of the three manuscripts that represent this thesis.

#### a. Manuscript I:

**‘Microstructures in shells of the freshwater gastropod *Viviparus viviparus*: A potential sensor for temperature change?’**

Central statement:

*Water temperature influenced the appearance of crossed-lamellar microstructures in shells of the freshwater gastropod *Viviparus viviparus*.*

To test the influence of different water temperatures on shell microstructures, specimens of the freshwater gastropod *Viviparus viviparus* were exposed to different temperature regimes in a six-week-long tank experiment. To facilitate the temporal alignment of different shell portions, shells were marked with calcein at the beginning of each new experimental period (= new temperature regime).

During different temperature regimes, crossed-lamellar structures, the predominating microstructure in shells of *Viviparus viviparus*, differed distinctly in appearance. Whereas 1<sup>st</sup>-order lamellae were highly unordered, showed branching and sudden stops when formed *de novo* during cold and highly variable water temperature, the same structures were characterized by a uniform and ordered appearance when warmer and more stable growth conditions prevailed. When deposited onto existing shell material with well-ordered 1<sup>st</sup>-order lamellae, structures were always uniformly ordered irrespective of temperature variability. It is hypothesized that the calcification front contains a template that guides the appearance of 1<sup>st</sup>-order lamellae. However, when this template is missing and new material is formed

*de novo*, for example at the ventral margin, microstructures are primarily influenced by the prevailing environmental conditions. During particular stressful situations, such as calcein staining or the removal from habitat, the influence of the template seems to be mitigated. In fact, these events initiated the formation of disturbance lines, characterized by an evolutionary older and more primitive microstructure (= irregular fibrous prisms) that differed distinctly from the surrounding crossed-lamellar structure.

Future studies need to evaluate to which extent microstructural variations are influenced by other environmental (e.g., food availability) or biological (e.g., growth rates) parameters and if other microstructures are likewise sensitive to temperature change. Furthermore, it should be tested if results presented here can be confirmed in specimens from natural habitats.

## **b. Manuscript II:**

### **‘Strontium/lithium ratio in aragonitic shells of *Cerastoderma edule* (Bivalvia) – A new potential temperature proxy for brackish environments’**

#### Central statement:

*Sr/Li<sub>shell</sub> ratios of the studied specimens of Cerastoderma edule were strongly correlated to water temperature. It is hypothesized that the normalization of Sr/Ca<sub>shell</sub> to Li/Ca<sub>shell</sub> ratios mathematically adjusted for some vital effects that typically hamper temperature reconstructions based on element-to-calcium ratios in bivalves.*

In order to test if the combination of element-to-calcium ratios is a possibility to reconstruct water temperature from trace elements ratios of bivalve shells, Sr/Ca<sub>shell</sub> and Li/Ca<sub>shell</sub> ratios of *Cerastoderma edule* collected from the intertidal zone of the North Sea (Schillig, Germany) were determined with sub-annual resolution. Using sclerochronological methods, geochemical data of the shells were temporally aligned and compared to an extensive dataset of environmental parameters (monitoring period = spring 2013 to spring 2014).

As expected, Sr/Ca<sub>shell</sub> and Li/Ca<sub>shell</sub> ratios of *C. edule* were severely vitally affected. In fact, element-to-calcium ratios of shells significantly underestimated respective values of the ambient water and calculated distribution coefficients differed distinctly from those determined in synthetic aragonite. Neither growth rates, salinity, chlorophyll a or respective element concentrations of the ambient water exerted

strong control on the incorporation of both trace elements into the shell. Although, the correlation between water temperature and  $(\text{Sr}, \text{Li})/\text{Ca}_{\text{shell}}$  were statistically significant and followed trends expected from abiogenic precipitation experiments or theoretical calculations, only  $\text{Sr}/\text{Li}_{\text{shell}}$  values were strongly negatively correlated to temperature. In fact, when ratios of four individuals were averaged, 81% of the  $\text{Sr}/\text{Li}_{\text{shell}}$  variation was mathematically explained by water temperature. When this new potential proxy was applied to  $\text{Sr}/\text{Li}_{\text{shell}}$  ratios of *C. edule*, it was possible to estimate temperatures with an average uncertainty of  $\pm 1.5$  °C. It is hypothesized that the normalization of Sr/Ca to Li/Ca mathematically reduces vital effects that otherwise hamper temperature reconstructions based on trace elements.

However, although temperatures reconstructed based on  $\text{Sr}/\text{Li}_{\text{shell}}$  ratios were similar to the instrumental record, clear differences were observed, especially close to the annual growth lines. These variations might be the result of findings presented in manuscript III. Further studies need to evaluate if the newly found proxy is also applicable to other bivalve species at other localities and if the same correlation also exists in other calcium carbonate polymorphs.

### c. Manuscript III:

**‘Minute co-variations of Sr/Ca ratios and microstructures in the aragonitic shell of *Cerastoderma edule* (Bivalvia) – Are geochemical variations on the ultra-scale masking potential environmental signals?’**

#### Central statement:

*Sr/Ca<sub>shell</sub> ratios in Cerastoderma edule co-varied with microstructural changes along annual and circatidal growth patterns. It is likely that microstructures or the mechanisms in charge of their formation control the amounts of strontium co-precipitated during shell formation.*

The third manuscript combines insights from manuscript I and II by means of contextualizing ultra-high resolution geochemical (i.e., ion microprobe, NanoSIMS) and microstructural analyses across circatidal and annual growth patterns of *Cerastoderma edule* collected from the intertidal zone of the North Sea (Schillig, Germany).

Findings of this study demonstrate that strontium and sulfur (analyzed as representative for organics) in shells *C. edule* are heterogeneously distributed and

co-vary with microstructural variations associated with annual and circatidal growth patterns. Whereas  $\text{Sr}/\text{Ca}_{\text{shell}}$  ratios were enriched at circatidal and annual growth lines, respective values were considerably lower in portions between consecutive growth lines, i.e., in increments.  $\text{Sr}/\text{Ca}_{\text{shell}}$  ratios at annual growth lines exceeded those measured at circatidal growth lines. Sr levels also differed between the three shell layers, which were also characterized by different microstructures. Sulfur-to-calcium ratios (= S/Ca) were likewise heterogeneously distributed, with highest concentrations measured at annual growth lines and within circatidal increments. Abruptly increasing strontium levels near circatidal and annual growth lines can neither be explained by variations of temperature or strontium levels in the ambient water, nor by abiogenic crystal kinetic effects. Based on the intimate link between abruptly changing  $\text{Sr}/\text{Ca}_{\text{shell}}$ ,  $\text{S}/\text{Ca}_{\text{shell}}$  and microstructures it is hypothesized that microstructures or the mechanisms in charge of their formation likely affect the incorporation of  $\text{Sr}^{2+}$  ions into shells of *C. edule*.

The observed small-scale geochemical variations would have remained unnoticed if conventional analytical techniques such as LA-ICP-MS or wet chemical analysis of milled/drilled samples were applied. In fact, as the average sample size (e.g., laser spot  $\sim 55 \mu\text{m}$ ;  $300 \mu\text{m}$  drill hole) of these techniques can already be larger than a single growth increment, obtained trace element concentrations likely represent mixed signals of  $\text{Sr}/\text{Ca}_{\text{shell}}$  ratios of different growth structures and different microstructures. Since strontium levels between consecutively formed circatidal growth lines and increments differ by up to  $0.9 \text{ mmol/mol}$ , averaging  $\text{Sr}/\text{Ca}_{\text{shell}}$  ratios of both growth structures results in  $\text{Sr}/\text{Ca}_{\text{shell}}$  time-series which are challenging to interpret. For example, a potential temperature signal with a temperature sensitivity similar to that of abiogenic aragonite ( $0.04 \text{ mmol/mol}/^\circ\text{C}$ ) would be masked.

Findings of this manuscript indicate that the usability of  $\text{Sr}/\text{Ca}_{\text{shell}}$  ratios as paleothermometer in *C. edule* can likely be improved if geochemical analyses are limited to portions of the shell that consist of the same microstructure. Additionally, measurements should be completed within the same shell layer and sample size should match the studied growth structures.

In conclusion, findings of this thesis indicate that:

- (i) shell microstructures and  $\text{Sr}/\text{Li}_{\text{shell}}$  ratios may potentially serve as alternative means to estimate temperature from bivalves with high temporal resolution. However, both approaches have to be rigorously tested;
- (ii) understanding the distribution of strontium on the sub-micron scale can help to make better use of  $\text{Sr}/\text{Ca}_{\text{shell}}$  as potential temperature proxy;
- (iii) accurate temperature reconstructions based on mollusk shells require a detailed understanding of the complex processes of their formation.

## 3.2 Open questions and future outlook

Testing novel and established environmental proxies on different species, localities and shells of different carbonate polymorphs can improve the understanding of how universally a proxy can be applied. However, to improve the reliability of temperature quantifications from specific shell parameters, such as the geochemical composition, it is at least equally important to understand the underlying controlling mechanisms. This is especially true for trace elements and shell microstructures, because processes controlling properties of these potential proxy systems are complex and barely understood. The following lists urgent research topics, which I personally believe will help to achieve more accurate paleoclimate estimates. The last paragraph of this chapter outlines a more general outlook of how the capabilities of mollusk shells as climate archives can be enhanced.

In my opinion it is inevitable to understand (i) to what extent active and passive  $\text{Ca}^{2+}$ -transport mechanisms also transport impurities such as  $\text{Sr}^{2+}$ , (ii) to what extent vesicles of amorphous calcium carbonate (= ACC) are part of the shell formation and which elements they contain, (iii) to which phase (i.e., organic or crystal) ions preferentially bind, (iv) if specific crystal faces favor the incorporation of specific ions and thus if certain crystallographic orientations are associated with higher or lower trace element levels, (v) if organic macromolecules have binding sites that attract specific trace element ions, (vi) if and how the concentration of organic macromolecules at the biomineralization front changes with ontogeny and season, (vii) if and how changes in the crystal lattice are related to higher or lower levels of other trace elements. Answering the questions will likely help to differentiate between the different parameters that influence the concentrations of trace elements in shells and thus to evaluate to which amount these variations are caused by environmental factors such as water temperature. In fact, only if a trace element is incorporated into the crystal phase, its concentration likely follows trends similar as those in abiogenic precipitation experiments. For instance, whereas strontium is known to substitute for  $\text{Ca}^{2+}$  in the crystal lattice of molluscan aragonite (Foster et al., 2009) and thus shows the a similar negative thermodynamic relationship as in abiogenic precipitates (Kinsman and Holland, 1969), magnesium is bound to the organic phase of aragonitic shells (Schöne et al., 2010) and thus unlikely provide reliable temperature estimates in aragonitic shells. However, if shell portions with a high organic content are formed during specific seasons, for example during lower or higher temperatures, correlations between temperature and the magnesium content might be detected, even though there is no true thermodynamic control on the incorporation. Thus, it is particularly important to test for these spurious correlations by understanding the processes controlling the incorporation of trace elements.

To advance the application of microstructures as an environmental proxy, I believe it is important to study (i) if a quantifiable relationship exists between temperature and microstructural variability, (ii) the influence of other factors likely controlling microstructures such as food availability, age or growth rate, (iii) the susceptibility of microstructures to diagenesis, (iv) the influence of organic templates on the formation of microstructures.

Findings of manuscript III indicate that in order to advance the reliability of reconstructed temperatures from mollusk shells, it is of utmost importance to gain a more detailed understanding of the archive, i.e. the shell, itself. This includes understanding shells not as simple instrumental recorders, but as products of biological processes (Willbur and Saleuddin, 1983). Thereby, it is important to acknowledge that the formation of mollusk shell material does not occur via simple precipitation from a calcium carbonate-supersaturated fluid, but is a prime example for mineralization occurring under full biological control (Marin et al., 2012) – a process, which is in focus of an own research area known as biomineralization (see Lowenstam and Weiner, 1981; Dove et al., 2004 and Cuif et al., 2011 for comprehensive reviews). In comparison to analytical methods used in sclerochronology, biomineralogical analyses of bivalve shells typically focus on the interplay between specific organic macromolecules and forming crystals on the nano-scale. Although knowledge of the biological control of shell formation is still in an early stage, research on biomineralization greatly contributed to the understanding of the complex processes of shell formation. However, due to the application of high-resolution analytical techniques, the big picture can get lost. Sclerochronological analyses on the other hand aim to extract environmental information of longer time periods from mollusk shells and are thus commonly conducted on larger shell areas. While this is typically better achieved with lower sampling resolution, the data are much more complicated to interpret and underlying controlling mechanisms are often not sufficiently considered.

Since sclerochronology and biomineralization study the same materials, both disciplines could greatly benefit from a combined approach. This way, sclerochronological findings could help to set biomineralogical results into a broader context. In turn, a detailed understanding of biomineralization can help to shed light on ‘vital effects’ (Urey, 1951; Weiner and Dove, 2003) and thus improve the temperature estimates using mollusk shells.

### 3.3 References

- Cuif, J.-P., Dauphin, Y., Sorauf, J.E., 2011. *Biominerals and fossils through time*. Cambridge University Press, Cambridge (490 pp.).
- Foster, L.C., Allison, N., Finch, A.A., Andersson, C., 2009. Strontium distribution in the shell of the aragonite bivalve *Arctica islandica*. *Geochem. Geophys. Geosyst.* 10, Q03003.
- Kinsman, D.J.J., Holland, H.D., 1969. The co-precipitation of cations with CaCO<sub>3</sub> - IV. The co-precipitation of Sr<sup>2+</sup> with aragonite between 16° and 96 °C. *Geochim. Cosmochim. Acta* 33, 1–17.
- Lowenstam, H.A., Weiner, S., 1989. *On Biomineralization*. Oxford University Press, Oxford (324 pp.).
- Marin, F., Le Roy, N., Marie, B., 2012. The formation and mineralization of mollusk shell. *Front. Biosci.* S4, 1099–1125.
- Schöne, B.R., Zhang, Z., Jacob, D., Gillikin, D.P., Tütken, T., Garbe-Schönberg, D., McConnaughey, T., Soldati, A., 2010. Effect of organic matrices on the determination of the trace element chemistry (Mg, Sr, Mg/Ca, Sr/Ca) of aragonitic bivalve shells (*Arctica islandica*) – comparison of ICP-OES and LA-ICP-MS data. *Geochem. J.* 44, 23–37.
- Urey, H.C., 1951. Measurement of paleotemperatures and temperatures of the Upper Cretaceous of England, Denmark, and the southeastern United States. *Geol. Soc. Am. Bull.* 62, 399–416.
- Weiner, S., Dove, P.M., 2003. An overview of biomineralization processes and the problem of the vital effect. *Rev. Mineral. Geochem.* 54, 1–29.
- Wilbur, K.M., Saleuddin, A.S.M., 1983. Shell formation. In: Saleuddin, A.S.M., Wilbur, K.M. (Eds.), *The Mollusca*. Vol. 4. Physiology, Part 1. Academic Press, Toronto, pp. 235–287.





# Appendix

## **Curriculum vitae**

Not displayed for reasons of data protection.



## **Conference contributions**

Not displayed for reasons of data protection.